HELSINKI UNIVERSITY OF TECHNOLOGY
Department of Micro and Nanosciences
Electron Physics Group

Aapo Varpula

Modelling of electrical properties of granular semiconductors

Licentiate's thesis submitted in partial fulfilment of the requirements for the degree of Licentiate of Science in Technology

Espoo, 7.10.2009

Supervisors: Professor Juha Sinkkonen
Professor Pekka Kuivalainen

Author: Aapo Varpula
Faculty: Faculty of Electronics, Communications and Automation
Date: 7.10.2009 Language: English Number of pages: 116

Title: Modelling of electrical properties of granular semiconductors
Title in Finnish: Rakeisten puolijohteiden sähköisten ominaisuuksien mallintaminen
Chair: S-69 Electron physics, Electrophysics
Supervisors: Prof. Juha Sinkkonen
Prof. Pekka Kuivalainen

Abstract:

In this Thesis the electrical properties of granular n-type semiconductor are modelled using analytical and numerical simulation methods. The numerical simulation is performed with SILVACO ATLAS device simulation software. The analytical DC and AC models of the granular n-type semiconductor are presented. In the model the grain boundaries are infinitely thin and have acceptor-type electronic interface states with a single discrete energy level. The whole granular material is modelled with a number of identical grain boundaries separated by bulk regions.

The use of different grain-boundary potential profiles in the calculation of DC current density and the electron density at the grain boundary is compared. All potential profiles give very similar results. The calculated I–V curves of the material have four characteristic regions: linear, sub-linear, super-linear (nonlinear), and series resistance limited (linear). The sub-linear region is caused by the electronic trapping at grain boundaries. The agreement between the analytical and numerical results is excellent in a large voltage range.

In the course of the small-signal AC analysis of the granular semiconductor the electrical equivalent circuit (EEC) model of the material is presented. The model shows that a granular semiconductor material exhibits negative admittance and capacitance, when the electronic trapping at grain boundaries is present and a DC bias voltage is applied across the material. The analytical and numerical results are in a very good agreement in the whole frequency range at low DC bias voltages.

Keywords: Granular semiconductors, metal oxides, drift-diffusion theory, barrier model, electronic interface states, electronic trapping, electrical equivalent circuit

Tekijä: Aapo Varpula
Tiedekunta: Elektroniikan, tietoliikenteen ja automaation tiedekunta

Päivämäärä: 7.10.2009 Kieli: Englanti Sivumäärä: 116

Työn nimi: Rakeisten puolijohteiden sähköisten ominaisuuksien mallintaminen
Title in English: Modelling of electrical properties of granular semiconductors
Professuurin koodi ja nimi: S-69 Elektronifysiikka, Sähköfysiikka
Työn valvojat: Prof. Juha Sinkkonen
Prof. Pekka Kuivalainen

Tiivistelmä:

Työssä mallinnetaan rakeisen n-tyypin puolijohteen sähköisiä ominaisuuksia analyyttisin ja numeerisin menetelmin. Numeerinen simulointi tehdään SILVACO ATLAS –komponenttisimulointiohjelmalla. Työssä esitetään rakeisen n-tyypin puolijohteen analyyttiset DC ja AC-mallit. Mallissa raerajat ovat äärettömän ohuita ja niissä on akseptori-tyypin elektronisia pintatiloja, joilla on yksi diskreetti energiataso. Mallissa koko rakeinen aine koostuu identtisistä raerajoista, joita yhdistää väliaine.

Erilaisten potentiaaliprofiilien käyttöä DC-virran ja raerajalla olevan elektronitiheyden laskemisessa vertaillaan. Kaikki potentiaaliprofiilit antavat hyvin samankaltaisia tuloksia. Lasketuilla aineen I-V käyrillä on neljä luonteenomaista aluetta: lineaarinen, alilinearinen, ylilineaarinen (epälineaarinen), sekä sarjavastusrajoitteinen (lineaarinen). Alilineaarinen johtuu elektronien loukkuuntumisesta raerajoilla. Analyyttiset ja numeeriset tulokset pitävät erinomaisesti yhtä laajalla jännitealueella.

Rakeisen puolijohteen AC-piensignaalianalyysin yhteydessä esitetään aineen vastinpiirimalli. Mallin mukaan rakeisessa puolijohteessa havaitaan negatiivista admittanssia ja kapasitanssia, kun aineessa esiintyy elektronien loukkuuntumista ja aineen yli kytketään DC-jännite. Analyyttiset ja numeeriset tulokset pitävät erittäin hyvin yhtä koko taajuusalueella alhaisilla DC-jännitteillä.

Avainsanat: Rakeiset puolijohteet, metallioksidit, drift-diffuusioteoria, vallimalli, elektroniset tilat rajapinnoilla, elektronien loukkuuntuminen, vastinpiiri

Preface

The research work of this thesis was performed in the Electron Physics Group of the Department of Micro and Nanosciences at the Helsinki University of Technology (TKK) in Micronova building.

I thank my supervisors professors Juha Sinkkonen and Pekka Kuivalainen for the opportunity to work in the fascinating field of semiconductor physics and guidance in the theoretical part of this work. I am also obliged to D.Sc. Marko Yli-Koski and M.Sc. Ville Vähänissi, whose help was invaluable in the use of the numerical simulation sofware Silvaco.

The financial support of the Academy of Finland is gratefully acknowledged.

Finally I thank my friends and family for their encouragement. Especially, I express my gratitude to my wife Sointu for her love and support.

Otaniemi, Espoo, 7th of October 2009

Matti Aapo Ilari Varpula

Contents

1 Introduction **1**

2 Grain boundaries in semiconductors **4**
2.1 Non-degenerate semiconductors 4
2.2 Electronic traps in semiconductors 6
2.3 Features of semiconductor grain boundaries 8
2.3.1 Depletion, inversion, and accumulation regions 10
2.3.2 Additional effects 12
2.4 Modelling granular material 13
2.4.1 Theories for calculating charge transport in semiconductors . . 16

3 Modelling of electrical properties of grain boundaries in n-type semiconductors **18**
3.1 Numerical calculation of electric properties 19
3.2 Potential in grain-boundary region 21
3.2.1 General solution 21
3.2.2 Depletion region approximation 26
3.2.3 Other approximative solutions 28
3.2.4 Comparison of general and approximative solutions 29
3.2.5 Depletion region approximation with external electric field applied 31
3.2.6 Comparison of potential profiles 36
3.3 Calculation of DC current and electron density 41
3.3.1 Linear potential 43
3.3.2 Useful formulas for integration in quadratic potential case . . 46
3.3.3 Quadratic potential without bulk electric field 46
3.3.4 Quadratic potential with bulk electric field 48
3.3.5 Comparison of formulas 50

3.4 Electronic trapping at grain boundary 54
3.4.1 Correction to rate equation 57
3.4.2 Steady state solution of rate equation 58
3.4.3 Normalization of rate equation 58
3.5 Dynamical electric model of grain boundary 60
3.5.1 Calculation using linear potential and approximations 62
3.5.2 Electrical equivalent circuit model 63
3.5.3 Electrical equivalent circuit conversion 73
3.6 Additional modelling considerations 74

4 I–V characteristics of granular semiconductor 76
4.1 DC model of granular semiconductor 76
4.2 Comparison of modelling results 78
4.3 Effect of parameters 82

5 Small signal analysis of granular semiconductor 91
5.1 Electrical equivalent circuit model 91
5.2 Effect of parameters 94

6 Conclusions 104

Bibliography 106

Chapter 1

Introduction

Polycrystalline materials consist of crystallites (i.e. grains) which have various sizes, shapes, and crystal orientation. As an example, images of a polycrystalline semiconductor material, iron oxide, are shown in Fig. 1.1. Polycrystalline semiconductors are materials which often have unusual electrical properties [1, 2]. These electrical properties originate from electrically active grain boundaries existing in the material [1,2]. They can either benefit or harm the operation of devices in which granular materials are employed. In addition, polycrystalline semiconductors, for example polycrystalline silicon (poly-Si), are widely used as low-cost and versatile material in microfabrication of devices and integrated circuits [1, 2]. In this technological application the presence of the electrically active grain boundaries in the material is often deleterious. For example in solar cells fabricated from polycrystalline materials the grain boundaries reduce the efficiency of the solar cells considerably [1]. Therefore much effort is placed in the passivation of the grain boundaries [1].

Several devices are based directly on the unusual electrical properties of grain boundaries: Varistors (i.e. variable resistors or voltage-dependent resistors (VDR)), positive temperature coefficient (PTC) resistors, grain-boundary capacitors, pressure gauges, light detectors, and gas sensors [1, 4]. In polycrystalline semiconductors the transport of charge carriers across the grain boundaries depend exponentially on the height of the potential barrier located at the grain boundary [1]. This results in nonlinear I–V characteristics [1]. The height of the grain-boundary potential barrier in turn depends quadratically on the charge at the grain boundary [1]. Hence due to the exponential dependence very small changes in the grain-boundary charge re-

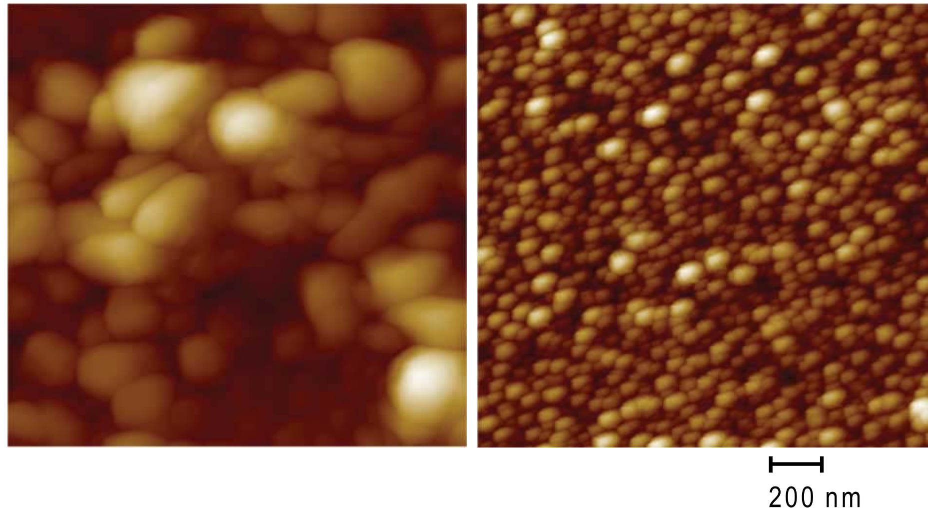

Figure 1.1: Atomic force microscopy (AFM) images of iron oxide thin films [3].

sult in large changes in the electric current. This exponential amplification effect is exploited in very sensitive sensor devices.

The use of polycrystalline semiconductors in the varistor application arises from their highly nonlinear I–V characteristics [1, 4]. Metal oxides, for example ZnO, are usually employed because of their large-energy-handling capabilities [1, 4]. Applications of varistors range from power switching in electrical transmission systems to voltage surge protection in automobile and semiconductor electronics [4]. The physical operation principle of a varistor as a solid-state switch is simple: In the off-state the varistor is operated in the Ohmic part of the I–V curve, and only leakage current flows through the device. In the on-state the non-linear part of the I–V curve, where the current is high, is employed.

Metal-oxide semiconductors are frequently used as gas sensors [5–8]. The most common gas sensor is the resistive sensor where the electrical resistance of the gas-sensitive material changes in the presence of target gas molecules. Gas-sensitive metal oxides are often deposited as porous polycrystalline films, through which gas molecules can pass. The most common gas sensing mechanism is based on atmospheric oxygen which is adsorbed on the surfaces of the metal-oxide grains as ions [5–7, 9]. Elevated temperatures (usually at 200–500 ^{o} [6]) are required for the oxygen ionosorption to take place. Due to the electric charge of the preadsorbed oxygen ions potential barriers are formed at the grain boundaries [5, 9]. As stated before, these potential barriers impede the flow of electric current substantially. The

gas-sensing effect is acquired, when the target gas molecules react with the preadsorbed oxygen, thus reducing the amount of grain-boundary charge and thereby increasing the flow of electric current [5, 9].

In this work the electrical properties of granular large band-gap n-type semiconductor are modelled using analytical and numerical simulation methods. The aim is to derive an accurate analytical model for the material. Compared to numerical simulations analytical models allow simple and fast calculations. In addition, fitting an analytical model to experimental data is much simpler and faster than fitting a numerical one. The analytical models presented in this work can be used in the modelling of granular semiconductor materials and devices and sensors based on them. The analytical models are compared with the results from numerical simulations, which are performed with the SILVACO ATLAS device simulation software [10].

In the modelling the effect of holes in the material is neglected. However, with minor model modifications, the results presented in this work can also be applied to a p-type semiconductor. In this work the DC and the AC models of the n-type semiconductor grain boundary, which were earlier briefly presented in Refs. [11] and [12], are improved in many ways and extended to the case of the whole granular material, which is modelled with a number of identical grain boundaries separated by bulk regions. However, in the numerical simulations the granular material has only a single grain boundary. In the model the grain boundaries are infinitely thin and they have acceptor-type electronic interface states with a single discrete energy level. Numerous studies (see for example Refs. [1, 2, 9] and references therein) have shown that this approach is enough to explain the most of the experimental results. The approach can also be considered as a type of geometrical model of a granular material [2]. In spite of the simplified approach the model semiconductor structure displays extraordinary electric properties, such as highly nonlinear I–V characteristics [1, 11] and negative admittance and capacitance [1, 12].

This Thesis is divided into several chapters. In chapter 2 the general properties of grain boundaries in semiconductors and related theories and models are discussed. The numerical and the analytical models of a grain boundary in an n-type semiconductor are presented in chapter 3. The models of chapter 3 are applied to the whole granular material in the DC and the AC cases in chapters 4 and 5, respectively.

Chapter 2

Grain boundaries in semiconductors

2.1 Non-degenerate semiconductors

This section summarizes the fundamental semiconductor physics of non-degenerate semiconductors related to this work. Only non-degenerate semiconductors are considered.

In non-degenerate semiconductors densities of donors and acceptors are sufficiently small for the Fermi level to lie in the forbidden energy gap [13]. Often the Fermi level is far from the conduction and valence band edges, i.e. $E_c - E_F \gg k_B T$ and $E_F - E_v \gg k_B T$. In this case Maxwell-Boltzmann statistics can be used instead of Fermi-Dirac statistics. In Maxwell-Boltzmann statistics, which are employed in this work, the electron and hole densities are given by [13–15]

$$n = N_c e^{-(E_c - E_F)/k_B T} \tag{2.1}$$

$$p = N_v e^{-(E_F - E_v)/k_B T}, \tag{2.2}$$

where N_c and N_v are the effective densities of states of the conduction and valence

bands, which are defined by [13, 14]

$$N_c = 2\left(\frac{m_n^* k_B T}{2\pi\hbar^2}\right)^{3/2} \tag{2.3}$$

$$N_v = 2\left(\frac{m_p^* k_B T}{2\pi\hbar^2}\right)^{3/2}, \tag{2.4}$$

where m_n^* and m_p^* are the effective masses of electrons and holes, respectively. If the semiconductor has no doping the Fermi level is equal to the intrinsic energy [13,15,16]

$$E_i = \frac{1}{2}\left(E_c + E_v\right) - \frac{1}{2} k_B T \ln \frac{N_c}{N_v}. \tag{2.5}$$

If the effective densities of states N_c and N_v are equal, E_i lies exactly in the middle of the gap. The position of the Fermi level relative to E_i defines the type of the semiconductor [15]: If $E_F = E_i$, the semiconductor is intrinsic. In the case $E_F > E_i$ the semiconductor is n-type, and p-type in the case $E_F < E_i$, respectively. Using the intrinsic carrier density [13, 16]

$$n_i = \sqrt{np} = \sqrt{N_c N_v} e^{-E_g/(2k_B T)}, \tag{2.6}$$

where E_g is the forbidden energy gap of the semiconductor, Eqs. 2.1 and 2.2 can be written as

$$n = n_i e^{-(E_i - E_F)/k_B T} \tag{2.7}$$

$$p = n_i e^{-(E_F - E_i)/k_B T}. \tag{2.8}$$

Another important quantity describing semiconductor material is the Debye length. The Debye length is the distance over which charge carriers screen out (i.e. neutralize) electric fields and charge imbalances in the material under steady-state or equilibrium conditions. The extrinsic Debye length is given by [17]

$$L_D = \sqrt{\frac{\varepsilon k_B T}{q^2\left(n_b + p_b\right)}}, \tag{2.9}$$

where n_b and p_b are the electron and hole densities, respectively. The formula of the intrinsic Debye length is obtained by replacing $n_b + p_b$ by n_i in Eq. 2.9 [16]. As Eq. 2.9 shows the Debye length is essentially determined by the density of charge carriers. Because of this L_D is usually much larger in semiconductors than in metals.

Finally, the following Einstein's relation is frequently used in this work [18]

$$D = \frac{k_B T}{q}\mu. \tag{2.10}$$

Table 2.1: Charging characters of electronic trap states [15].

Type of state	Occupied by electron (Empty of holes)	Empty of electrons (Occupied by hole)
Donor	0	+
Acceptor	−	0

2.2 Electronic traps in semiconductors

This section summarizes the physics of electronic traps in semiconductors. Only the electronic traps in the bulk of the semiconductor are considered. However, the model presented here can be easily extended to the cases of interface and surface traps (see section 3.4).

Existence of foreign atoms or defects in semiconductor crystals can give rise to local electronic states within the energy gap [17]. Similar electronic states can exist also on surfaces and in interfaces of materials [15]. The electronic states act as traps for electrons and holes. If the trap state is occupied by an electron, then it is empty of holes, and vice versa.

The type of the electronic traps states are either donor or acceptor. Depending on the occupancy and type of the trap state the electric charge of the trap state is either positive (+), neutral (0), or negative (−). The possible combinations are listed in Table 2.1.

The electron and hole trapping and releasing from the electronic trap state with energy level of E_T is shown in Fig. 2.1. All the processes shown in Fig. 2.1 can be described by a rate equation. The rate equation describing the density of trap states occupied by an electron N_T is given by [17]

$$\frac{dN_T}{dt} = (c_n n + e_p)\left(N_T^{tot} - N_T\right) - (c_p p + e_n) N_T, \tag{2.11}$$

where n is the density of electrons, p the density of holes, N_T^{tot} the total density of trap states, and e_n and e_p the emission (i.e. releasing) coefficients of electrons and holes, respectively. The capture (i.e. trapping) coefficients of electrons and holes c_n and c_p are defined by [17]

$$c_n = \sigma_n v_{Tn} \tag{2.12}$$

$$c_p = \sigma_p v_{Tp}, \tag{2.13}$$

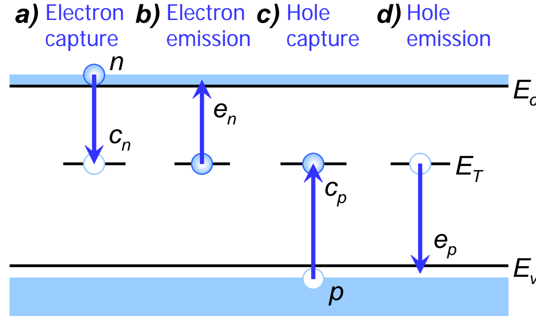

Figure 2.1: Energy-band illustration of the trapping phenomena: *a)* Electron capture from the conduction band to the electronic trap state, *b)* electron emission to the conduction band, *c)* hole capture from the valence band to the electronic trap state, and *d)* hole emission to the valence band. E_c is the bottom of the conduction band, E_v the top of the valence band, E_T the energy level of the trap state, n the density of electrons, p the density of holes, e_n the emission coefficient of electrons, e_p the emission coefficient of holes, c_n the capture coefficient of electrons, and c_p the capture coefficient of holes, respectively.

where σ_n and σ_p are the capture cross-sections and υ_{Tn} and υ_{Tn} the thermal velocities of electrons and holes, respectively. The thermal velocities are [13, 17]

$$\upsilon_{Tn} = \sqrt{\frac{3k_BT}{m_n^*}} \tag{2.14}$$

$$\upsilon_{Tp} = \sqrt{\frac{3k_BT}{m_p^*}}. \tag{2.15}$$

In the thermodynamical equilibrium the occupation probabilities of the trap states are given by [19]

$$f_n = \frac{1}{1 + \frac{g_p}{g_n} \exp\left(\frac{E_T - E_F}{k_BT}\right)} \tag{2.16}$$

$$f_p = \frac{1}{1 + \frac{g_n}{g_p} \exp\left(\frac{E_F - E_T}{k_BT}\right)}, \tag{2.17}$$

where g_n and g_p are the statistical weights of the states occupied by an electron and a hole, respectively. The weights correspond to the number of ways these states may be realized. If the degeneracy is only due to the electron spin, then $g_n = 2$ and $g_p = 1$. When the degeneracy is neglected (i.e. $g_n/g_p = 1$), the Fermi-Dirac

distribution functions for electrons and holes are given by

$$f_n = \frac{1}{1 + \exp\left(\frac{E_T - E_F}{k_B T}\right)} \tag{2.18}$$

$$f_p = \frac{1}{1 + \exp\left(\frac{E_F - E_T}{k_B T}\right)}. \tag{2.19}$$

The use of these Fermi-Dirac distribution functions instead of Eqs. 2.16 and 2.17 gives an error to the value of energy level. The error is in the order of $k_B T$ or less (see Refs. [16] or [19]), which is usually low enough for practical calculations.

Relations between the emission and the capture coefficients can be obtained by using the principle of detailed balance [17]. According to the principle each fundamental process and its inverse must balance independent of any other process that may be occuring inside the material under thermodynamical equilibrium conditions [17]. If the trap occupancy statistics are calculated using the Fermi-Dirac distribution functions (Eqs. 2.18 and 2.19), then the relations are [17]

$$e_n = c_n n_i e^{-(E_i - E_T)/k_B T} = c_n N_c e^{-(E_c - E_T)/k_B T} \tag{2.20}$$

$$e_p = c_p n_i e^{-(E_T - E_i)/k_B T} = c_p N_v e^{-(E_T - E_v)/k_B T}, \tag{2.21}$$

where Eqs. 2.1, 2.2, 2.7, and 2.8 were used. Usually it is assumed that Eqs. 2.20 and 2.21 hold also under non-equilibrium conditions.

A more detailed thermodynamical consideration (see Ref. [17]) reveals that in addition to the correct statistics (Eqs. 2.16 and 2.17) the entropy change must be taken into account when deriving the relations of Eqs. 2.20 and 2.21. In addition, the capture cross-sections σ_n and σ_p can depend exponentially on the temperature (i.e. activation energy is related to the capture process). These corrections will not be considered in this work.

2.3 Features of semiconductor grain boundaries

Surfaces and interfaces by themselves perturb the periodicity of the crystal. The perturbation can create local electronic states inside the energy band gap of the semiconductor [15, 16]. Real surfaces and interfaces have often surface impurities and defects [15, 20]. The surface and interface states related to the material itself

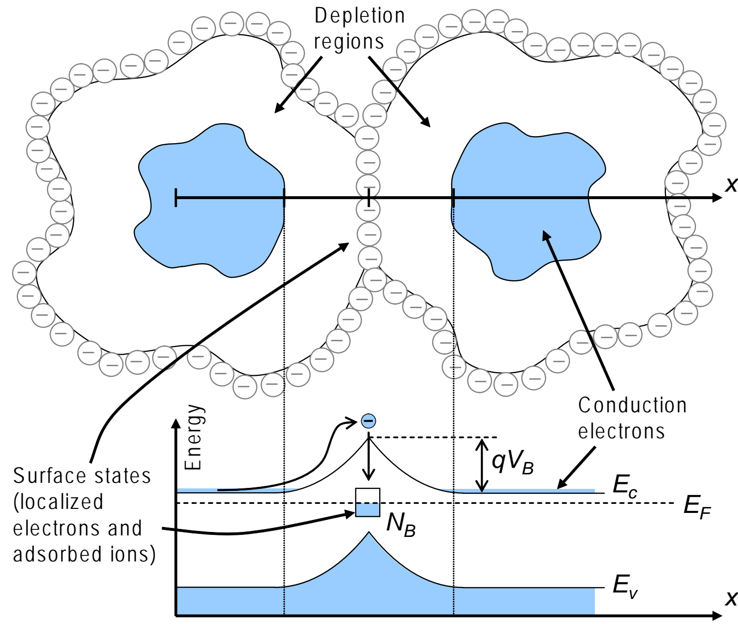

Figure 2.2: Schematic picture of two connected grains of n-type semiconductor material. The energy bands along the x-axis in the grain-boundary region are plotted, and trapping of a conduction electron in an acceptor-type electronic interface state is illustrated. N_B is the density of occupied interface states, E_c the bottom of the conduction band, E_v the top of the valence band, E_F the Fermi level, q the unit charge, and V_B the grain-boundary potential barrier, respectively.

are called intrinsic states [2, 20]. In addition to intrinsic states, extrinsic states can be generated by adsorption of gases [2, 19–21]. (However, Lüth [15] defines only the surface states related to ideal surfaces as intrinsic and the others as extrinsic surface states.) The existence of the local electronic states gives rise to electronic trapping processes, which can be modelled in the similar way as the bulk trap states (see section 2.2). In the case of trapping in an adsorbed atom or molecule (extrinsic state) the process is also known as ionization.

Two connected semiconductor grains and the electronic energy band in the grain-boundary region are illustrated in Fig. 2.2. The semiconductor is n-type and the electronic interface states at the grain boundary are acceptor-type in Fig. 2.2. Trapping of electron in the interface state shown in Fig. 2.2 gives rise to local charge at the grain boundary (density N_B per area). The local charge, in turn, causes the bending of electronic energy bands, which is discussed below. The band bending is characterized by a grain-boundary potential barrier V_B (see Fig. 2.2), which determines the transport of electrons across the grain boundary.

The thickness of the grain boundary (i.e. the intergranular phase) in materials, where the electrical activity of grain boundaries is high, varies from less than a monolayer up to several monolayers [1, 22]. The typical thickness is 2–10 nm [1], but the diffusion of atoms can result in thicknesses of 100 nm or higher [1]. However, in the typical case the thickness of the grain boundary is so small that it can be considered as infinitely thin [1]. This approach is utilized in this work. In some cases the diameter of the grains has much larger effect on the electronic properties of the granular semiconductor. If the depletion regions shown in Fig. 2.2 extend across the whole grains, the electronic properties change considerably [2]. This effect is discussed in more detail below.

2.3.1 Depletion, inversion, and accumulation regions

In a semiconductor material electric fields cause depletion or accumulation of major charge carriers of the material [15, 16]. The type and width of these regions inside the material depend on the sign and magnitude of the electric field and on the type and density of charge carriers in the material [15, 16]. If the depletion of major charge carriers is strong enough, the minority charge carriers begin to accumulate in the region [15, 16]. This is called inversion. Electric field inside the material can be caused by an external source, contact potential (for example in metal-semiconductor contact), and surface or interface states [16]. In this work only interface states are considered.

The depletion, inversion, and accumulation phenomena can also be viewed differently by considering electric potential corresponding to the applied electric field. The electric potential changes, i.e. bends, the electronic energy bands locally. The band bending, in turn, causes the depletion or accumulation of majority or minority charge carriers depending on the direction of the bending.

The depletion, inversion, and accumulation regions around a grain boundary are sketched in Fig. 2.3. Acceptor interface states in an n-type semiconductor give rise to depletion or inversion regions. Donor interface states result in accumulation region. In a p-type semiconductor the cases are the opposite: donor states result in depletion or inversion, and acceptor states in accumulation, respectively. Fig. 2.3 shows that in the inversion case the width of the region where the density of minority charge carriers exceeds the density of majority charge carriers is very small. In fact, the dimension of the region is such small that quantum effects [15] must be taken

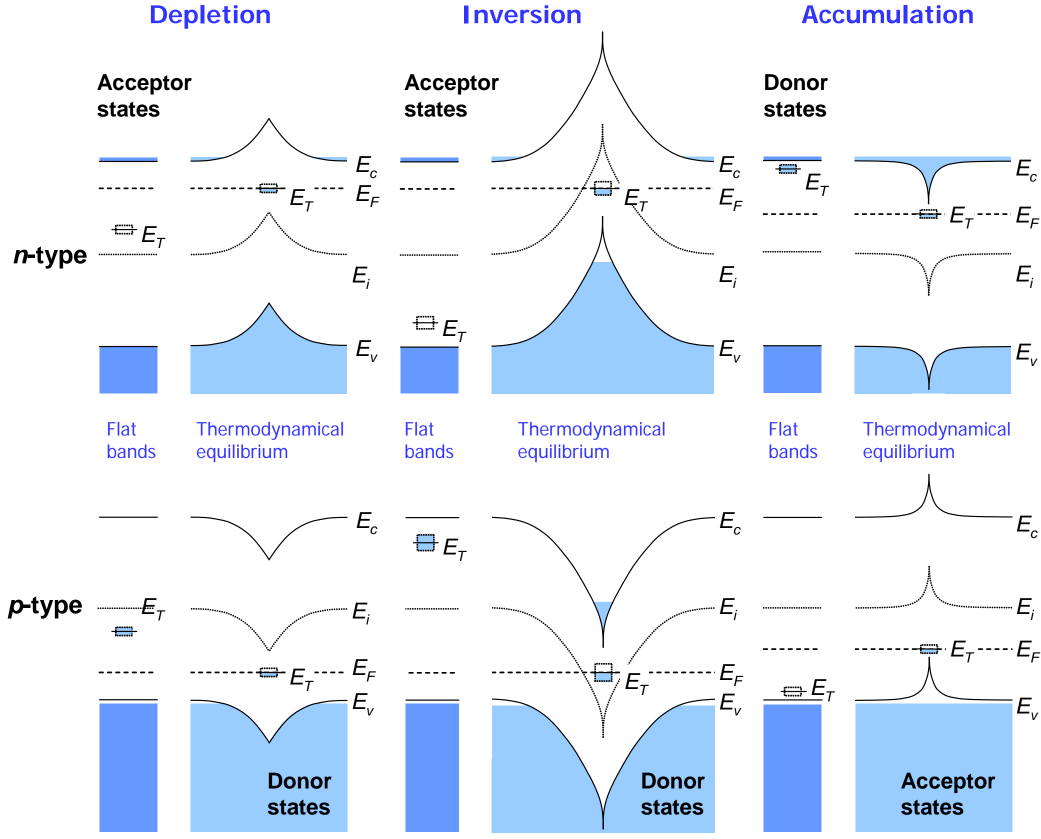

Figure 2.3: Illustration of energy bands of grain boundaries with depletion (*left*), inversion (*middle*), and accumulation (*right*) regions in n-type (*top*) and p-type semiconductors (*bottom*), respectively. The cases of flat-band and thermodynamical equilibrium are shown. E_c is the bottom of the conduction band, E_v the top of the valence band, E_F the Fermi level, and E_T the energy level of the trap state at the grain boundary, respectively. The type of the interface state (donor or acceptor) is indicated in each case.

into account in inversion regions.

The total electric charge corresponding to the interface states is Q_i. This charge is screened (i.e. compensated) by the total net charge in the semiconductor, which is often called the total space charge Q_{sc}. The overall charge neutrality requires that

$$Q_i = -Q_{sc}. \tag{2.22}$$

Q_i can be calculated by integrating over all the interface states and Q_{sc} by integrating over the whole volume of the semiconductor (excluding the interface states).

As stated before, in some cases the diameter of the grains has a large effect on

the electronic properties of granular semiconductor. If the depletion regions (see Fig. 2.2) extend across the whole grains and no bulk regions would lie between two grain boundaries, the charge neutrality condition (Eq. 2.22) must be applied in the whole material. This would result in a very different kind of material, where the interface and surface states are acting as effective bulk donors and acceptors [2, 23].

The electric potential ϕ can be solved from Poisson's equation which is in homogeneous linear medium given by [15, 24]

$$\nabla^2 \phi = -\frac{\rho}{\varepsilon}, \tag{2.23}$$

where ε is the permittivity of the medium and ρ the density of free charge, respectively. Furthermore, the electric field is given by $\vec{E} = -\vec{\nabla}\phi$, and the density of free charge in semiconductor by

$$\rho = q\left(p - N_a^- - n + N_d^+\right), \tag{2.24}$$

where q is the unit charge, p the density of holes, N_a^- the density of ionized acceptors, n the density of electrons, and N_d^+ the density of ionized donors, respectively. In the general case p, N_a^-, n, and N_d^+ vary in space. In one dimension Eqs. 2.23 and 2.24 give

$$\frac{d^2\phi(x)}{dx^2} = -\frac{q}{\varepsilon}\left[p(x) - N_a^-(x) - n(x) + N_d^+(x)\right]. \tag{2.25}$$

Now, Eqs. 2.22 and 2.25 can be used to solve the electric potential and band bending in the semiconductor. In the grain-boundary region this is performed in section 3.2.

In this work the potential for electrons V is often used. It is defined by

$$V = -\phi. \tag{2.26}$$

2.3.2 Additional effects

In this section additional effects observed at grain boundaries are briefly presented. They are not discussed further in this work. However, the effects listed should be considered when the models presented in this work are developed further.

- Grain-boundary scattering of charge carriers [2, 25].
- Tunneling effects.

  - Tunnelling through the top of the grain-boundary potential barrier [1].
  - Tunnelling directly from the conduction or valence band in the bulk to the trap state.

- Minority charge carrier effects [1, 2].
  - Minority charge carrier trapping, generation, and recombination [1].
  - Potential barrier modulation by minority carriers [1, 2].

- Hot electron phenomena [1].
  - Minority charge carrier generation by impact ionisation of valence sites (due to high potential drop, requires usually high bulk doping) [1].
  - Barrier-controlled avalanche breakdown [1].

- Ion and atom movement.
  - Grain-boundaries can act as rapid diffusion paths for atoms [22]. Therefore, impurities can be segregated at grain-boundaries [1, 2, 22].
  - Several metal-oxide materials (which are often large-band gap semiconductors), for example WO_3 [26] and SnO_2 [27], exhibit high oxygen diffusion coefficients.

2.4 Modelling granular material

Granular materials are usually very complex and their structures are far from ideal. A real granular film is sketched in Fig. 2.4a. The grains consisting of conductive material are surrounded by material which is poorly or non-conductive, such as air. As Fig. 2.4a shows size, shape, and orientation of the grains may vary. In addition the adjacent grains may be connected to each other with small or large contact area, or they may not be connected at all.

Generally a film consisting of grains can be modelled with a electric circuit consisting of equivalent circuit presentations of the grains and grain boundaries. However, mathematically this approach is challenging. In order to calculate the electric current passing through the granular film the electric properties of each grain and grain-boundary must be known. In practice experimental determination of the each

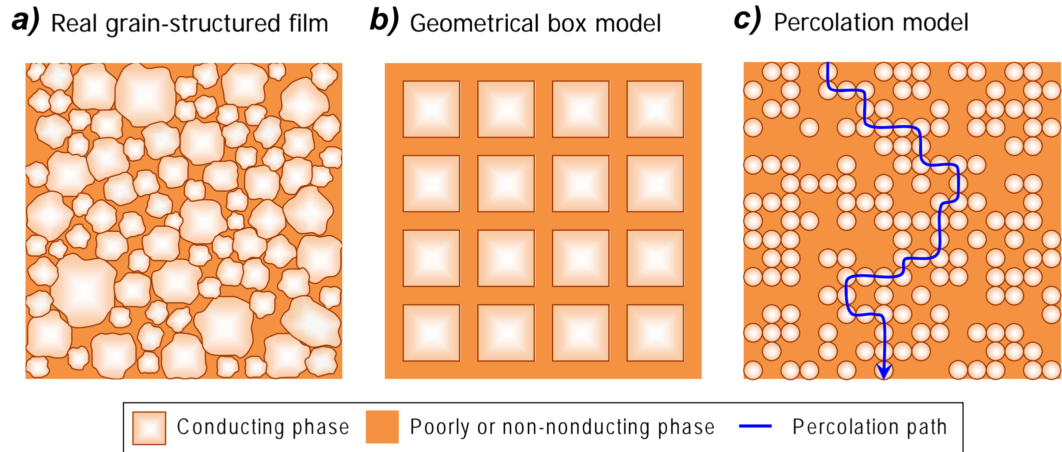

Figure 2.4: *a)* Schematic picture of a real granular film. *b)* Two-dimensional box model of granular film. *c)* Two-dimensional percolation model of a granular film at the percolation threshold. The percolation path is shown.

part of the film is, of course, impossible. Several approximative models exist for the calculation of the electric current passing through an inhomogeneous material: Geometrical models, and percolation and effective medium theories [2]. The largest difference between the models is that in the geometrical models the material is assumed to be highly ordered, and in the percolation and effective medium theories completely random [2]. In other words, they apply to fundamentally different problems. A large number of publications are available, where the percolation theory (see for example Refs. [2, 28–31]) and the effective medium theory (see for example Refs. [2, 29–34]) are presented.

In the geometrical models the material is presented by highly idealised structures. One of the simplest model is the cubic or box model, where the grains are presented by cubes or boxes arranged in a square lattice (see Fig. 2.4b). The cubic model is sometimes called the brick layer model (BLM). The advantage of the geometrical models is that although the calculation of the electrical properties is fairly simple, yet they can yield somewhat realistic results. In addition, a number of electric properties of the geometrical models are insensitive to the precise geometry considered [2]: For example, if the layer separating the grains (i.e. the poorly conductive region in Fig. 2.4b) is thin, a cubic model has exactly the same total resistance as the corresponding geometrical model consisting of spheres [2]. The cubic model has been compared with a realistic model of polycrystals: When the grain-boundary resistance dominates the total resistance of the realistic polycrystal is according

to numerical simulations roughly 17 % less in 3D [35] and roughly 10 % less in 2D [36] than the total resistance of the corresponding cubic model. In other words, although it could seem unlikely, the cubic model is a fair approximation of a real polycrystalline material.

In the percolation and effective medium theories the volume (or area) fraction of the conductive and (poorly or) non-conductive phases in the material is considered. Mixing ratio is the ratio of the volume (or area) of the phase in question and the total volume. Usually the percolation theories apply in the case of low mixing-ratio of the conductive phase. The effective medium theory in turn applies usually in the case of high mixing-ratio of the conductive phase. However, similar results can be obtained with the both theories in the same mixing ratio range.

In the percolation theory the material is divided into regions. Each region belongs either to the conductive or to the non-conductive phase (see Fig. 2.4c). The percolation theory has two general approaches: the site and the bond model. The sites are points in space. Each site corresponds to a region in the material. These sites are connected to the neighbouring sites by bonds. In the site model the sites are either conductive or non-conductive in random. In the bond model the bonds are random. An important property of material exhibiting percolation-type electrical conduction is the percolation threshold. The percolation threshold is the minimum volume (or area) fraction of the conductive phase, when the current begins to flow through the material. The material at the percolation threshold and the percolation path are illustrated in Fig. 2.4c. The percolation threshold of a bond-model of cubic lattice is 0.5 in 2D and 0.25 in 3D [29].

In the effective medium theory each grain of the material is treated as if it were surrounded by a homogeneous medium. The effective physical quantity of the whole material is determined self-consistently. Several approaches and effective medium approximations exist. In addition, many non-linear models have been proposed (see for example Refs. [37–40]).

In this work mostly the properties of single grain-boundaries are considered. The whole granular material is modelled by a one-dimensional model shown in Fig. 2.5a, where identical grain-boundary regions are connected in series. This allows the total current flowing through the whole material to be calculated in a simple manner. One might think that this assumption of the structure of the whole material is quite far from reality. However, the assumption made is that all the relevant grain

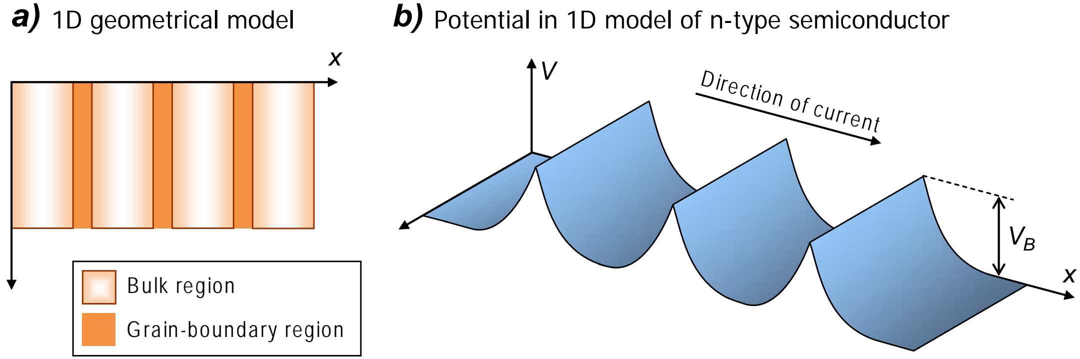

Figure 2.5: *a)* One-dimensional geometrical model of a granular material. *b)* Sketch of the electron potential V in the one-dimensional model of n-type semiconductor with acceptor-type electronic traps at the grain boundaries.

boundaries in the material can be presented by a set of identical grain boundaries. In other words, the properties of the identical grain boundaries of the model project the properties of all grain-boundaries in the path of the current. Numerous studies (see for example Refs. [1,2,9] and references therein) have shown that this approach is enough to explain the most of the experimental results. The electron potential V in the granular n-type semiconductor materials of Fig. 2.5a is sketched in Fig. 2.5b.

2.4.1 Theories for calculating charge transport in semiconductors

The two most common theories for calculating charge transport in semiconductors are the thermionic emission and the drift-diffusion theories. The former theory applies usually to high-mobility and the latter to low-mobility semiconductors [18]. In addition, a third theory, the so-called thermionic emission – diffusion theory, which is a mixture of the first two theories, have been synthesised [18]. In all of the theories it is assumed that the height of grain-boundary potential barrier is much larger than $k_B T$, and the charge carriers on both sides of the grain boundary can be described by their thermal equilibrium distributions in spite of the current flow [18].

In all these models the mean free path of charge carriers must be less than the diameter of grains. Otherwise the charge carriers which have enough energy could travel across multiple grain boundaries before a scattering event occurs [2]. Conversely the charge carriers without enough energy to surmount the grain boundary could be

trapped within the grains, because they do not obtain energy from the scattering interactions with phonons [2]. However, it must be noted that the grain-boundaries itself act as strong scatterers [2,25], hence it is very unlikely that a charge carrier can travel across multiple grain boundaries without scattering. In addition, scattering events are needed to establish thermal equilibrium of the charge carriers in the bulk of the grains.

The applicability of the theory is evaluated by the mean free path of the charge carriers: If the width of the grain-boundary potential barrier (i.e. grain-boundary region) is equal or less than the mean free path of the charge carriers [9], then the thermionic emission theory applies. In this case the charge carriers experience no collisions in the grain-boundary region, hence for calculation of the current flow is enough to count only the charge carries which have enough energy to surmount the grain-boundary potential barrier [18]. The drift-diffusion theory applies when the width of the grain-boundary potential barrier is much larger than the mean free path of the charge carriers [9]. In this case the charge carriers experience many collisions in the grain-boundary region, i.e. their motion is characterized by a diffusion process.

Chapter 3

Modelling of electrical properties of grain boundaries in n-type semiconductors

In this chapter the electrical properties of grain boundaries in n-type semiconductors are calculated analytically. The use of numerical simulation method is also presented, but in this chapter numerical simulations are employed only in the potential calculations. The calculations are performed in the model structure of the grain boundary region shown in Fig. 3.1. The grain boundary itself, whose thickness is neglected, is located at $x = 0$. The acceptor-type interface states with a single discrete energy level E_T are located at the grain-boundary. Often interface states with various shapes of the density of states are considered [1]. However, in this work only a single discrete interface state is studied. The total density of the interface states is N_B^{tot} (per unit area). The density (per unit area) of the interface states occupied by electrons is denoted by N_B.

The surrounding regions I–IV consist all of the bulk semiconductor material and their properties (including doping) are the same. The difference between the bulk (III and IV) and the grain-boundary regions (I and II) is that the negative electric charge at the grain boundary (density N_B per area) affects them by band-bending. Usually the regions I and II are depletion regions. In this work it is assumed that the depletion regions (i.e. regions I and II) do not extend across the whole grain. In other words, bulk regions (regions III and IV) always exist between two grain boundaries.

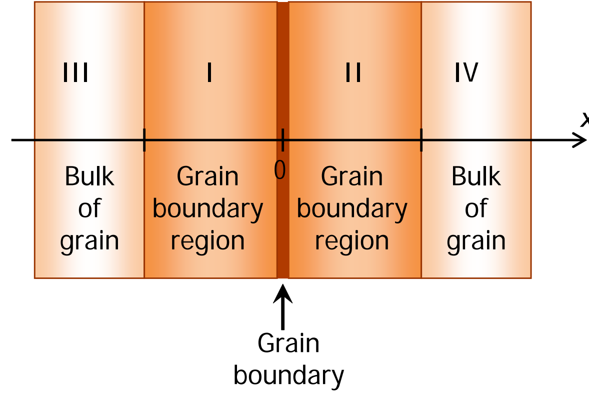

Figure 3.1: Definition of the grain-boundary (I and II) and bulk regions (III and IV) for the mathematical calculations. The infinitesimally thin grain boundary is at $x = 0$. The acceptor-type electronic interface states with a single discrete energy level E_T and total density N_B^{tot} (per area) are located at the grain-boundary. The density (per area) of grain-boundary negative charge (i.e. the density of the interface states occupied by electron) is N_B. The electron potential at the grain boundary is V_B. The doping is the same in the regions I–IV.

Although the model shown in Fig. 3.1 consists of only a single grain boundary, the analytical model presented in this chapter is extended later in chapters 4 and 5 to the case of the whole granular material by considering identical grain-boundary regions connected in series (see discussion in section 2.4). The most of the numerical simulation results are presented in chapters 4 and 5.

3.1 Numerical calculation of electric properties

In addition to the analytical model presented in this chapter the SILVACO ATLAS device simulation software [10] is used for calculating the electric properties of granular semiconductors. The SILVACO ATLAS device simulation software can be used for calculating the electrical behaviour of semiconductor structures and devices in two and three dimensions. First the structure to be modelled is presented by a grid, where each node (i.e. grid point) represents a point in the structure. Due to the fact that the number of nodes is finite the grid is always an approximation of the structure. After the grid is formed the electric behaviour is calculated using discretized differential equations.

In this work the one-dimensional structure shown in Fig. 3.1 is presented by a two-

Table 3.1: Selected values for material parameters in the numerical calculations.

Band gap E_g	3.0 eV at all temperatures
Dielectric constant ε_r	9
Effective mass of electron m_n^*/m_0	0.3
Effective mass of hole m_p^*/m_0	0.3
Effective density of states of conduction band N_c	$4.12342 \cdot 10^{18}$ cm^{-3} at 300 K
Effective density of states of valence band N_v	$4.12342 \cdot 10^{18}$ cm^{-3} at 300 K
Shockley-Read-Hall recombination lifetime for electrons	10^{10} s
Shockley-Read-Hall recombination lifetime for holes	10^{10} s
Trap state degeneracy factor	1
All the other material parameters have the default values for Silicon.	
I–V calculation	
Lifetime for electrons in the trap level†	1 s
Lifetime for holes in the trap level†	10^{10} s
Small signal analysis	
Capture cross-section of the trap for holes c_p	10^{-35} cm^2

†Not included in the analytical model. m_0 = mass of free electron.

Table 3.2: Physical properties of common large band gap semiconductors.

Material	Band gap at 300 K E_g (eV)	Static dielectric constant ε_r	Effective mass of electron m_n^*/m_0	Effective mass of hole m_p^*/m_0	Refs.
SnO_2	3.6 D	$\|\|c$: 9.6 $\perp c$: 13.5	$\|\|c$: 0.2 $\perp c$: 0.3		[41, 42]
ZnO	3.4 D	$\|\|c$: 8.75 $\perp c$: 7.8			[41, 42]
ZnO	3.35 D	8.8	0.27		[43]
TiO_2	Rutile 3.0 I Anatase 3.2 I				[44]
ZnS	3.68 D	8.5	0.40	0.58	[43]
CdS	2.42 D	11.6	0.21	0.80	[43]
GaN	3.36 D	12.2	0.19	0.60	[43]

D = direct, I = indirect. $||c$ = parallel to c-axis, $\perp c$ = perpendicular to c-axis.

dimensional structure, which is only two nodes wide. The spacing between the nodes varies gradually: At the grain boundary it is 5 pm (0.005 nm) and on the edges of the structure 10 nm, respectively. In the software the maximum number of nodes is 20 000 [10]. The electronic interface states are created at the grain boundary with the INTRAP statement of ATLAS. The Blaze module [10] of ATLAS is used in the calculation. The selected values for material parameters in the numerical calculations are listed in Table 3.1. These values represent the typical values of common large band gap semiconductors, which are listed in Table 3.2.

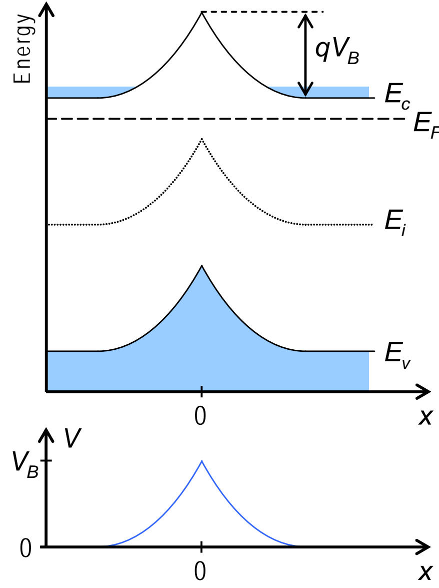

Figure 3.2: Schematic picture of the energy bands and the potential V in the grain-boundary region. E_c is the bottom of the conduction band, E_v the top of the valence band, E_F the Fermi level, E_i the intrinsic energy, q the electron charge, and V_B the grain-boundary potential barrier.

3.2 Potential in grain-boundary region

3.2.1 General solution

The following solution of Poisson's equation in the grain-boundary region applies to non-degenerate semiconductors in the case where no external electric field is applied in the material. The degenerate case is considered for example in Refs. [15, 16].

The terms used in the derivation of the solution of potential are depicted in Fig. 3.2. Using the dimensionless potentials

$$u(x) = \frac{q}{k_B T}\left[E_F - E_i(x)\right] \tag{3.1}$$

and

$$v(x) = \frac{qV(x)}{k_B T} = -\frac{q\phi(x)}{k_B T} \tag{3.2}$$

Eqs. 2.7 and 2.8 can be written as [15]

$$n = n_b e^{-v} = n_i e^{u} = n_i e^{-v+u_b} \tag{3.3}$$
$$p = p_b e^{v} = n_i e^{-u} = n_i e^{v-u_b}, \tag{3.4}$$

where $n_b = n_i e^{u_b}$ and $p_b = n_i e^{-u_b}$ are the electron and hole densities and u_b the value of u in the bulk (i.e. far away from the grain-boundary region), respectively. Plugging Eqs. 3.3 and 3.4, and $n_b = N_d^+$ and $p_b = N_a^-$ in Eq. 2.25 gives [15]

$$\frac{d^2v}{dx^2} = \frac{q^2}{k_B T \varepsilon}\left(n_b - p_b - n_b e^{-v} + p_b e^{v}\right) = \frac{1}{L_D^2}\left[\frac{\sinh(v-u_b)}{\cosh(u_b)} + \tanh(u_b)\right], \tag{3.5}$$

where Eq. 2.9 was used. Using $\frac{d^2v}{dx^2} = \frac{1}{2}\frac{d}{dv}\left(\frac{dv}{dx}\right)^2$ in Eq. 3.5, multiplying both sides of the equation by $2dv$, and integrating with the condition $\frac{dv}{dx} = 0$ at $v = 0$ leads to [15]

$$\frac{dv}{dx} = \mp\frac{\sqrt{2}}{L_D}\sqrt{\frac{\cosh(v-u_b)}{\cosh(u_b)} + v\tanh(u_b) - 1}, \tag{3.6}$$

where the minus sign corresponds to $v > 0$ and the plus sign to $v < 0$. The final integration of Eq. 3.6,

$$\frac{x}{L_D} = \int_{v_B}^{v} \frac{dv}{\mp\sqrt{2}\sqrt{\frac{\cosh(v-u_b)}{\cosh(u_b)} + v\tanh(u_b) - 1}}, \tag{3.7}$$

has to be calculated numerically. Numerical solutions and approximative solutions are represented below in section 3.2.4.

Using Gauss's law [24] in the vicinity of the grain boundary gives a relation for the maximum of the electric field in the grain-boundary region when no external electric field is applied [37]:

$$E_0^{max} = \left|\frac{qN_B}{2\varepsilon}\right|. \tag{3.8}$$

For the electric field, $E = -\frac{d\phi}{dx} = \frac{k_B T}{q}\frac{dv}{dx}$, Eq. 3.6 gives

$$\begin{aligned} |E| &= \frac{k_B T}{q}\frac{\sqrt{2}}{L_D}\sqrt{\frac{\cosh(v-u_b)}{\cosh(u_b)} + v\tanh(u_b) - 1} \\ &= \sqrt{2k_B T}\sqrt{\frac{n_b + p_b}{\varepsilon}}\sqrt{\frac{\cosh(v-u_b)}{\cosh(u_b)} + v\tanh(u_b) - 1}. \end{aligned} \tag{3.9}$$

The maximum of the electric field is at the grain-boundary: $E_0^{max} = |E(v = v_B)|$. The electron potential at the grain boundary $V_B = -\phi(x = 0) = \frac{k_B T}{q} v_B$ can be solved from Eqs. 3.8 and 3.9. Assuming that V_B is of the same order or larger than the thermal voltage $\frac{k_B T}{q}$ and $|u_b|$ is large gives an approximative formula for the grain-boundary potential when no external eletric field is applied [37]:

$$|V_B| = \frac{q N_B^2}{8\varepsilon (n_b + p_b)} + \frac{k_B T}{q}. \tag{3.10}$$

The assumption made that $|u_b|$ is large means that the Fermi level E_F is far away from the intrinsic energy level E_i. In other words, the semiconductor is either n-($n_b \gg p_b$) or p-type ($p_b \gg n_b$).

The normalized potential v, the electron density n/n_i, and the hole density p/n_i are plotted as a function of x/L_D with various values of u_b in n- and p-type semiconductors in Figs. 3.3 and 3.4, respectively. The grain-boundary potential v_B in Figs. 3.3 and 3.4 is set either to $v_B = 20$ or $v_B = -20$. Positive grain-boundary potential v_B in an n-type semiconductor gives rise to depletion or inversion (see Fig. 3.3) and in a p-type semiconductor to accumulation (see Fig. 3.4), respectively. With negative grain-boundary potential v_B the behavior of the semiconductors is the opposite.

Figs. 3.3 and 3.4 show that if the value of u_b is low enough, the depletion can turn in to inversion. Inversion occurs also with higher values of u_b when the grain-boundary potential is large enough. The inversion occurs when the density of minority charge carriers exceeds the density of the majority charge carriers at the grain boundary (see Figs. 3.3 and 3.4). Figs. 3.3 and 3.4 show that the width of the inversion region is very small. Because of the small dimension of the inversion region, quantum mechanical approach [15] should be used instead of the classical theory employed here.

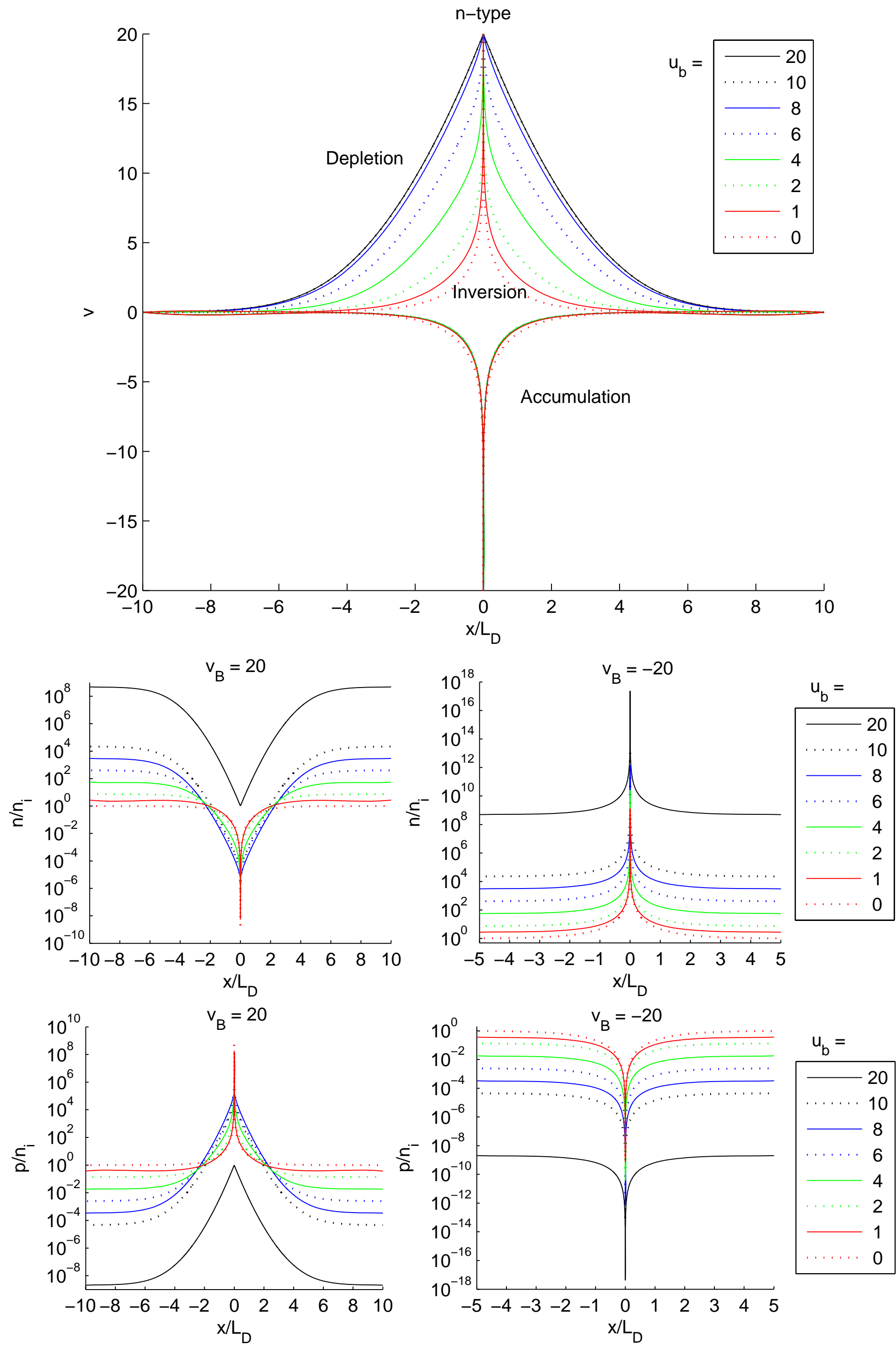

Figure 3.3: Normalized potential v, electron density n/n_i, and hole density p/n_i plotted as a function of x/L_D with various values of u_b in n-type semiconductor. Calculated using Eqs. 3.3, 3.4, and 3.7 and the MATLAB function `quadl` (numerical integration).

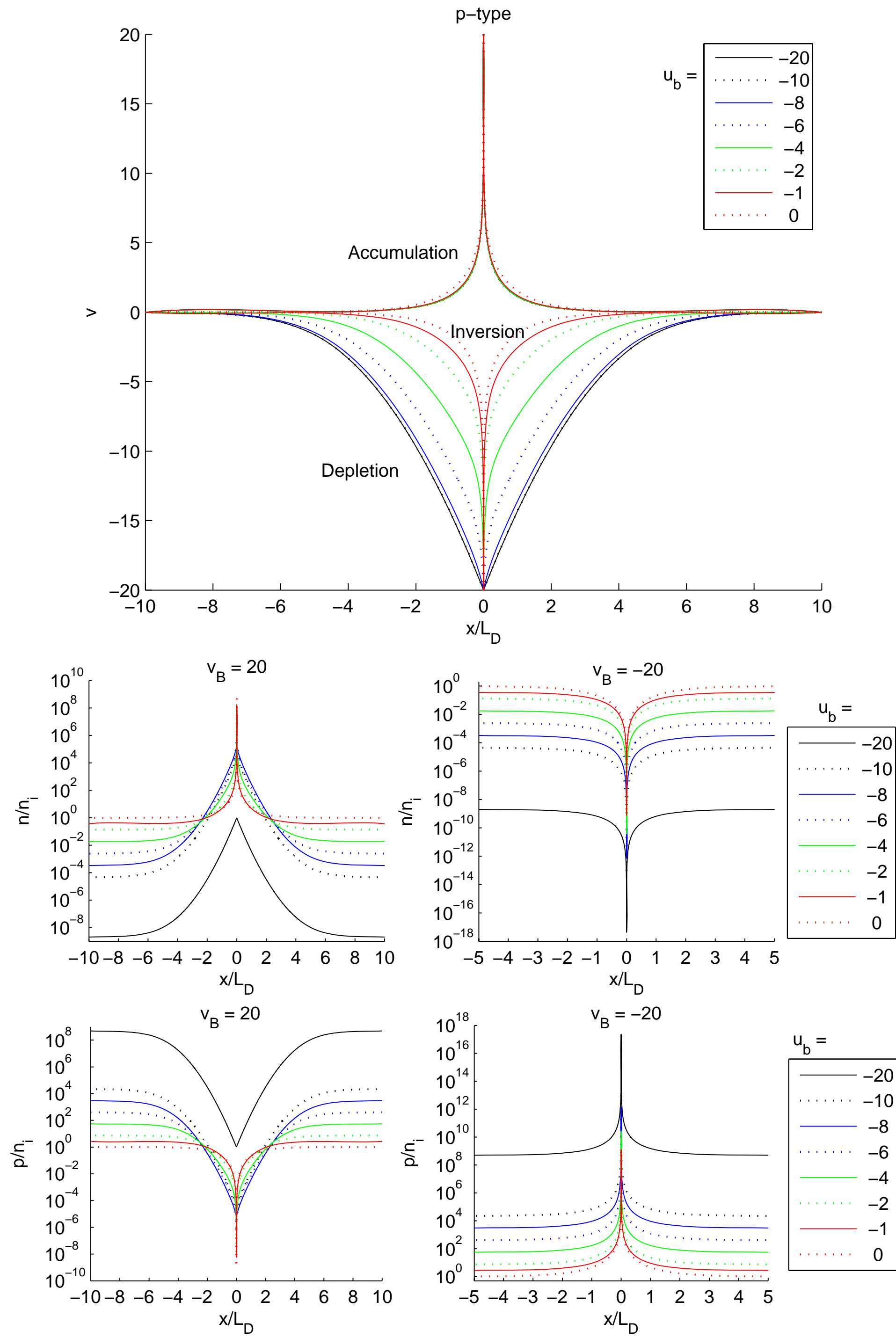

Figure 3.4: Normalized potential v, electron density n/n_i, and hole density p/n_i plotted as a function of x/L_D with various values of u_b in p-type semiconductor. Calculated using Eqs. 3.3, 3.4, and 3.7 and the MATLAB function `quadl` (numerical integration).

3.2.2 Depletion region approximation

Poisson's equation (Eq. 2.25) can be solved fairly simply by using the Schottky or depletion region approximation. In this approximation it is assumed that the electrons are totally depleted from the depletion regions, and the ionized donor atoms are left as static charge in this region. In Fig. 3.1 the depletion regions are regions I and II.

The widths of the first (region I) and second (region II) depletion regions are x_{d_1} and x_{d_2}, respectively. According to the charge neutrality condition (Eq. 2.22) the total width of the depletion regions is constant:

$$L_d = x_{d_1} + x_{d_2} = \frac{N_B}{N_d}. \tag{3.11}$$

Eq. 3.11 applies also in the case where eletric field or voltage is applied across the grain-boundary region.

The density of the free charge can be written as

$$\rho(x) = \begin{cases} qN_d & \text{when } -x_{d_1} \leq x < 0 \quad \textit{Region I} \\ -qN_B & \text{when } x = 0 \quad \textit{Grain boundary} \\ qN_d & \text{when } 0 < x \leq x_{d_2} \quad \textit{Region II} \\ 0 & \text{otherwise} \quad \textit{Regions III and IV,} \end{cases} \tag{3.12}$$

where N_d is the donor density, and N_B is the grain-boundary charge density, respectively.

When no electric field is applied the depletion widths in the regions I and II are equal,

$$x_d = x_{d_1} = x_{d_2}, \tag{3.13}$$

and the boundary conditions for Poisson's equation become

$$\begin{aligned} \left.\frac{d\phi(x)}{dx}\right|_{x=\pm x_d} &= 0 \quad \textit{No electric field inside the grains} \\ \phi(x = \pm x_d) &= 0. \end{aligned} \tag{3.14}$$

The solution of Poisson's equation and Eq. 3.12 is illustrated in Fig. 3.5. The maximum of the electric field, E_0^{max}, is given by Eq. 3.8. The potential is given by

$$V(x) = V_{B_0}\left(\frac{x}{x_d} \pm 1\right)^2, \tag{3.15}$$

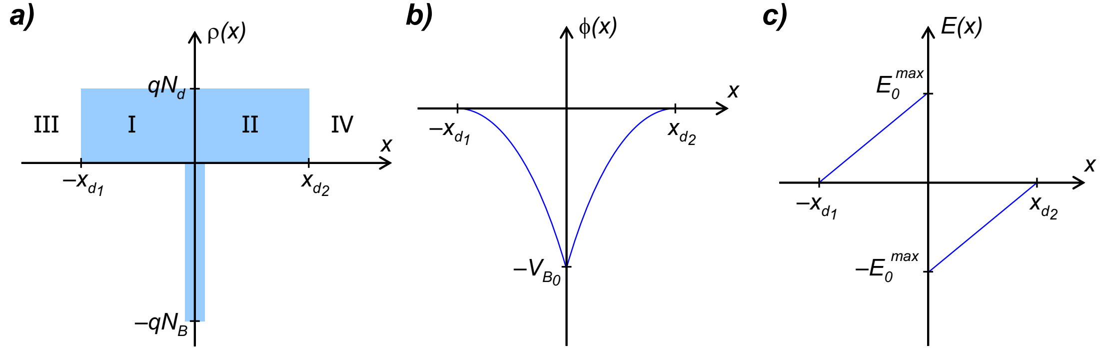

Figure 3.5: *a)* The density of free charge, *b)* the electric potential, and *c)* the electric field in the grain-boundary region in the case where no voltage is applied across the grain boundary. The widths of the depletion regions x_{d_1} and x_{d_2} are equal.

where the plus sign corresponds to region I ($x < 0$) and minus to region II ($x > 0$), and

$$V_{B_0} = \frac{qN_B^2}{8\varepsilon N_d} \tag{3.16}$$

is the potential at the grain boundary estimated by the depletion region approximation. Comparison of Eqs. 3.10 and 3.16 shows that the thermal voltage $\frac{k_BT}{q}$ is missing in Eq. 3.16. In other words, the correct formula for the potential at the grain boundary is

$$V_{B_0} = \frac{qN_B^2}{8\varepsilon N_d} + \frac{k_BT}{q} \tag{3.17}$$

instead of Eq. 3.16.

With the help of Eqs. 3.16 and 3.11 the depletion width in the depletion region approximation can written as

$$x_d = \frac{1}{2}L_d = \sqrt{\frac{2\varepsilon\,|V_{B_0}|}{qN_d}} = L_D\sqrt{2\,|v_{B_0}|}, \tag{3.18}$$

where v_{B_0} is the normalized potential (see Eq. 3.2) at the grain boundary given by the depletion region approximation (Eq. 3.16). However, because Eq. 3.16 is not exact, Eq. 3.17 must be used instead. Therefore, the formula of the depletion width changes to

$$x_d = \frac{1}{2}L_d = \sqrt{\frac{2\varepsilon}{qN_d}\left(|V_{B_0}| - \frac{k_BT}{q}\right)} = L_D\sqrt{2\left(|v_{B_0}| - 1\right)}, \tag{3.19}$$

where Eq. 2.9 was used. However, because the edge of the depletion region is not abrupt: the distribution tail of the majority carriers extend into the depletion region thereby reducing its width [18]. This effect can be taken into account by reducing the height of the potential barrier in the formula (V_{B_0}) by $\frac{k_B T}{q}$, hence the Eq. 3.19 must be changed to [18]

$$x_d = \sqrt{\frac{2\varepsilon}{qN_d}\left(|V_{B_0}| - \frac{2k_B T}{q}\right)} = L_D\sqrt{2\left(|v_{B_0}| - 2\right)}. \tag{3.20}$$

Using Eqs. 2.9, 3.17, and 3.20 the total width of the depletion region can be written as

$$L_d^{corr} = 2x_d = \sqrt{L_d^2 - 8L_D^2} = L_d\sqrt{1 - 8\left(\frac{L_D}{L_d}\right)^2}, \tag{3.21}$$

where $L_d = \frac{N_B}{N_d}$ is the total width of the depletion region estimated by the charge neutrality condition (Eq. 3.11).

With the aid of Eq. 3.8, Eq. 3.17 can be written as

$$V_{B_0} - \frac{k_B T}{q} = \frac{1}{4}E_0^{max} L_d, \tag{3.22}$$

which in the depletion region approximation (i.e. when Eq. 3.16 is used instead of Eq. 3.17) reduces to

$$V_{B_0} = \frac{1}{4}E_0^{max} L_d. \tag{3.23}$$

For later use Eq. 3.15 can be normalized as

$$v(x) = v_B\left(\frac{L_D}{x_d}\cdot\frac{x}{L_D} \pm 1\right)^2, \tag{3.24}$$

where Eq. 3.2 was used.

3.2.3 Other approximative solutions

In addition to the depletion region approximation several approximative solutions of Poisson's equation are available in the book by Many et al. [16].

In the strong accumulation layers ($|v| \geq 3$) the potential can be calculated using [16]

$$\frac{x}{L_D} \approx \sqrt{2}\left(e^{-\frac{1}{2}|v|} - e^{-\frac{1}{2}|v_B|}\right). \tag{3.25}$$

In the depletion layers($|v| \geq 3$, and $0 > v > -2u_b$ for n-type and $0 < v < -2u_b$ for p-type) the potential is approximately given by [16]

$$|v| \approx \frac{1}{2}\left(\sqrt{2|v_B|-2} - \frac{x}{L_D}\right)^2 + 1 = (|v_B|-1)\left(\frac{1}{\sqrt{2}\sqrt{|v_B|-1}} \cdot \frac{x}{L_D} - 1\right)^2 + 1. \tag{3.26}$$

In strong inversion layers (large $|v|$) the potential profile can be calculated by using [16]

$$\frac{x}{L_D} \approx \sqrt{2}\left[e^{-\frac{1}{2}(2|u_b|-|v|)} - e^{-\frac{1}{2}(2|u_b|-|v_B|)}\right]. \tag{3.27}$$

3.2.4 Comparison of general and approximative solutions

Dependence of grain-boundary potential on grain boundary charge

Normalizing the grain-boundary potential V_B given by Eq. 3.10 by the thermal voltage k_BT/q leads, with help of Eq. 2.9, to

$$|v_B| = \frac{q\,|V_B|}{k_BT} = \frac{1}{8}\left[\frac{N_B}{L_D\,(n_b + p_b)}\right]^2 + 1 = v_{B_0}, \tag{3.28}$$

where v_{B_0} is the normalized value of the grain-boundary potential (see Eq. 3.17).

The normalized grain-boundary potential v_B as a function of the normalized grain boundary charge density N_B is plotted in Fig. 3.6. Fig. 3.6 shows that Eq. 3.28 is a very good approximation when $|v_B| > 2$, i.e. V_B is larger than twice the thermal voltage k_BT/q.

Fig. 3.6 also shows that the increase of v_B with increasing normalized N_B is first quadratic and after a certain point the rate of increase drops. This point shows up earlier with lower values of u_b. This is related to the fact that the Fermi level lies low when u_b is low (see Eq. 3.1). Hence, it seems that depending on the position of the Fermi level in the semiconductor only a specific band bending (given by v_B) can exist in the material. Although the energy level of the interface state was not included in the calculation of the potential, the behaviour is often explained by the pinning of the Fermi level E_F on the interface level E_T, i.e. v_B increases slowly after E_F drops below E_T [2, 15].

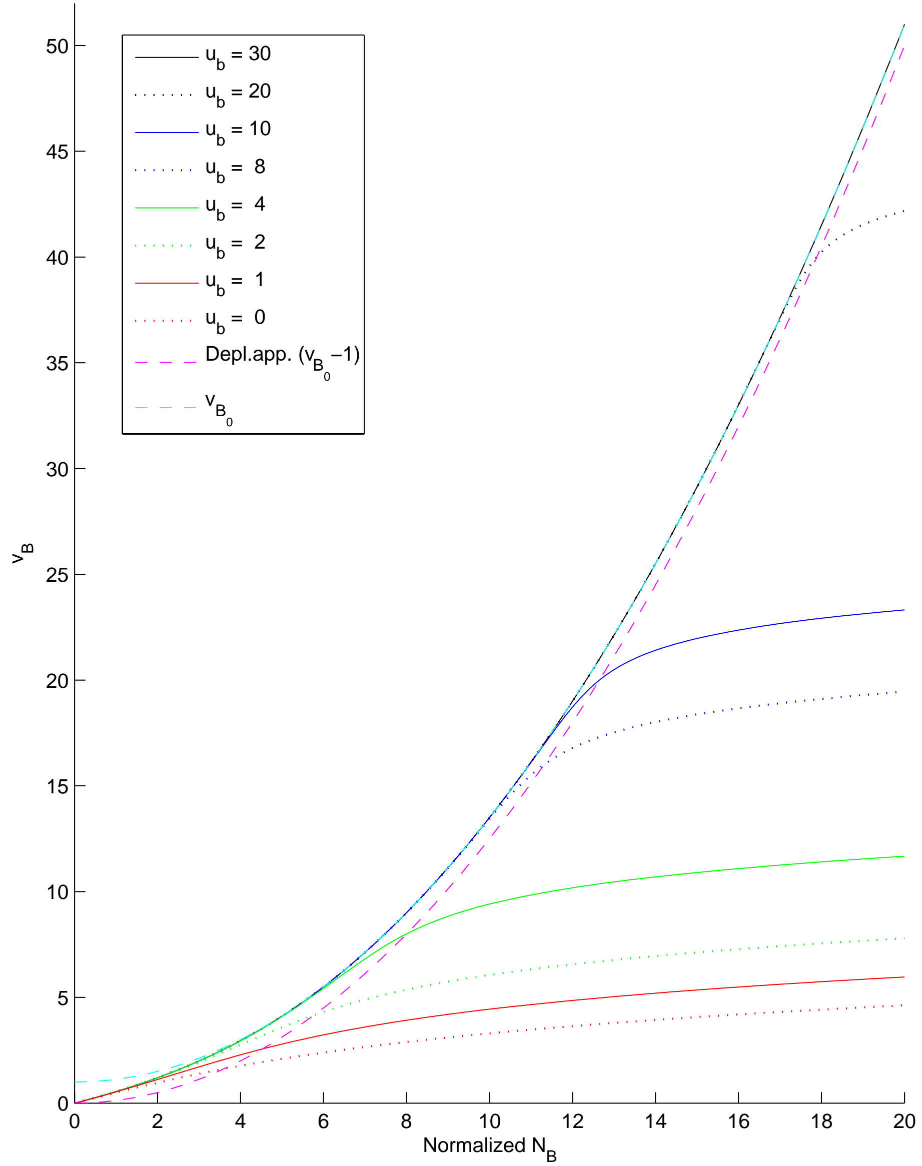

Figure 3.6: Normalized grain-boundary potential $v_B = k_B T V_B/q$ plotted as a function of the normalized grain boundary charge density N_B with various values of u_b in n-type semiconductor. N_B normalized with $L_D(n_b + p_b)$. v_B is numerically solved from Eqs. 3.8 and 3.9 by using the MATLAB function `fsolve`. The value estimated by the depletion region approximation (Eq. 3.16) and the approximative solution v_{B_0} (Eq. 3.28) are shown.

Solution of potential

The normalized potential profiles v and the electron densities n/n_b in the grain-boundary region with various values of v_B in a n-type semiconductor ($u_b = 20$) are shown in Fig. 3.7. Fig. 3.7 shows that the formulas of the uncorrected (Eqs. 3.18 and 3.24) and corrected (Eqs. 3.20 and 3.24) depletion region approximation are able to describe the potential profile near the top of the potential barrier ($x/L_D = 0$) in a good accuracy. The depletion region approximation formulas predict that the potential drops faster with x/L_D than it should be. The discrepancy increases when the height of the potential barrier v_B is lowered. The formula of Many et al. (Eq. 3.26) gives the best approximation of the potential profile. However, the potential stays at $v = 1$ and it does not drop to zero.

In addition, Fig. 3.7 shows that whereas the corrected depletion region approximation formula (Eq. 3.20) gives slightly worse potential profiles, the formulas are able to predict the total width of the depletion regions correctly (the depletion region is roughly the region when $n/n_b < 0.5$). The uncorrected formula (Eq. 3.18) overestimates the total width of the depletion regions. Therefore, Eq. 3.21 should be used when calculating the total width of the depletion regions.

3.2.5 Depletion region approximation with external electric field applied

The solution of Poisson's equation by using the depletion region approximation when a bias voltage U_{GB} is applied across the grain boundary is given in Ref. [11]. The solution in this case is illustrated in Fig. 3.8. However, the effect of the electric field inside the grains is not taken into account in the solution of Ref. [11].

In this section the Poisson's equation is solved using the depletion region approximation when, in addition to the bias voltage U_{GB}, a static external electric field is applied in the whole material. The solution in this case is depicted in Fig. 3.9.

The boundary conditions for Poisson's equation are

$$\begin{aligned} &\left.\frac{d\phi(x)}{dx}\right|_{x=x_{d_1}} = \left.\frac{d\phi(x)}{dx}\right|_{x=x_{d_2}} = -E_{bulk} && \textit{The electric field inside the grains} \\ &\phi(x = -x_{d_1}) = 0 && \\ &\phi(x = x_{d_2}) = -U_{GB} && \textit{Voltage across the boundary.} \end{aligned} \tag{3.29}$$

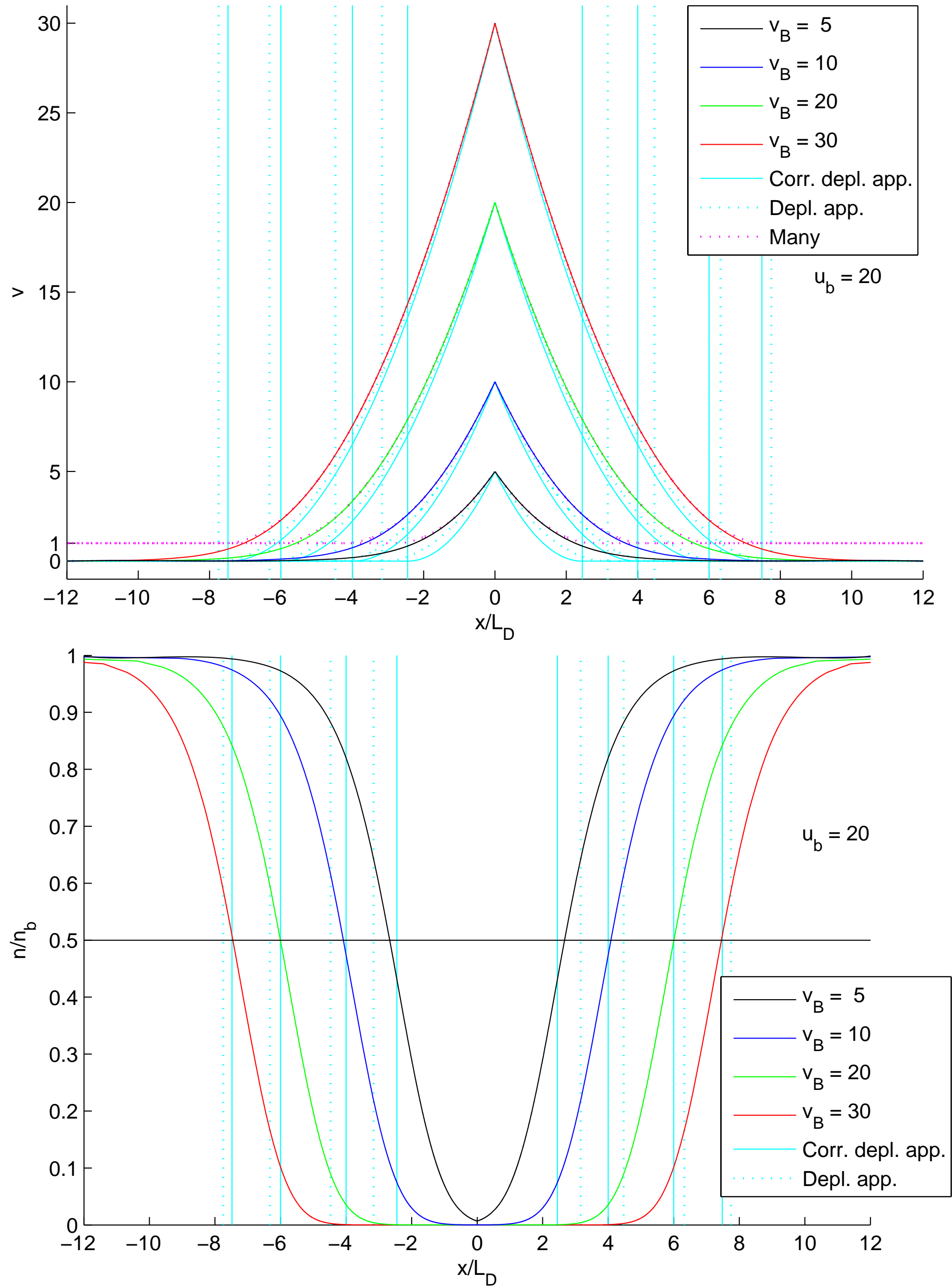

Figure 3.7: Normalized potential v and electron density n/n_b plotted as a function of x/L_D with various values of v_B in n-type semiconductor ($u_b = 20$). The numerical solution (calculated using Eqs. 3.3, 3.4, and 3.7 and the MATLAB function `quadl`), the corrected depletion region approximation (Eqs. 3.20 and 3.24), the depletion region approximation (Eqs. 3.18 and 3.24), and the formula of Many et al. (Eq. 3.26) are compared. The edges of the depletion regions are indicated by vertical lines.

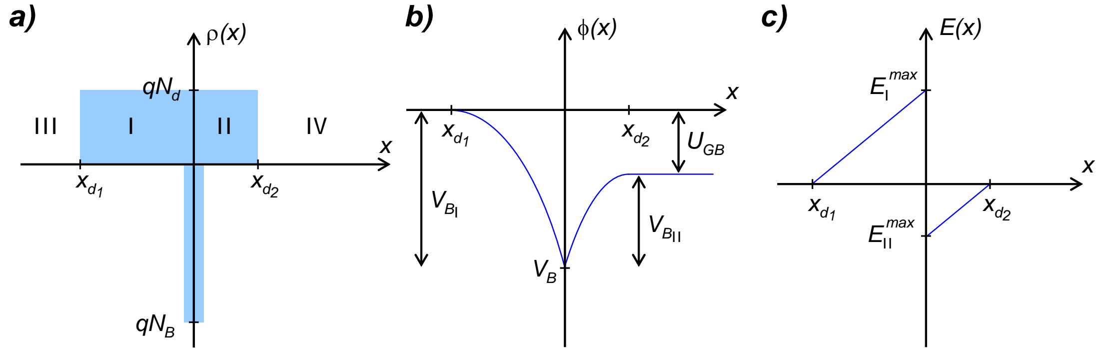

Figure 3.8: *a)* The density of free charge, *b)* the electric potential, and *c)* the electric field in the grain-boundary region in the case where voltage U_{GB} is applied across the grain boundary.

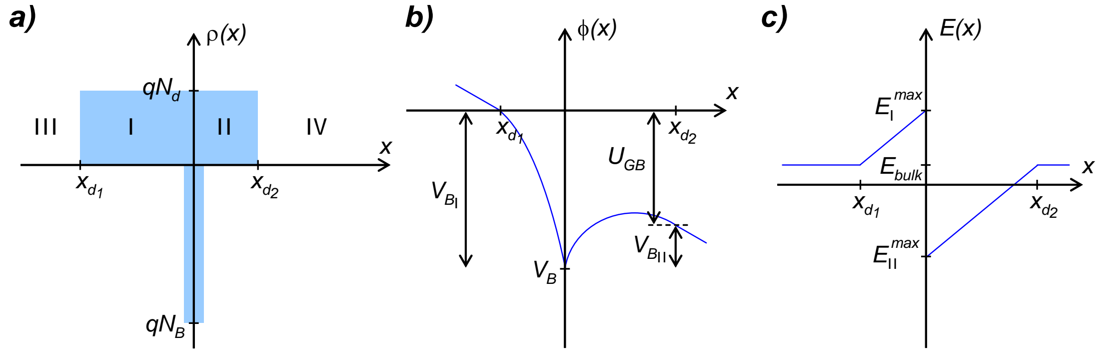

Figure 3.9: *a)* The density of free charge, *b)* the electric potential, and *c)* the electric field in the grain-boundary region in the case where voltage U_{GB} is applied across the grain boundary and electric field E_{bulk} in the whole material.

With these boundary conditions Eqs. 2.23 and 3.12 give

$$\phi(x) = \begin{cases} 0 & \text{when } x = -x_{d_1} \\ -\frac{qN_d}{2\varepsilon}\left(x + x_{d_1}\right)^2 - E_{bulk}\left(x + x_{d_1}\right) & \text{when } -x_{d_1} < x \leq 0 \quad \textit{R. I} \\ -\frac{qN_d}{2\varepsilon}\left(x - x_{d_2}\right)^2 - E_{bulk}\left(x - x_{d_2}\right) - U_{GB} & \text{when } 0 \leq x < x_{d_2} \quad \textit{R. II} \\ -U_{GB} & \text{when } x = x_{d_2}. \end{cases} \tag{3.30}$$

For the electric field Eq. 3.30 gives

$$E(x) = \begin{cases} \frac{qN_d}{\varepsilon}\left(x + x_{d_1}\right) + E_{bulk} & \text{when } -x_d \leq x < 0 \quad \textit{Region I} \\ \frac{qN_d}{\varepsilon}\left(x - x_{d_2}\right) + E_{bulk} & \text{when } 0 < x \leq x_d \quad \textit{Region II} \\ E_{bulk} & \text{otherwise} \quad \textit{Regions III and IV}. \end{cases} \tag{3.31}$$

Eq. 3.30 gives relations for the grain-boundary potentials seen from the regions I

and II (see Fig. 3.9):

$$\begin{aligned} V_{B_I} &= \frac{qN_d}{2\varepsilon} x_{d_1}^2 + E_{bulk} x_{d_1} \\ V_{B_{II}} &= \frac{qN_d}{2\varepsilon} x_{d_2}^2 - E_{bulk} x_{d_2}. \end{aligned} \tag{3.32}$$

These are interrelated as (cf. Eq. 3.30)

$$U_{GB} = V_{B_I} - V_{B_{II}} = \frac{qN_B}{2\varepsilon}\left(x_{d_1} - x_{d_2}\right) + \frac{N_B}{N_d} E_{bulk}, \tag{3.33}$$

where Eq. 3.11 was used. The depletion region widths x_{d_1} and x_{d_2} can be solved from Eqs. 3.11 and 3.33 giving

$$\begin{aligned} x_{d_1} &= \frac{\varepsilon U_{GB}}{qN_B} - \frac{\varepsilon E_{bulk}}{qN_d} + \frac{N_B}{2N_d} = \left(\frac{U_{GB}}{4V_{B_0}} - \frac{E_{bulk}}{E_0^{max}} + 1\right)\frac{L_d}{2} \\ x_{d_2} &= -\frac{\varepsilon U_{GB}}{qN_B} + \frac{\varepsilon E_{bulk}}{qN_d} + \frac{N_B}{2N_d} = \left(-\frac{U_{GB}}{4V_{B_0}} + \frac{E_{bulk}}{E_0^{max}} + 1\right)\frac{L_d}{2}, \end{aligned} \tag{3.34}$$

where Eqs. 3.8, 3.11, and 3.16 were used. The depletion widths must be positive, thus an important condition is obtained for the applied voltage and electric field:

$$\frac{U_{GB}}{4V_{B_0}} + 1 > \frac{E_{bulk}}{E_0^{max}} > \frac{U_{GB}}{4V_{B_0}} - 1. \tag{3.35}$$

If $E_{bulk} = 0$, then Eq. 3.35 reduces to [11]

$$|U_{GB}| < 4V_{B_0}. \tag{3.36}$$

Substituting Eq. 3.34 into Eq. 3.32 and 3.31 gives for the potentials

$$\begin{aligned} V_{B_I} &= V_{B_0}\left[\left(1 + \frac{U_{GB}}{4V_{B_0}}\right)^2 - \left(\frac{E_{bulk}}{E_0^{max}}\right)^2\right] \\ V_{B_{II}} &= V_{B_0}\left[\left(1 - \frac{U_{GB}}{4V_{B_0}}\right)^2 - \left(\frac{E_{bulk}}{E_0^{max}}\right)^2\right] \end{aligned} \tag{3.37}$$

and the electric field maxima

$$\begin{aligned} E_I^{max} &= E_0^{max}\left(1 + \frac{U_{GB}}{4V_{B_0}}\right) = \frac{4V_{B_0} + U_{GB}}{L_d} \\ E_{II}^{max} &= E_0^{max}\left(1 - \frac{U_{GB}}{4V_{B_0}}\right) = \frac{4V_{B_0} - U_{GB}}{L_d}, \end{aligned} \tag{3.38}$$

where Eqs. 3.8, 3.11, and 3.16 were used. The formulas for the maxima of the electric fields (Eq. 3.38) are exactly the same as in the case without E_{bulk} [11]. Eqs. 3.8, 3.11, 3.16, 3.30, 3.31, 3.34, and 3.38 allow the electric field and the potential $V(x)$ to be written as

$$E(x) = \begin{cases} (E_I^{max} - E_{bulk})\left(1 + \frac{x}{x_{d_1}}\right) + E_{bulk} & \text{when } -x_d \le x < 0 \quad \textit{Region I} \\ (-E_{II}^{max} - E_{bulk})\left(1 - \frac{x}{x_{d_2}}\right) + E_{bulk} & \text{when } 0 < x \le x_d \quad \textit{Region II} \end{cases} \tag{3.39}$$

and

- $V(x) = 0$, when $x = -x_{d_1}$.
- Region I ($-x_{d_1} < x \le 0$):

$$\begin{aligned} V(x) =& V_{B_0}\left(1 + \frac{U_{GB}}{4V_{B_0}} - \frac{E_{bulk}}{E_0^{max}}\right)^2 \left(\frac{x}{x_{d_1}} + 1\right)^2 \\ &+ 2V_{B_0}\left(\frac{E_{bulk}}{E_0^{max}}\right)\left(\frac{U_{GB}}{4V_{B_0}} + 1 - \frac{E_{bulk}}{E_0^{max}}\right)\left(\frac{x}{x_{d_1}} + 1\right). \end{aligned} \tag{3.40}$$

- Region II ($0 \le x < x_{d_2}$):

$$\begin{aligned} V(x) =& V_{B_0}\left(1 - \frac{U_{GB}}{4V_{B_0}} + \frac{E_{bulk}}{E_0^{max}}\right)^2 \left(\frac{x}{x_{d_2}} - 1\right)^2 \\ &+ 2V_{B_0}\left(\frac{E_{bulk}}{E_0^{max}}\right)\left(-\frac{U_{GB}}{4V_{B_0}} + 1 + \frac{E_{bulk}}{E_0^{max}}\right)\left(\frac{x}{x_{d_2}} - 1\right) + U_{GB}. \end{aligned} \tag{3.41}$$

- $V(x) = U_{GB}$, when $x = x_{d_2}$.

If $E_{bulk} = 0$, then Eqs. 3.37, 3.40, and 3.41 reduce to [1, 11, 45]

$$\begin{aligned} V_{B_I} &= V_{B_0}\left(1 + \frac{U_{GB}}{4V_{B_0}}\right)^2 \\ V_{B_{II}} &= V_{B_0}\left(1 - \frac{U_{GB}}{4V_{B_0}}\right)^2 \end{aligned} \tag{3.42}$$

and

$$V(x) = \begin{cases} 0 & \text{when } x \le -x_{d_1} \quad \textit{III} \\ V_{B_0}\left(1 + \frac{U_{GB}}{4V_{B_0}}\right)^2\left(\frac{x}{x_{d_1}} + 1\right)^2 & \text{when } -x_{d_1} < x \le 0 \quad \textit{I} \\ V_{B_0}\left(1 - \frac{U_{GB}}{4V_{B_0}}\right)^2\left(\frac{x}{x_{d_2}} - 1\right)^2 + U_{GB} & \text{when } 0 \le x < x_{d_2} \quad \textit{II} \\ U_{GB} & \text{when } x \ge x_{d_2} \quad \textit{IV.} \end{cases} \tag{3.43}$$

Later the solution given by the formulas of Eqs. 3.40 and 3.41 are referred as the quadratic potential profile with the bulk electric field E_{bulk} taken into account, and the formula of Eq. 3.43 as the quadratic potential profile without E_{bulk}, respectively.

Linear approximation of potential $V(x)$

The further calculation of the electric properties can be simplified remarkably by approximating the quadratic potential profile with a linear one. The electric field maxima in the cases with and without bulk electric field are given by Eq. 3.38. Hence, a linear approximation of the potential can be written as

$$V(x) = \begin{cases} V_{B_I} + E_I^{max} x & \text{when } x_{lin0-} < x < 0 \quad \textit{Region I} \\ V_{B_I} - E_{II}^{max} x & \text{when } 0 < x < x_{lin0+} \quad \textit{Region II}, \end{cases} \tag{3.44}$$

where

$$\begin{array}{ll} x_{lin0-} = -\frac{V_{B_I}}{E_I^{max}} & \textit{Region I} \\ x_{lin0+} = \frac{V_{B_I} - U_{GB}}{E_{II}^{max}} = \frac{V_{B_{II}}}{E_{II}^{max}} & \textit{Region II.} \end{array} \tag{3.45}$$

Eq. 3.33 was used in the derivation of Eq. 3.45. In Eq. 3.44 x_{lin0-} and x_{lin0+} define the edges of the linearized grain-boundary potential barrier, because $V(x_{lin0-}) = 0$ and $V(x_{lin0+}) = U_{GB}$. The height of the potential barrier V_{B_I} in the case without the bulk electric field is given by Eq. 3.42 and in the case with the bulk electric field by Eq. 3.37, respectively.

3.2.6 Comparison of potential profiles

The potential V, the electric field E, and the electron density n with various values of the applied voltage in the grain-boundary region is plotted in Figs. 3.10 and 3.11. The numerical calculation and the analytical formulas of the depletion region approximation are compared in Figs. 3.10 and 3.11. Fig. 3.10 shows that at low values of the applied voltage the depletion region approximation and the numerical simulation is in a very good agreement: only the tails of the potential barrier and the corresponding electric field are underestimated. When the applied voltage is increased, the density of electrons in the depletion region increases exponentially (see Figs. 3.10 and 3.11). In the high voltages ($U > 2$ V) the density of electrons in the depletion region is higher than 10 % of the doping density N_d (see Fig. 3.11). At this point the depletion region cannot be considered to be empty of electrons anymore,

and therefore the depletion region approximation fails. However, the formulas of the depletion region approximation still give some estimation for the potential profile, although the values are lower than they should be.

The different approximative formulas derived in section 3.2.5 and the numerical results are compared in Fig. 3.12, where the potential V and electric field E are plotted in the grain-boundary region. The only essential difference between the quadratic potential profile with the bulk electric field E_{bulk} (Eqs. 3.40 and 3.41) and without E_{bulk} (Eq. 3.43) is the electric field in the bulk part. The linear potential profile (Eqs. 3.44 and 3.45) is in very good agreement with the quadratic profile and the numerical results near the top of the grain-boundary potential barrier. However, it greatly underestimates the tails and width of the potential barrier.

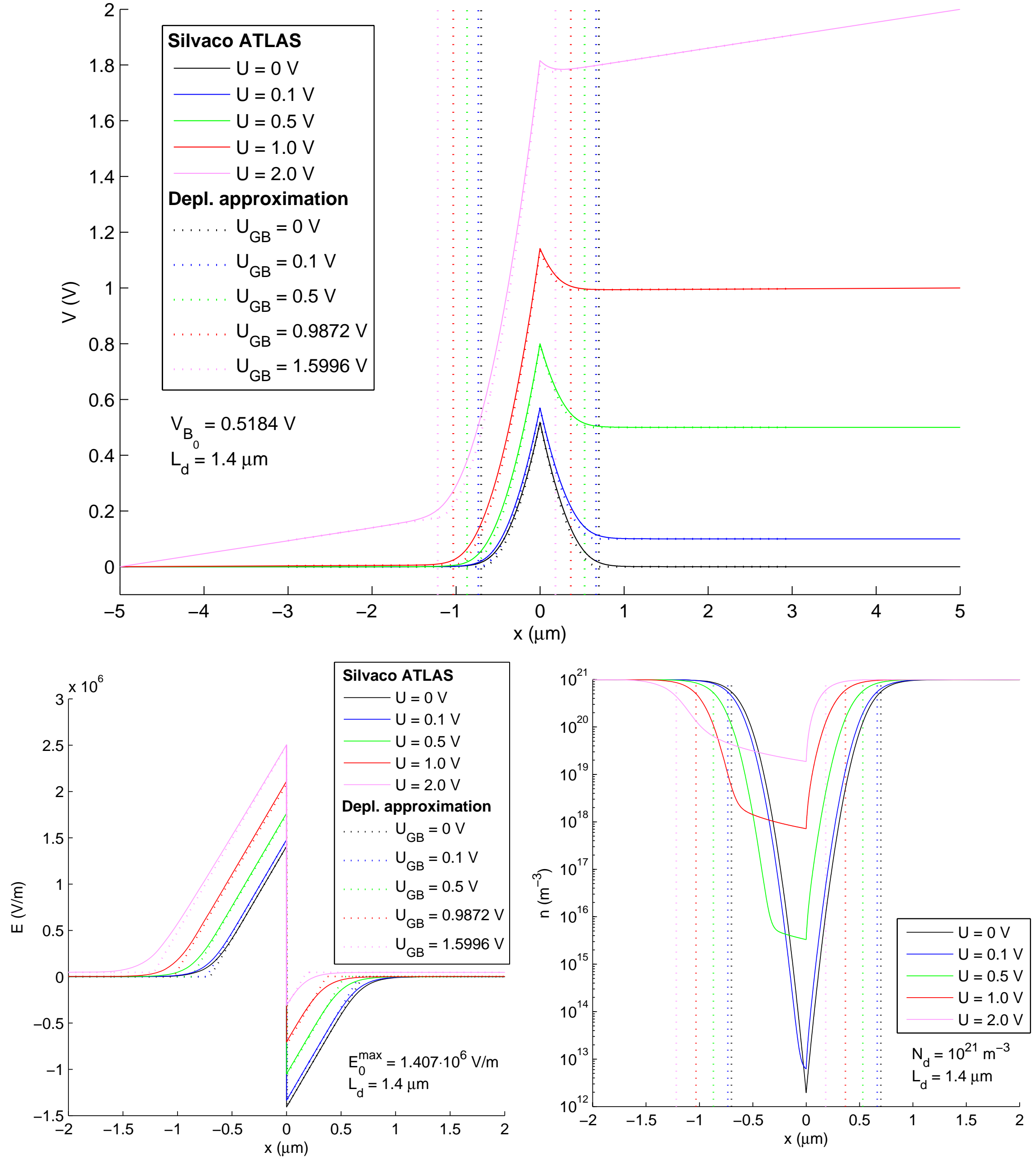

Figure 3.10: Potential V, electric field E, and electron density n plotted in the grain-boundary region with various voltages U applied across the sample. The numerical results obtained with Silvaco ATLAS and the depletion approximation (see section 3.2.5) are compared. Calculated using Eqs. 3.17, 3.39, 3.40, and 3.41. The values for U_{GB} and E_{bulk} were obtained from the Silvaco ATLAS results. The parameter values (see also Table 3.1) are $N_B = 1.4{\cdot}10^{15}$ m^{-2}, $N_d = 10^{21}$ m^{-3}, $\mu = 1000$ cm^2/(Vs), $E_c - E_T = 2$ eV (all traps filled), and $T = 300$ K.

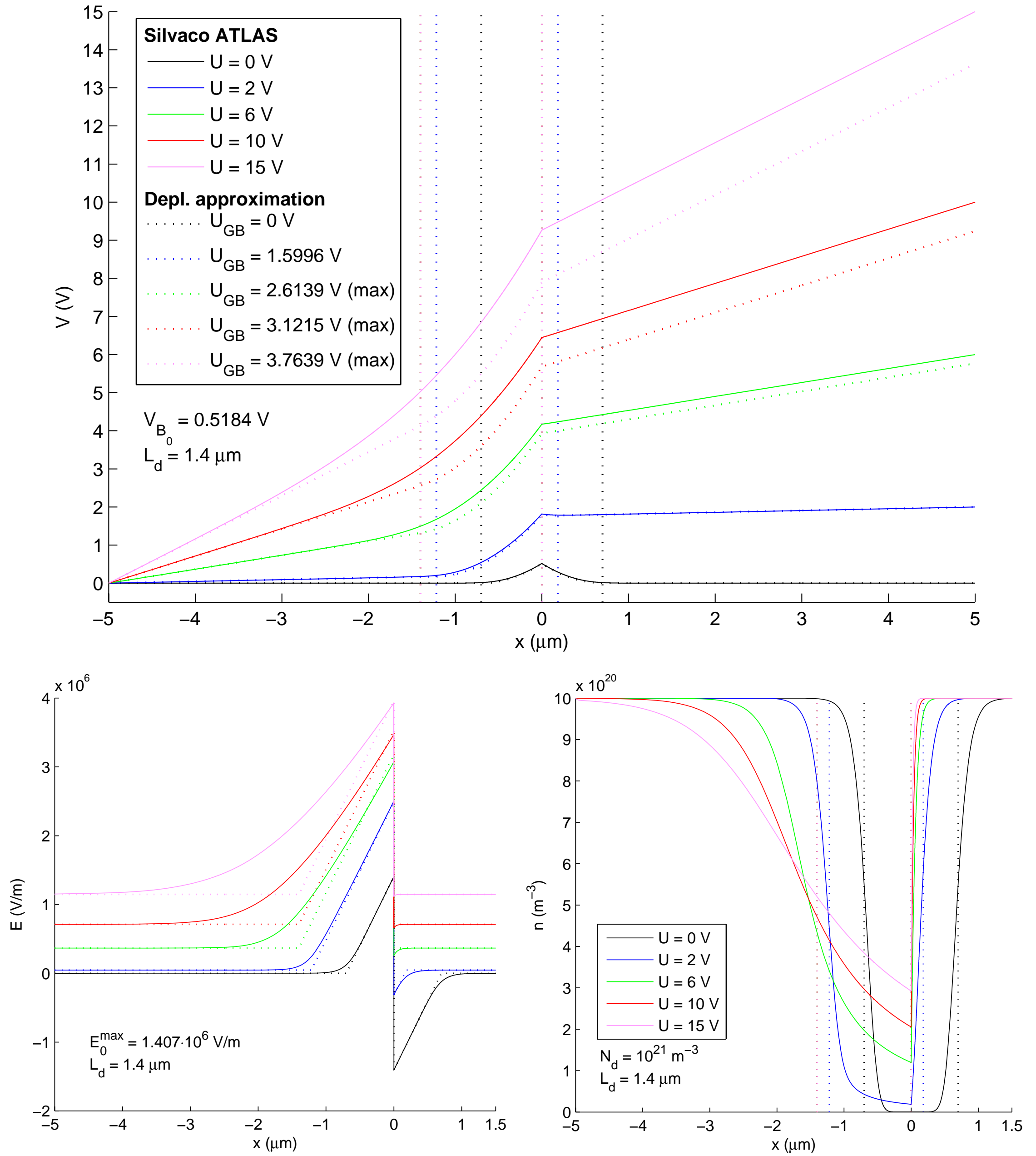

Figure 3.11: Potential V, electric field E, and electron density n plotted in the grain-boundary region with various voltages U applied across the sample. The numerical results obtained with Silvaco ATLAS and the depletion approximation (see section 3.2.5) are compared. Calculated using Eqs. 3.17, 3.39, 3.40, and 3.41. The values for U_{GB} and E_{bulk} were obtained from the Silvaco ATLAS results. The parameter values (see also Table 3.1) are $N_B = 1.4 \cdot 10^{15}$ m^{-2}, $N_d = 10^{21}$ m^{-3}, $\mu = 1000$ cm^2/(Vs), $E_c - E_T = 2$ eV (all traps filled), and $T = 300$ K.

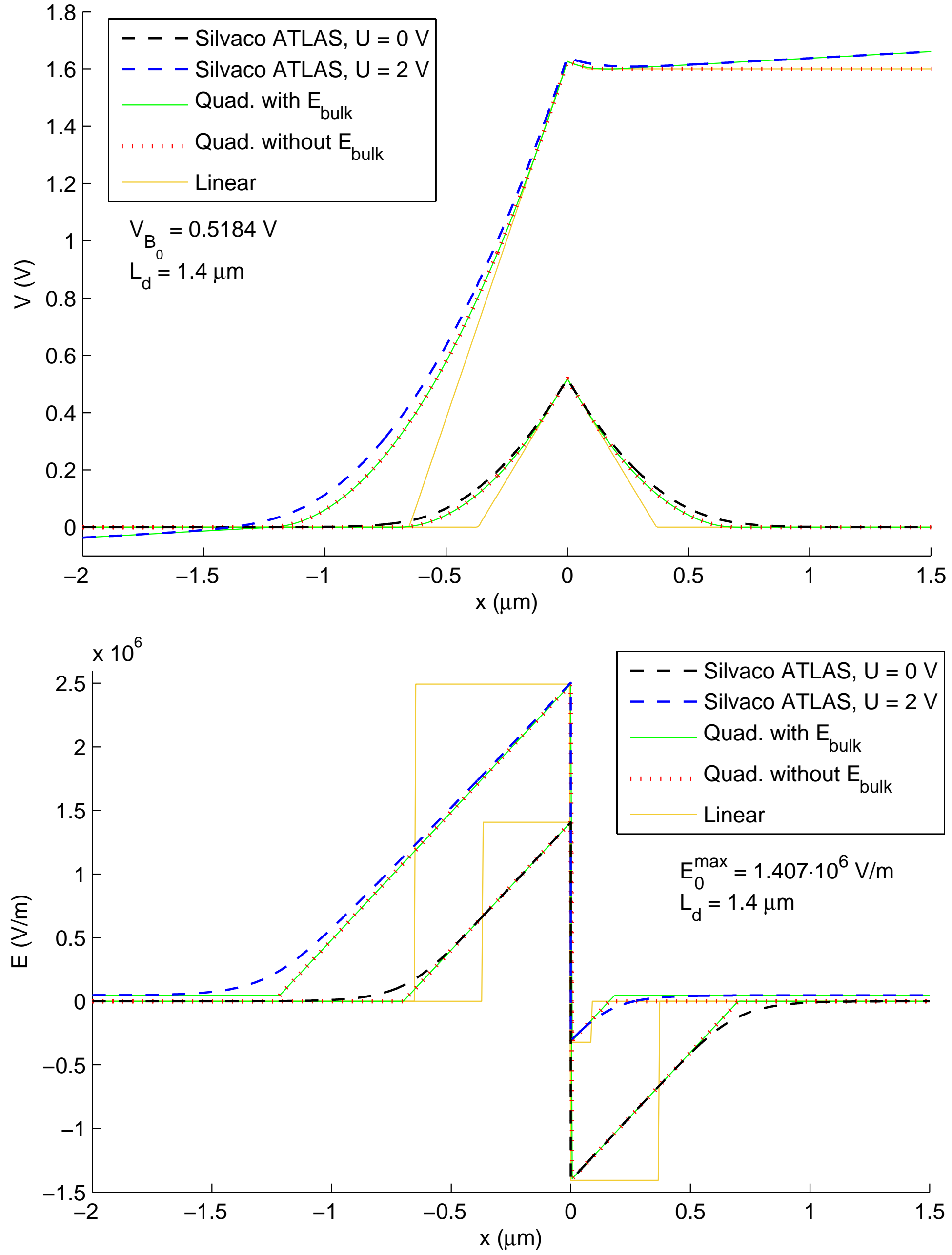

Figure 3.12: Potential V and electric field E plotted in the grain-boundary region with and without voltage U applied across the sample. The numerical results obtained with Silvaco ATLAS and various approximative potential profiles (see section 3.2.5) are compared. Calculated using Eqs. 3.17, 3.39, 3.40, 3.41, 3.43, 3.44, and 3.45. The values for U_{GB} and E_{bulk} were obtained from the Silvaco ATLAS results. The parameter values (see also Table 3.1) are $N_B = 1.4 \cdot 10^{15}$ m^{-2}, $N_d = 10^{21}$ m^{-3}, $\mu = 1000$ cm^2/(Vs), $E_c - E_T = 2$ eV (all traps filled), and $T = 300$ K.

3.3 Calculation of DC current and electron density

In this section the drift-diffusion theory is used for calculating the DC electric current through the grain-boundary region and the electron density at the grain boundary. The generation or recombination processes and holes are not taken into account.

In the drift-diffusion theory the electric current caused by electrons is given by [18]

$$\vec{J} = qD\vec{\nabla}n + q\mu n\vec{E}. \tag{3.46}$$

Using Einstein's relation (Eq. 2.10) Eq. 3.46 can be written in the one-dimensional case as

$$\frac{dn(x)}{dx} + \frac{qE(x)}{k_BT}n(x) = \frac{J(x)}{qD}. \tag{3.47}$$

Now, using the relation between the electric field and the electric potential, $\int E(x)\,dx = -\phi(x)$, and the general solution of a linear first order differential equation [46] a formula is obtained for the density of electrons

$$n(x) = \exp\left(\frac{q\phi(x)}{k_BT}\right)\left[\int_0^x \exp\left(-\frac{q\phi(x')}{k_BT}\right)\frac{J(x')}{qD}\,dx' + C\right], \tag{3.48}$$

where C is a constant.

The energy bands of electrons in the cases with and without the applied voltage U_{GB} are shown in Figs. 3.13a and b. Using Eq. 3.48 and setting the electric current density J constant in regions I and II a formula can be written for the region I

$$n(x) = \exp\left(-\frac{qV(x)}{k_BT}\right)\left[C_I + \frac{J_I}{qD}\int_{-x_{d_1}}^{x} \exp\left(\frac{qV(x')}{k_BT}\right)dx'\right]. \tag{3.49}$$

Because of the electron density outside the depletion region is $n(-x_{d_1}) = N_d$ and $V(-x_{d_1}) = 0$, Eq. 3.49 gives $C_I = n(-x_{d_1}) = N_d$. Now for the electron density at the grain boundary Eq. 3.49 gives [11]

$$n_B \equiv n(0) = \exp\left(-\frac{qV_B}{k_BT}\right)\left[N_d + \frac{J_I\mathcal{I}_I}{qD}\right], \tag{3.50}$$

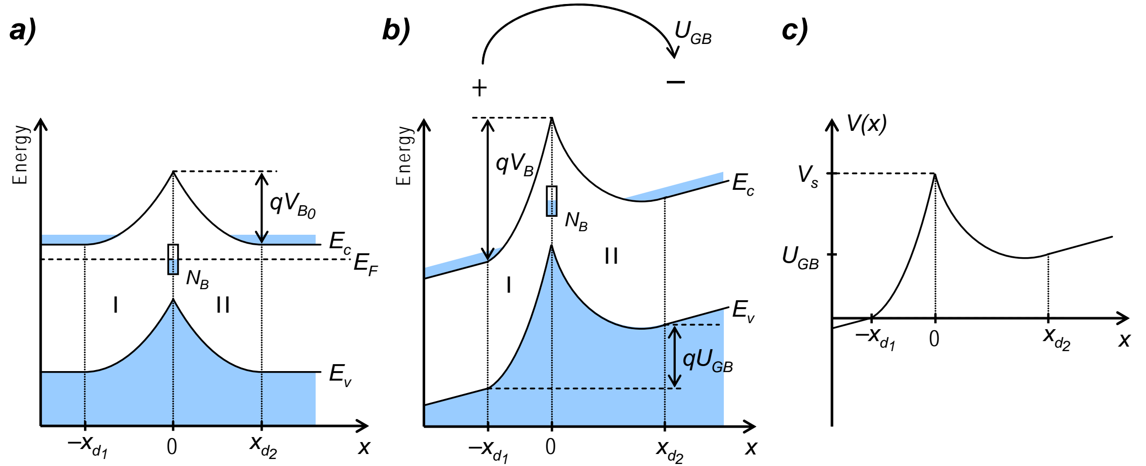

Figure 3.13: Energy bands of electrons in the grain-boundary region in the case where *a)* no voltage is applied across the boundary and *b)* voltage U_{GB} is applied across the grain boundary. The regions I and II are indicated. *c)* A plot of the potential $V(x)$ in the grain boundary region.

where

$$\mathcal{I}_I = \int_{-x_{d_1}}^{0} \exp\left(\frac{qV(x)}{k_BT}\right) dx. \tag{3.51}$$

Similarly, using Eq. 3.48 and constant J a formula can be written for the region II

$$n(x) = \exp\left(-\frac{qV(x)}{k_BT}\right)\left[C_{II} - \frac{J_{II}}{qD}\int_{x}^{x_{d_2}} \exp\left(\frac{qV(x')}{k_BT}\right) dx'\right]. \tag{3.52}$$

Substituting $V(x_{d_2}) = U_{GB}$ into Eq. 3.52 gives $n(x_{d_2}) = \exp\left(-\frac{qU_{GB}}{k_BT}\right)C_{II}$. On the other hand, $n(x_{d_2}) = N_d$, which in turn with the previous formula gives $C_{II} = N_d \exp\left(\frac{qU_{GB}}{k_BT}\right)$. Finally for the electron density at the grain boundary Eq. 3.52 gives

$$n_B = \exp\left(-\frac{qV_B}{k_BT}\right)\left[N_d \exp\left(\frac{qU_{GB}}{k_BT}\right) - \frac{J_{II}\mathcal{I}_{II}}{qD}\right], \tag{3.53}$$

where

$$\mathcal{I}_{II} = \int_{0}^{x_{d_2}} \exp\left(\frac{qV(x)}{k_BT}\right) dx. \tag{3.54}$$

Equating Eqs. 3.50 and 3.53 gives

$$J_I\mathcal{I}_I + J_{II}\mathcal{I}_{II} = qN_dD\left[\exp\left(\frac{qU_{GB}}{k_BT}\right) - 1\right]. \tag{3.55}$$

In the steady state the electric current is constant and continuous across the grain-boundary region, i.e. $J_I = J_{II} = J_{GB}^{DC}$. In this case Eq. 3.55 gives a formula for the electric current density through the grain boundary region [11]

$$J_{GB}^{DC} = \frac{qN_dD\left(e^{\frac{qU_{GB}}{k_BT}} - 1\right)}{\mathcal{I}_{tot}} = \frac{qN_dD\left(e^{\frac{qU_{GB}}{k_BT}} - 1\right)}{\int\limits_{-x_{d_1}}^{x_{d_2}} e^{\frac{qV(x)}{k_BT}}dx}, \tag{3.56}$$

where

$$\mathcal{I}_{tot} = \mathcal{I}_I + \mathcal{I}_{II} = \int\limits_{-x_{d_1}}^{x_{d_2}} \exp\left(\frac{qV(x)}{k_BT}\right)dx. \tag{3.57}$$

Eq. 3.56 can be solved by choosing a suitable function for the potential $V(x)$.

3.3.1 Linear potential

Here the linear potential profile (Eq. 3.44) without the bulk electric field is used in the calculation of the DC electric current through the grain-boundary region.

First the intergal in Eq. 3.56 is calculated. Using Eqs. 3.44 and 3.45 the integrals in the regions I and II are

$$\mathcal{I}_I = \int\limits_{-x_{d_1}}^{0} e^{\frac{qV(x)}{k_BT}}dx = \int\limits_{x_{lin0-}}^{0} e^{\frac{q\left(V_B + E_I^{max}x\right)}{k_BT}}dx = \frac{k_BT}{qE_I^{max}}\left(e^{\frac{qV_B}{k_BT}} - 1\right) \tag{3.58}$$

and

$$\mathcal{I}_{II} = \int\limits_{0}^{x_{d_2}} e^{\frac{qV(x)}{k_BT}}dx = \int\limits_{0}^{x_{lin0+}} e^{\frac{q\left(V_B - E_{II}^{max}x\right)}{k_BT}}dx = \frac{k_BT}{qE_{II}^{max}}\left(e^{\frac{qV_B}{k_BT}} - e^{\frac{qU_{GB}}{k_BT}}\right). \tag{3.59}$$

Now, substituting Eqs. 3.58 and 3.59 into Eq. 3.56 and using Einstein's relation (Eq. 2.10) gives

$$J_{GB}^{DC} = \frac{q\mu N_d e^{-\frac{qV_B}{k_BT}}\left(e^{\frac{qU_{GB}}{k_BT}} - 1\right)}{\frac{1}{E_I^{max}}\left(1 - e^{-\frac{qV_B}{k_BT}}\right) + \frac{1}{E_{II}^{max}}\left(1 - e^{\frac{q(U_{GB} - V_B)}{k_BT}}\right)}. \tag{3.60}$$

Substituting Eqs. 3.56, 3.58, and 3.59 into Eq. 3.50 gives

$$n_B = N_d e^{-\frac{qV_B}{k_BT}} \left[1 + \frac{e^{\frac{qU_{GB}}{k_BT}} - 1}{1 + \frac{E_I^{max}}{E_{II}^{max}} \frac{1-e^{\frac{q(U_{GB}-V_B)}{k_BT}}}{1-e^{-\frac{qV_B}{k_BT}}}} \right]. \tag{3.61}$$

Next, Eq. 3.38 is plugged into Eqs. 3.60 and 3.61. This gives

$$J_{GB}^{DC} = \frac{q\mu N_d E_0^{max} \left[1 - \left(\frac{U_{GB}}{4V_{B_0}}\right)^2\right] e^{-\frac{q}{k_BT}\left(V_B - \frac{1}{2}U_{GB}\right)} \sinh \frac{qU_{GB}}{2k_BT}}{1 - e^{-\frac{q}{k_BT}\left(V_B - \frac{1}{2}U_{GB}\right)} \left[\cosh \frac{qU_{GB}}{2k_BT} + \frac{U_{GB}}{4V_{B_0}} \sinh \frac{qU_{GB}}{2k_BT}\right]} \tag{3.62}$$

and

$$n_B = \frac{N_d e^{-\frac{q}{k_BT}\left(V_B - \frac{1}{2}U_{GB}\right)} \left[\cosh \frac{qU_{GB}}{2k_BT} - \frac{U_{GB}}{4V_{B_0}} \sinh \frac{qU_{GB}}{2k_BT} - e^{-\frac{q}{k_BT}\left(V_B - \frac{1}{2}U_{GB}\right)}\right]}{1 - e^{-\frac{q}{k_BT}\left(V_B - \frac{1}{2}U_{GB}\right)} \left[\cosh \frac{qU_{GB}}{2k_BT} + \frac{U_{GB}}{4V_{B_0}} \sinh \frac{qU_{GB}}{2k_BT}\right]}. \tag{3.63}$$

In the case without the bulk electric field it is useful to write Eq. 3.42 in the form

$$V_B = V_{B_I} = V_{B_0} \left(\frac{U_{GB}}{4V_{B_0}} + 1\right)^2 = V_{B_0} \left[1 + \left(\frac{U_{GB}}{4V_{B_0}}\right)^2\right] + \frac{1}{2}U_{GB}. \tag{3.64}$$

Substitution of Eq. 3.64 into Eq. 3.62 gives

$$J_{GB}^{DC} = \frac{J_0 \sqrt{2} \sqrt{V_{B_0} - \frac{k_BT}{q}} \left[1 - \left(\frac{U_{GB}}{4V_{B_0}}\right)^2\right] e^{-\frac{qV_{B_0}}{k_BT}\left[1+\left(\frac{U_{GB}}{4V_{B_0}}\right)^2\right]} \sinh \frac{qU_{GB}}{2k_BT}}{1 - e^{-\frac{qV_{B_0}}{k_BT}\left[1+\left(\frac{U_{GB}}{4V_{B_0}}\right)^2\right]} \left[\cosh \frac{qU_{GB}}{2k_BT} + \frac{U_{GB}}{4V_{B_0}} \sinh \frac{qU_{GB}}{2k_BT}\right]}, \tag{3.65}$$

where (see Eqs. 3.8 and 3.17)

$$J_0 = \sigma_{bulk} \frac{E_0^{max}}{\sqrt{2}\sqrt{V_{B_0} - \frac{k_BT}{q}}} = \mu \sqrt{\frac{q^3 N_d^3}{\varepsilon}} \tag{3.66}$$

and σ_{bulk} is the bulk conductivity of the material,

$$\sigma_{bulk} = q\mu N_d. \tag{3.67}$$

Neglecting the term $-e^{-\frac{q}{k_BT}\left(V_B-\frac{1}{2}U_{GB}\right)}$ in the numerator (because $V_B \gg \frac{k_BT}{q}$) and substituting Eq. 3.64 into Eq. 3.63 gives

$$n_B \approx \frac{N_d e^{-\frac{qV_{B_0}}{k_BT}\left[1+\left(\frac{U_{GB}}{4V_{B_0}}\right)^2\right]}\left[\cosh\frac{qU_{GB}}{2k_BT}-\frac{U_{GB}}{4V_{B_0}}\sinh\frac{qU_{GB}}{2k_BT}\right]}{1-e^{-\frac{qV_{B_0}}{k_BT}\left[1+\left(\frac{U_{GB}}{4V_{B_0}}\right)^2\right]}\left[\cosh\frac{qU_{GB}}{2k_BT}+\frac{U_{GB}}{4V_{B_0}}\sinh\frac{qU_{GB}}{2k_BT}\right]}. \tag{3.68}$$

At lower voltages Eqs. 3.65 and 3.68 can be approximated by

$$J_{GB}^{DC} \approx J_0\sqrt{2}\sqrt{V_{B_0}-\frac{k_BT}{q}}\left[1-\left(\frac{U_{GB}}{4V_{B_0}}\right)^2\right]e^{-\frac{qV_{B_0}}{k_BT}\left[1+\left(\frac{U_{GB}}{4V_{B_0}}\right)^2\right]}\sinh\frac{qU_{GB}}{2k_BT} \tag{3.69}$$

and

$$n_B \approx N_d e^{-\frac{qV_{B_0}}{k_BT}\left[1+\left(\frac{U_{GB}}{4V_{B_0}}\right)^2\right]}\left[\cosh\frac{qU_{GB}}{2k_BT}-\frac{U_{GB}}{4V_{B_0}}\sinh\frac{qU_{GB}}{2k_BT}\right]. \tag{3.70}$$

At even lower voltages the U_{GB}^2 terms can be neglected in Eqs. 3.69 and 3.70 giving [11, 37]

$$J_{GB}^{DC} \approx q\mu N_d E_0^{max} e^{-\frac{qV_{B_0}}{k_BT}}\sinh\frac{qU_{GB}}{2k_BT} = J_0\sqrt{2}\sqrt{V_{B_0}-\frac{k_BT}{q}}e^{-\frac{qV_{B_0}}{k_BT}}\sinh\frac{qU_{GB}}{2k_BT} \tag{3.71}$$

and [11]

$$n_B \approx N_d e^{-\frac{qV_{B_0}}{k_BT}}\cosh\frac{qU_{GB}}{2k_BT}. \tag{3.72}$$

At very low applied voltages, in the linear regime, $\sinh\frac{qU_{GB}}{2k_BT} \approx \frac{qU_{GB}}{2k_BT}$ which gives a linear formula for the electric current density

$$J_{GB}^{DC} \approx \frac{q^2\mu N_d E_0^{max}}{2k_BT}e^{-\frac{qV_{B_0}}{k_BT}}U_{GB} = \frac{qJ_0\sqrt{V_{B_0}-\frac{k_BT}{q}}}{\sqrt{2}\,k_BT}e^{-\frac{qV_{B_0}}{k_BT}}U_{GB}. \tag{3.73}$$

In the linear regime Eq. 3.72 reduces to

$$n_B \approx N_d e^{-\frac{qV_{B_0}}{k_BT}}. \tag{3.74}$$

3.3.2 Useful formulas for integration in quadratic potential case

Before calculation of the electric current a few integrals are considered. An important integral can be calculated using Wolfram Mathematica Online Integrator [47]

$$\int \exp\left(ax^2+bx\right)dx = -i\frac{1}{2}\sqrt{\frac{\pi}{a}}e^{-\frac{b^2}{4a}}\operatorname{erf}\left(i\frac{b+2ax}{2\sqrt{a}}\right)+\text{const.}, \tag{3.75}$$

where erf is the error function. Eq. 3.75 can be written as

$$\int \exp\left(ax^2+bx\right)dx = \frac{1}{2}\sqrt{\frac{\pi}{-a}}e^{-\frac{b^2}{4a}}\operatorname{erf}\left(-\frac{b+2ax}{2\sqrt{-a}}\right)+\text{const.}, \tag{3.76}$$

which has only real numbers if $a < 0$. Using the imaginary error function, defined as [48]

$$\operatorname{erfi}(x) \equiv \frac{\operatorname{erf}(ix)}{i} = -i\operatorname{erf}(ix), \tag{3.77}$$

Eq. 3.75 can be written as

$$\int \exp\left(ax^2+bx\right)dx = \frac{1}{2}\sqrt{\frac{\pi}{a}}e^{-\frac{b^2}{4a}}\operatorname{erfi}\left(\frac{b+2ax}{2\sqrt{a}}\right)+\text{const.} \tag{3.78}$$

With $b = 0$ this reduces to

$$\int \exp\left(ax^2\right)dx = \frac{1}{2}\sqrt{\frac{\pi}{a}}\operatorname{erfi}\left(\sqrt{a}x\right)+\text{const.} \tag{3.79}$$

3.3.3 Quadratic potential without bulk electric field

In the case without the bulk electric field the potential profile is given by Eq. 3.43. In this case the first part of the integral in Eq. 3.56 reads

$$\int\limits_{-x_{d_1}}^{0} \exp\left[\frac{qV(x)}{k_BT}\right]dx = \int\limits_{-x_{d_1}}^{0} \exp\left[\frac{qV_{B_0}}{k_BT}\left(\frac{U_{GB}}{4V_{B_0}}+1\right)^2\left(\frac{x}{x_{d_1}}+1\right)^2\right]dx. \tag{3.80}$$

Substituting

$$a = \frac{qV_{B_0}}{k_BT}\left(\frac{U_{GB}}{4V_{B_0}}+1\right)^2 \tag{3.81}$$

and

$$y = \frac{x}{x_{d_1}} + 1 \tag{3.82}$$

in Eq. 3.80 and using Eq. 3.79 gives

$$\int_{-x_{d_1}}^{0} \exp\left(\frac{qV(x)}{k_B T}\right) dx = x_{d_1} \int_{0}^{1} \exp\left(ay^2\right) dy = \frac{\sqrt{\pi}}{2} \frac{x_{d_1}}{\sqrt{a}} \mathrm{erfi}\left(\sqrt{a}\right). \tag{3.83}$$

The second part of the integral in Eq. 3.56 reads

$$\int_{0}^{x_{d_2}} \exp\left[\frac{qV(x)}{k_B T}\right] dx = \int_{0}^{x_{d_2}} \exp\left[\frac{qV_{B_0}}{k_B T}\left(\frac{U_{GB}}{4V_{B_0}} - 1\right)^2 \left(\frac{x}{x_{d_2}} - 1\right)^2 + U_{GB}\right] dx. \tag{3.84}$$

Substituting

$$a' = \frac{qV_{B_0}}{k_B T}\left(\frac{U_{GB}}{4V_{B_0}} - 1\right)^2 \tag{3.85}$$

and

$$y' = \frac{x}{x_{d_2}} - 1 \tag{3.86}$$

in Eq. 3.84 and using Eq. 3.79 gives

$$\int_{0}^{x_{d_2}} \exp\left(\frac{qV(x)}{k_B T}\right) dx = x_{d_2} e^{\frac{qU_{GB}}{k_B T}} \int_{-1}^{0} \exp\left(a' {y'}^2\right) dy' = -\frac{\sqrt{\pi}}{2} \frac{x_{d_2}}{\sqrt{a'}} e^{\frac{qU_{GB}}{k_B T}} \mathrm{erfi}\left(-\sqrt{a'}\right). \tag{3.87}$$

Using Eqs. 3.34 ($E_{bulk} = 0$), 3.81, and 3.85 formulas are obtained for the ratios:

$$\begin{aligned} \frac{x_{d_1}}{\sqrt{a}} &= \frac{L_d}{2\sqrt{\frac{qV_{B_0}}{k_B T}}} \\ \frac{x_{d_2}}{\sqrt{a'}} &= -\frac{L_d}{2\sqrt{\frac{qV_{B_0}}{k_B T}}}. \end{aligned} \tag{3.88}$$

With the help of Eqs. Eqs. 3.83, 3.87, and 3.88 the total integral can be written as

$$\int_{-x_{d_1}}^{x_{d_2}} \exp\left(\frac{qV(x)}{k_B T}\right) dx = \frac{\sqrt{\pi}}{4} \frac{L_d}{\sqrt{\frac{qV_{B_0}}{k_B T}}} \left[\mathrm{erfi}\left(\sqrt{a}\right) + e^{\frac{qU_{GB}}{k_B T}} \mathrm{erfi}\left(-\sqrt{a'}\right)\right]. \tag{3.89}$$

Finally, plugging Eq. 3.89 into Eq. 3.56 the DC electric current density

$$J_{GB}^{DC} = \frac{J_0 \sqrt{\frac{8k_BT}{\pi q}} \left(1 - \frac{k_BT}{qV_{B_0}}\right)^{-1/2} \sinh \frac{qU_{GB}}{2k_BT}}{e^{-\frac{qU_{GB}}{2k_BT}} \operatorname{erfi}\left[\sqrt{\frac{qV_{B_0}}{k_BT}} \left(1 + \frac{U_{GB}}{4V_{B_0}}\right)\right] + e^{\frac{qU_{GB}}{2k_BT}} \operatorname{erfi}\left[\sqrt{\frac{qV_{B_0}}{k_BT}} \left(1 - \frac{U_{GB}}{4V_{B_0}}\right)\right]}, \quad (3.90)$$

where Eqs. 2.10, 3.22, 3.66, 3.67, 3.81, and 3.85 were used. Furthermore, plugging Eqs. 3.80, 3.89, and 3.90 in Eq. 3.50 gives for the electron density at the grain boundary

$$n_B = N_d \exp\left[-\frac{qV_{B_0}}{k_BT}\left(\frac{U_{GB}}{4V_{B_0}} + 1\right)^2\right] \left[1 + \frac{e^{\frac{qU_{GB}}{k_BT}} - 1}{1 + e^{\frac{qU_{GB}}{k_BT}} \frac{\operatorname{erfi}\left[\sqrt{\frac{qV_{B_0}}{k_BT}}\left(1 - \frac{U_{GB}}{4V_{B_0}}\right)\right]}{\operatorname{erfi}\left[\sqrt{\frac{qV_{B_0}}{k_BT}}\left(1 + \frac{U_{GB}}{4V_{B_0}}\right)\right]}}\right], \quad (3.91)$$

where Eqs. 2.10, 3.42 ($V_B = V_{B_I}$), 3.81, 3.85, and 3.88 were used.

3.3.4 Quadratic potential with bulk electric field

In the case with the bulk electric field the quadratic potential profile is given by Eqs. 3.40 and 3.41. In this case the first part of the integral in Eq. 3.56 reads

$$\begin{aligned} \int_{-x_{d_1}}^{0} \exp\left[\frac{qV(x)}{k_BT}\right] dx = \int_{-x_{d_1}}^{0} \exp\Bigg[\frac{qV_{B_0}}{k_BT}\left(\frac{U_{GB}}{4V_{B_0}} + 1 - \frac{E_{bulk}}{E_0^{max}}\right)^2 \left(\frac{x}{x_{d_1}} + 1\right)^2 \\ + 2\frac{qV_{B_0}}{k_BT}\left(\frac{E_{bulk}}{E_0^{max}}\right)\left(\frac{U_{GB}}{4V_{B_0}} + 1 - \frac{E_{bulk}}{E_0^{max}}\right)\left(\frac{x}{x_{d_1}} + 1\right)\Bigg] dx. \end{aligned} \quad (3.92)$$

Substituting

$$a = \frac{qV_{B_0}}{k_BT}\left(\frac{U_{GB}}{4V_{B_0}} + 1 - \frac{E_{bulk}}{E_0^{max}}\right)^2, \quad (3.93)$$

$$b = 2\frac{qV_{B_0}}{k_BT}\left(\frac{E_{bulk}}{E_0^{max}}\right)\left(\frac{U_{GB}}{4V_{B_0}} + 1 - \frac{E_{bulk}}{E_0^{max}}\right), \quad (3.94)$$

and

$$y = \frac{x}{x_{d_1}} + 1 \quad (3.95)$$

in Eq. 3.92 and using Eq. 3.78 gives

$$\int_{-x_{d_1}}^{0} \exp\left(\frac{qV(x)}{k_B T}\right) dx = \frac{\sqrt{\pi}}{2} \frac{x_{d_1}}{\sqrt{a}} e^{-\frac{b^2}{4a}} \left[\text{erfi}\left(\frac{b+2a}{2\sqrt{a}}\right) - \text{erfi}\left(\frac{b}{2\sqrt{a}}\right)\right]. \tag{3.96}$$

The second part of the integral in Eq. 3.56, which is calculated in the same way as the first part, reads

$$\begin{aligned}\int_{0}^{x_{d_2}} \exp\left[\frac{qV(x)}{k_B T}\right] dx = \int_{0}^{x_{d_2}} \exp\Bigg[\frac{qV_{B_0}}{k_B T}\left(\frac{U_{GB}}{4V_{B_0}} - 1 - \frac{E_{bulk}}{E_0^{max}}\right)^2 \left(\frac{x}{x_{d_2}} - 1\right)^2 \\ + 2\frac{qV_{B_0}}{k_B T}\left(\frac{E_{bulk}}{E_0^{max}}\right)\left(-\frac{U_{GB}}{4V_{B_0}} + 1 + \frac{E_{bulk}}{E_0^{max}}\right)\left(\frac{x}{x_{d_2}} - 1\right) + \frac{qU_{GB}}{k_B T}\Bigg] dx.\end{aligned} \tag{3.97}$$

Substituting

$$a' = \frac{qV_{B_0}}{k_B T}\left(\frac{U_{GB}}{4V_{B_0}} - 1 - \frac{E_{bulk}}{E_0^{max}}\right)^2, \tag{3.98}$$

$$b' = 2\frac{qV_{B_0}}{k_B T}\left(\frac{E_{bulk}}{E_0^{max}}\right)\left(-\frac{U_{GB}}{4V_{B_0}} + 1 + \frac{E_{bulk}}{E_0^{max}}\right), \tag{3.99}$$

and

$$y' = \frac{x}{x_{d_2}} - 1 \tag{3.100}$$

in Eq. 3.97 and using Eq. 3.78 gives

$$\int_{0}^{x_{d_2}} \exp\left(\frac{qV(x)}{k_B T}\right) dx = \frac{\sqrt{\pi}}{2} \frac{x_{d_2}}{\sqrt{a'}} e^{\frac{qU_{GB}}{k_B T}} e^{-\frac{b'^2}{4a'}} \left[\text{erfi}\left(\frac{b'}{2\sqrt{a'}}\right) - \text{erfi}\left(\frac{b'-2a'}{2\sqrt{a'}}\right)\right]. \tag{3.101}$$

By using Eqs. 3.34, 3.93 and 3.98 it can be shown that Eq. 3.88 also holds in the case with the bulk electric field. With Eqs. 3.93, 3.94, 3.98 and 3.99 a formula is obtained for the ratios

$$\frac{b^2}{4a} = \frac{b'^2}{4a'} = \frac{qV_{B_0}}{k_B T}\left(\frac{E_{bulk}}{E_0^{max}}\right)^2. \tag{3.102}$$

The total integral is given by the sum of Eqs. 3.96 and 3.101:

$$\begin{aligned}\int_{-x_{d_1}}^{x_{d_2}} \exp\left(\frac{qV(x)}{k_B T}\right) dx = \frac{\sqrt{\pi}}{4} \frac{L_d}{\sqrt{\frac{qV_{B_0}}{k_B T}}} e^{-\frac{qV_{B_0}}{k_B T}\left(\frac{E_{bulk}}{E_0^{max}}\right)^2} \cdot \\ \left\{\text{erfi}\left(\frac{b+2a}{2\sqrt{a}}\right) - \text{erfi}\left(\frac{b}{2\sqrt{a}}\right) - e^{\frac{qU_{GB}}{k_B T}}\left[\text{erfi}\left(\frac{b'}{2\sqrt{a'}}\right) - \text{erfi}\left(\frac{b'-2a'}{2\sqrt{a'}}\right)\right]\right\},\end{aligned} \tag{3.103}$$

where Eqs. 3.88 and 3.102 were used. Using Eqs. 3.93, 3.94, 3.98, and 3.99 formulas are obtained for the arguments

$$\begin{aligned}\frac{b}{2\sqrt{a}} &= \sqrt{\frac{qV_{B_0}}{k_BT}}\left(\frac{E_{bulk}}{E_0^{max}}\right)\\ \frac{b'}{2\sqrt{a'}} &= -\sqrt{\frac{qV_{B_0}}{k_BT}}\left(\frac{E_{bulk}}{E_0^{max}}\right)\\ \frac{b+2a}{2\sqrt{a}} &= \sqrt{\frac{qV_{B_0}}{k_BT}}\left(1+\frac{U_{GB}}{4V_{B_0}}\right)\\ \frac{b'-2a'}{2\sqrt{a'}} &= \sqrt{\frac{qV_{B_0}}{k_BT}}\left(1-\frac{U_{GB}}{4V_{B_0}}\right).\end{aligned} \tag{3.104}$$

Finally, plugging Eq. 3.103 in Eq. 3.56 gives for the DC electric current density

$$J_{GB}^{DC} = \frac{J_0\sqrt{\frac{8k_BT}{\pi q}}\left(1-\frac{k_BT}{qV_{B_0}}\right)^{-1/2} e^{\frac{qV_{B_0}}{k_BT}\left(\frac{E_{bulk}}{E_0^{max}}\right)^2}\sinh\frac{qU_{GB}}{2k_BT}}{e^{-\frac{qU_{GB}}{2k_BT}}\left[\operatorname{erfi}\left(\frac{b+2a}{2\sqrt{a}}\right)-\operatorname{erfi}\left(\frac{b}{2\sqrt{a}}\right)\right]-e^{\frac{qU_{GB}}{2k_BT}}\left[\operatorname{erfi}\left(\frac{b'}{2\sqrt{a'}}\right)-\operatorname{erfi}\left(\frac{b'-2a'}{2\sqrt{a'}}\right)\right]}, \tag{3.105}$$

where Eqs. 2.10, 3.22, 3.66, and 3.67 were used. Plugging Eqs. 3.92, 3.103 and 3.105 into Eq. 3.50 gives for the electron density at the grain boundary

$$n_B = N_d e^{-\frac{qV_{B_0}}{k_BT}\left[\left(1+\frac{U_{GB}}{4V_{B_0}}\right)^2-\left(\frac{E_{bulk}}{E_0^{max}}\right)^2\right]}\left[1+\frac{e^{\frac{qU_{GB}}{k_BT}}-1}{1-e^{\frac{qU_{GB}}{k_BT}}\frac{\operatorname{erfi}\left[\frac{b'}{2\sqrt{a'}}\right]-\operatorname{erfi}\left[\frac{b'-2a'}{2\sqrt{a'}}\right]}{\operatorname{erfi}\left[\frac{b+2a}{2\sqrt{a}}\right]-\operatorname{erfi}\left[\frac{b}{2\sqrt{a}}\right]}}\right], \tag{3.106}$$

where Eqs. 2.10, 3.37 ($V_B = V_{B_I}$), and 3.88 were used. The arguments are given in Eq. 3.104.

3.3.5 Comparison of formulas

Here the various formulas derived for the DC current density in the grain-boundary region J_{GB}^{DC} and the density of electrons at the grain boundary n_B are compared. The erfi function in Eqs. 3.90, 3.91, 3.105, and 3.106 is calculated with the complex function error function implemented in MATLAB [49].

First, the formulas derived in the case without the bulk electric field ($E_{bulk} = 0$) are compared. The DC current density in the grain-boundary region J_{GB}^{DC} and the

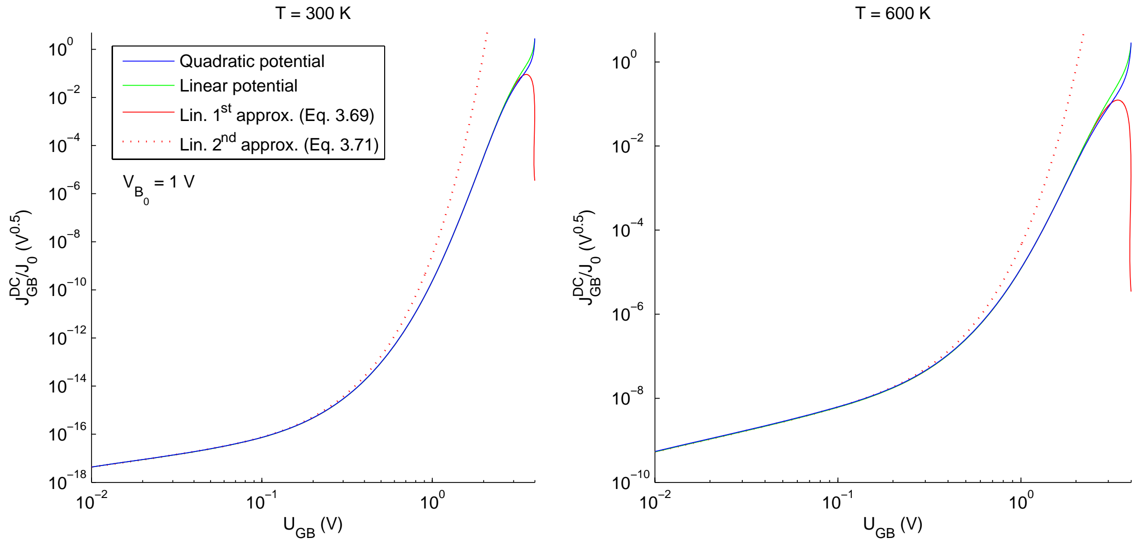

Figure 3.14: Normalized density of electric current flowing through the grain-boundary region plotted as a function of voltage U_{GB} with $V_B = 1$ V at temperatures of 300 K (*left*) and 600 K (*right*) when $E_{bulk} = 0$. Calculated using Eqs. 3.65, 3.69, 3.71, and 3.90.

density of electrons at the grain boundary n_B calculated with Eqs. 3.65 and 3.68 (the linear potential profile), 3.69 and 3.70 (the 1st approximation of the linear potential profile), 3.71 and 3.72 (the 2nd approximation of the linear potential profile), and 3.90 and 3.91 (the quadratic potential profile) at 300 K and 600 K are plotted against the applied voltage U_{GB} in Figs. 3.14 and 3.15, respectively. When the temperature is increased from 300 K to 600 K the low-voltage values of J_{GB}^{DC} and n_B increase exponentially in Figs. 3.14 and 3.15.

Figs. 3.14 and 3.15 show that the exact formulas of the linear and quadratic potential profiles differ essentially only at high voltages: With the linear potential profile J_{GB}^{DC} and n_B have a bit higher values than with the quadratic potential profile. However, the last point with the highest applied voltage before the condition of Eq. 3.36 is met, has roughly the same value with both formulas.

The first approximation of the linear potential profile formulas (Eqs. 3.69 and 3.70) is a good approximation when $U_{GB} \lesssim 1.5$ V (i.e. in this case $U_{GB} \lesssim 1.5 V_{B_0}$. However, the problem in Eqs. 3.69 and 3.70 is that Eq. 3.69 approaches zero at $U_{GB} = 4V_{B_0}$. Eq. 3.70 also approaches a very small number at $U_{GB} = 4V_{B_0}$. These properties are very problematic when these formulas belong to a set of formulas which are solved numerically: Often numerical algorithms work poorly with Eqs. 3.69 and

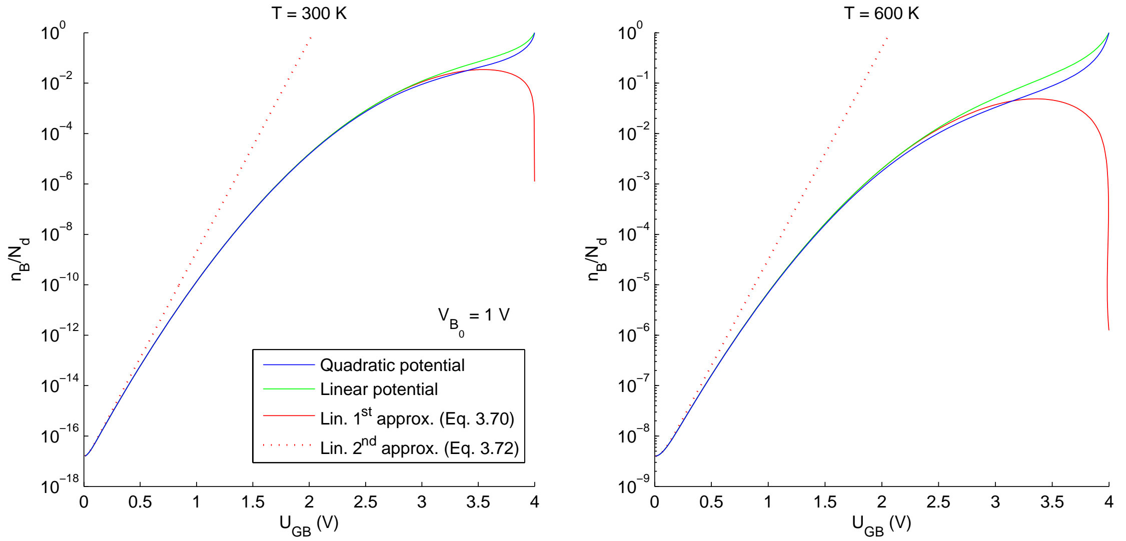

Figure 3.15: Relative electron density at the grain boundary plotted as a function of voltage U_{GB} with $V_B = 1$ V at temperatures of 300 K (*left*) and 600 K (*right*) when $E_{bulk} = 0$. Calculated using Eqs. 3.68, 3.70, 3.72, and 3.91.

3.70 because J_{GB}^{DC} and n_B decrease with voltage after certain point at high voltages, although in reality they should increase. These problems arise later when the electronic trapping is modelled and the I–V characteristics of granular semiconductor are calculated.

The second approximation of the linear potential profile formulas (Eqs. 3.71 and 3.72) is a good approximation at low voltages when $U_{GB} \lesssim 0.1$ V (i.e. in this case $U_{GB} \lesssim 0.1V_{B_0}$). The 2$^{\text{nd}}$ approximation formulas (Eqs. 3.71 and 3.72) do not have the same problem of decreasing values with increasing voltage as the 1$^{\text{st}}$ approximation formulas (Eqs. 3.69 and 3.70). However, the problem in the 2$^{\text{nd}}$ approximation formulas is the exponential increase of J_{GB}^{DC} and n_B with the voltage U_{GB}: At high voltages J_{GB}^{DC} and n_B are overestimated and in Figs. 3.14 and 3.15 the values of at J_{GB}^{DC} and n_B exceed the maximum values given by the other formulas at $U_{GB} \approx 2$ V (i.e. in this case $U_{GB} \approx 2V_{B_0}$).

Last, the formulas derived in the case of the quadratic potential profile with the bulk electric field are discussed. The DC current density in the grain-boundary region J_{GB}^{DC} and the density of electrons at the grain boundary n_B calculated with Eqs. 3.105 and 3.106 at 300 K and 600 K are plotted against the applied voltage U_{GB} with various values of the ratio of the bulk electric field and E_0^{max} (see Eq. 3.8) in

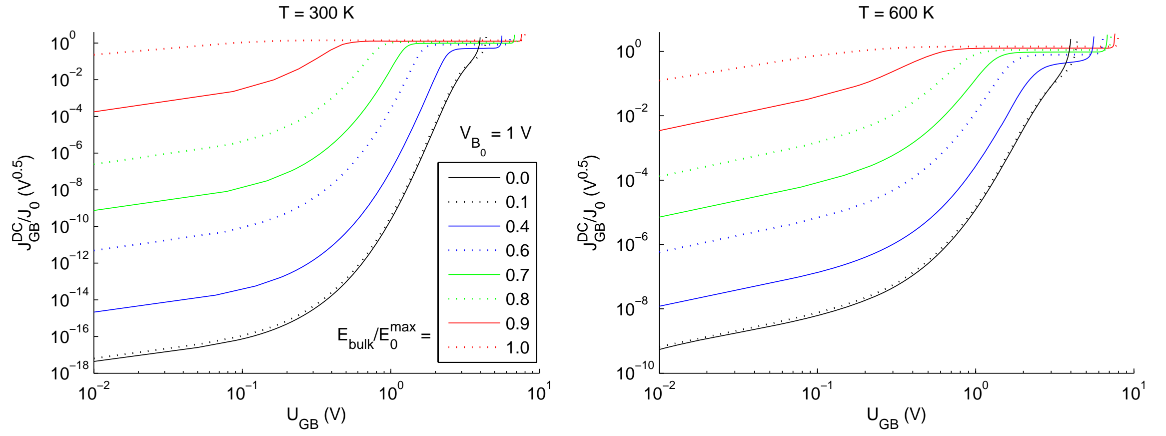

Figure 3.16: Normalized density of electric current flowing through the grain-boundary region plotted as a function of voltage U_{GB} with various values of the ratio of the electric fields E_{bulk}/E_0^{max} and $V_B = 1$ V at temperatures of 300 K (*left*) and 600 K (*right*). Calculated using Eq. 3.105.

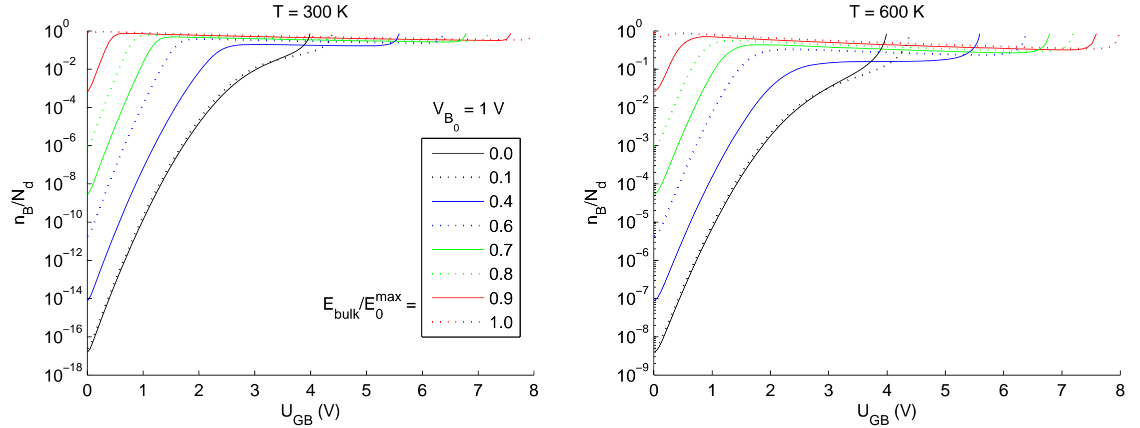

Figure 3.17: Relative electron density at the grain boundary plotted as a function of voltage U_{GB} with various values of the ratio of the electric fields E_{bulk}/E_0^{max} and $V_B = 1$ V at temperatures of 300 K (*left*) and 600 K (*right*). Calculated using Eq. 3.106.

Figs. 3.16 and 3.17, respectively. The effect of the bulk electric field E_{bulk} is shown at high voltages in Figs. 3.16 and 3.17: When the ratio E_{bulk}/E_0^{max} is increased a plateau appears in the graphs. The plateau effectively shifts the ends of the curves to higher voltages (cf. the condition of Eq. 3.35). This allows the voltage across the grain-boundary region U_{GB} to be higher than it can be in the case $E_{bulk} = 0$.

3.4 Electronic trapping at grain boundary

In a large band-gap n-type semiconductor the effect of holes can usually be neglected. In this case the electronic trapping at grain-boundaries the electronic trapping rate equation (Eq. 2.11) can be written as [50]

$$\frac{dN_B}{dt} = k_n n_B \left(N_B^{tot} - N_B\right) - k_{-n} N_c N_B, \tag{3.107}$$

where k_n and k_{-n} are the capture (i.e. trapping) and emission (i.e. releasing) coefficients of electrons, N_B the density of occupied grain-boundary electronic states, N_B^{tot} the total density of grain-boundary electronic states, and n_B the density of electrons at the grain boundary, respectively. Here the capture coefficient of electrons is denoted by k_n instead of c_n and it is given by Eq. 2.12. If the Fermi-Dirac statistics are used the capture and emission coefficients of electrons are interrelated by (cf. Eq. 2.20)

$$k_{-n} = k_n e^{-(E_c - E_T)/k_B T}. \tag{3.108}$$

Eq. 3.107 applies also to chemically induced electronic traps if the total density of chemically induced electronic traps (i.e. N_B^{tot} in Eq. 3.107) is constant [11]. In the case of chemisorbed gas atoms or molecules this is not always true.

The electronic energy bands in the grain-boundary region in the flat-band case and in the thermodynamical equilibrium are illustrated in Fig. 3.18. Based on Fig. 3.18 the difference between the Fermi level and the trap level can be written as

$$E_T - E_F = E_c^{bulk} - E_F + qV_B - \left(E_c^{GB} - E_T\right). \tag{3.109}$$

In the flat-band case $V_B = 0$ (see Fig. 3.18) and Eq. 3.109 reduces to

$$\left(E_T - E_F\right)_{V_B=0} = E_c^{bulk} - E_F - \left(E_c^{GB} - E_T\right), \tag{3.110}$$

where $E_c^{GB} = E_c^{bulk}$. The both of the terms in Eq. 3.110, the position of the Fermi level in the bulk and the position of the trap level, do not depend on the band bending, i.e. they are constant. Plugging Eq. 3.110 in Eq. 3.109 gives (cf. Ref. [51])

$$E_T - E_F = \left(E_T - E_F\right)_{V_B=0} + qV_B. \tag{3.111}$$

In the thermodynamical equilibrium the occupation probability of the trap states are given by the Fermi-Dirac distribution function (cf. Eqs. 2.16 and 2.18 and Ref. [19])

$$f_n = \frac{N_B^{eq}}{N_B^{tot}} = \frac{1}{1 + \exp\left(\frac{E_T - E_F}{k_B T}\right)} = \frac{1}{1 + \exp\left[\frac{(E_T - E_F)_{V_B=0} + qV_B^{eq}}{k_B T}\right]}, \tag{3.112}$$

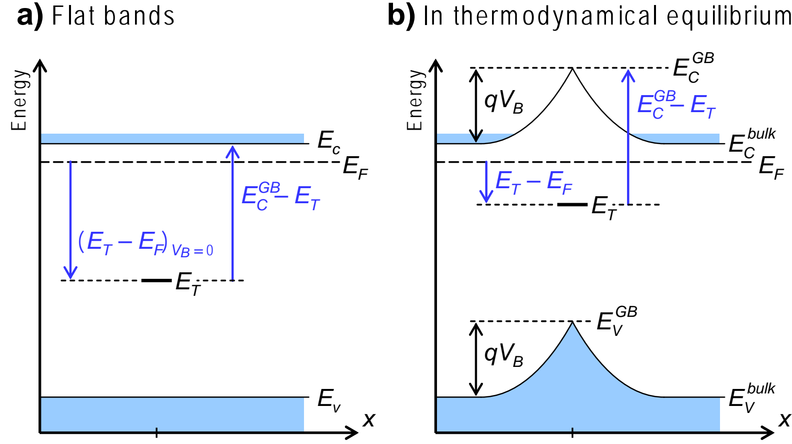

Figure 3.18: Schematic picture of electronic energy bands in the grain-boundary region in n-type semiconductor *a)* in the flat-band case (i.e. without band bending, $V_B = 0$) and *b)* in the thermodynamical equilibrium. E_c is the bottom of the conduction band, E_v the top of the valence band, E_F the Fermi level, E_T the acceptor-type interface trap state level, q the electron charge, and V_B the grain-boundary potential barrier, respectively.

where Eq. 3.111 was used. Here the values of N_B and V_B in the thermodynamical equilibrium are denoted by N_B^{eq} and V_B^{eq}. In Eq. 3.112 N_B^{eq} depends on V_B^{eq} via Eq. 3.10, hence it must be numerically solved from

$$N_B^{eq} = \frac{N_B^{tot}}{1 + \exp\left[\frac{(E_T - E_F)_{V_B=0} + \frac{\left(qN_B^{eq}\right)^2}{8\varepsilon N_d}}{k_B T} + 1\right]}. \tag{3.113}$$

With the help of Eq. 3.10 Eqs. 3.112 and 3.113 can also be written as

$$f_n = \sqrt{\frac{V_{B_0}^{eq} - \frac{k_B T}{q}}{V_{B_0}^{tot} - \frac{k_B T}{q}}} = \frac{1}{1 + \exp\left[\frac{(E_T - E_F)_{V_B=0} + qV_{B_0}^{eq}}{k_B T}\right]}, \tag{3.114}$$

where $V_{B_0}^{eq}$ is the value of V_{B_0} in the thermodynamical equilibrium and $V_{B_0}^{tot} = \frac{q\left(N_B^{tot}\right)^2}{8\varepsilon N_d} + \frac{k_B T}{q}$, respectively. V_B^{tot} is the height of the grain-boundary potential barrier when all the interface trap states are filled, i.e. it is the maximum height of the grain-boundary potential barrier.

The occupation probability of the acceptor-type interface trap states in the thermodynamical equilibrium f_n as a function of the energy level of the trap state

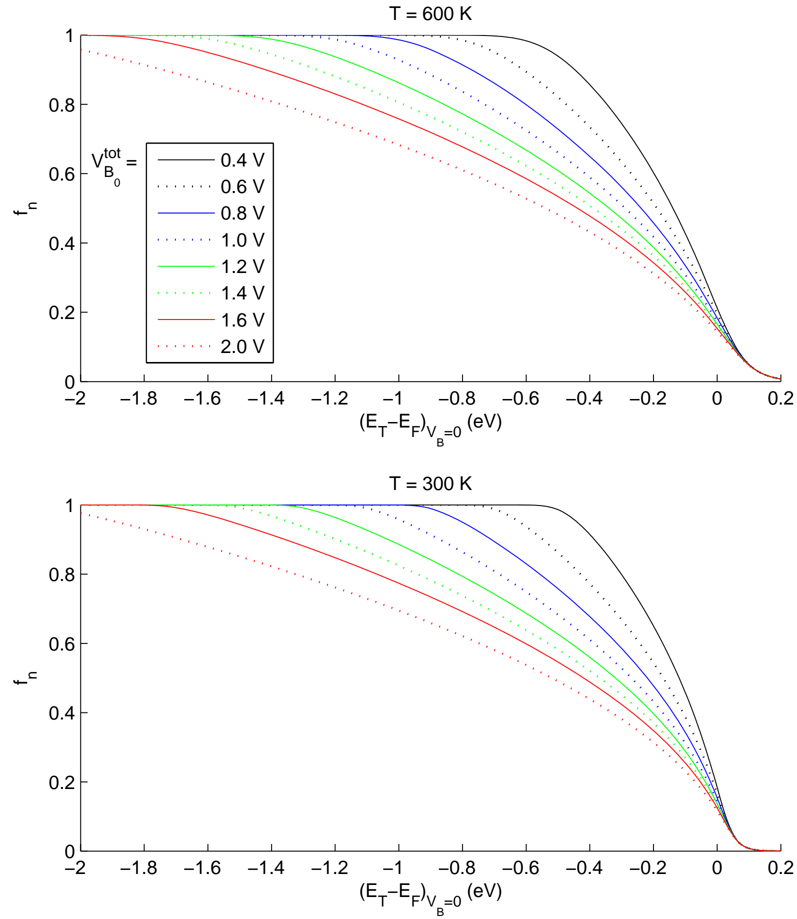

Figure 3.19: Occupation probability of the acceptor-type interface trap states in the thermodynamical equilibrium f_n plotted as a function of the energy level of the trap state $(E_T - E_F)_{V_B=0}$ with various values of $V_{B_0}^{tot}$ at temperatures of 600 K (*top*) and 300 K (*bottom*). Calculated numerically using Eq. 3.114.

$(E_T - E_F)_{V_B=0}$ with various values of $V_{B_0}^{tot}$ is plotted in Fig. 3.19. The typical features of the Fermi distribution function is shown in Fig. 3.19: the occupation probability is highly dependent on the difference between the energy level E_T and the Fermi level, and the shape of the curves broaden when the temperature is increased. Fig. 3.19 shows also that the trap state does not have to lie very deep below the Fermi level in order to be over half filled: for example even with a very high value of $V_{B_0}^{tot} = 2.0$ V the state, which lies in $(E_T - E_F)_{V_B=0} \leq -0.5$ V, is over 50 % filled ($f_n \geq 0.5$) at 300–600 K.

In this section the most of the formulas are given in the normalized form, in which

the dimensionless variable is the normalized density of the occupied grain-boundary states

$$\nu \equiv \frac{N_B}{N_B^{eq}}, \tag{3.115}$$

where N_B^{eq} is the value of the density of occupied grain-boundary states in the thermodynamical equilibrium. The normalized quantity of Eq. 3.115 allows the other important quantities to be written in terms of their thermodynamical equilibrium values:

$$L_d = \frac{N_B N_B^{eq}}{N_d N_B^{eq}} = \nu L_d^{eq} \tag{3.116}$$

and

$$V_{B_0} = \nu^2 \left(V_{B_0}^{eq} - \frac{k_B T}{q} \right) + \frac{k_B T}{q}, \tag{3.117}$$

where Eqs. 3.10, 3.11, and 3.16 were used. If Eq. 3.21 is used for calculating the total width of the depletion region, the Debye length L_D (Eq. 2.9) must be normalized as well:

$$L_D = L_D^{eq} \sqrt{\frac{T}{T_{eq}}}. \tag{3.118}$$

3.4.1 Correction to rate equation

It turns out that the accurate consideration of the electric properties of grain boundaries in the dynamical case yields a correction to the rate equation (see section 3.5): the density of electrons at the grain boundary n_B in Eq. 3.107 must be replaced with Eq. 3.151. Now, Eq. 3.107 can be written as

$$\frac{dN_B}{dt} = \frac{k_n n_B^{DC} \left(N_B^{tot} - N_B \right) - k_{-n} N_c N_B}{1 + \xi \frac{N_B^{tot} - N_B}{N_B}}, \tag{3.119}$$

where n_B^{DC} is the density of electrons at the grain boundary in steady state and

$$\xi = \frac{k_n \varepsilon \eta}{q \mu} \tag{3.120}$$

is the delay coefficient. The parameter η is defined by Eq. 3.136 (see section 3.5). The effect of the new term in the corrected rate equation (Eq. 3.119) is addition of delay to the changing rate of N_B. The delay is caused by the finite drift speed of electrons travelling across the grain-boundary region. Often the value of ξ is small and the delay effect can be neglected allowing the original rate equation (Eq. 3.107) to be used instead. In addition, the delay term has no effect in the steady state.

3.4.2 Steady state solution of rate equation

In the steady state Eqs. 3.107 and 3.119 reduce to

$$\frac{N_B}{N_B^{tot}} = \frac{n_B}{n_B + \frac{k_{-n}}{k_n} N_c} = \frac{1}{1 + \frac{N_c}{n_B} e^{-(E_c - E_T)/k_B T}}, \tag{3.121}$$

where Eq. 3.108 was used. In the thermodynamical equilibrium at temperature T_{eq} assuming that N_B^{tot} is constant Eq. 3.121 gives

$$N_c^{eq} = n_B^{eq} \frac{k_n^{eq}}{k_{-n}^{eq}} \left[\frac{N_B^{tot}}{N_B^{eq}} - 1 \right] = n_B^{eq} e^{(E_c - E_T)/k_B T_{eq}} \left[\frac{1}{f_n^{eq}} - 1 \right], \tag{3.122}$$

where Eq. 3.112 and $f_n^{eq} \equiv f_n(T_{eq}, V_B^{eq})$ were used and n_B^{eq}, k_n^{eq}, and k_{-n}^{eq} denote the quantities in the thermodynamical equilibrium. Eq. 2.3 gives a relation

$$\frac{N_c}{N_c^{eq}} = \left(\frac{T}{T_{eq}} \right)^{3/2}. \tag{3.123}$$

Plugging Eqs. 3.122 and 3.123 in Eq. 3.121 gives

$$\frac{N_B}{N_B^{tot}} = \frac{\frac{n_B}{n_B^{eq}}}{\frac{n_B}{n_B^{eq}} + \exp\left[\frac{E_c - E_T}{k_B} \left(\frac{1}{T_{eq}} - \frac{1}{T} \right) \right] \left(\frac{1}{f_n^{eq}} - 1 \right) \left(\frac{T}{T_{eq}} \right)^{3/2}}. \tag{3.124}$$

By writing $\frac{N_B}{N_B^{tot}} = \frac{N_B N_B^{eq}}{N_B^{eq} N_B^{tot}} = f_n^{eq} \frac{N_B}{N_B^{eq}}$ and using Eq. 3.124, N_B can be normalized in respect to N_B^{eq} as

$$\nu = \frac{N_B}{N_B^{eq}} = \frac{\frac{n_B}{n_B^{eq}}}{f_n^{eq} \frac{n_B}{n_B^{eq}} + \exp\left[\frac{E_c - E_T}{k_B} \left(\frac{1}{T_{eq}} - \frac{1}{T} \right) \right] (1 - f_n^{eq}) \left(\frac{T}{T_{eq}} \right)^{3/2}}. \tag{3.125}$$

At $T = T_{eq}$ Eq. 3.125 reduces to

$$\nu = \frac{\frac{n_B}{n_B^{eq}}}{1 + f_n^{eq} \left(\frac{n_B}{n_B^{eq}} - 1 \right)}. \tag{3.126}$$

3.4.3 Normalization of rate equation

Ordinary rate equation

Dividing the rate equation of Eq. 3.107 by N_B^{eq} gives

$$\frac{d\nu}{dt} = \frac{d}{dt} \left(\frac{N_B}{N_B^{eq}} \right) = k_n \frac{k_n^{eq}}{k_n^{eq}} n_B \left(\frac{1}{f_n^{eq}} - \nu \right) - k_{-n} N_c \nu, \tag{3.127}$$

where it was assumed that the total density of states N_B^{tot} is constant. Eq. 3.122 can be written as

$$k_n^{eq} = \frac{k_{-n}^{eq} N_c^{eq} f_n^{eq}}{n_B^{eq} (1 - f_n^{eq})}. \tag{3.128}$$

Plugging Eq. 3.128 into Eq. 3.127 gives

$$\frac{d\nu}{dt} = k_n^{eq} N_c^{eq} \frac{k_n}{k_n^{eq}} e^{-(E_c - E_T)/k_B T_{eq}} \frac{n_B}{n_B^{eq}} \frac{1 - f_n^{eq}\nu}{1 - f_n^{eq}} - k_n N_c e^{-(E_c - E_T)/k_B T} \nu, \tag{3.129}$$

where Eq. 3.108 was used. Eqs. 2.12 and 2.14 give the ratio of electron capture coefficients

$$\frac{k_n^{eq}}{k_n} = \frac{v_{Tn}(T_{eq})}{v_{Tn}(T)} = \sqrt{\frac{T_{eq}}{T}}. \tag{3.130}$$

Finally, substituting Eq. 3.130 in Eq. 3.129 gives

$$\frac{d\nu}{dt} = k_n^{eq} N_c^{eq} \sqrt{\frac{T}{T_{eq}}} \left[\frac{n_B}{n_B^{eq}} \left(\frac{1 - f_n^{eq}\nu}{1 - f_n^{eq}} \right) e^{-\frac{E_c - E_T}{k_B T_{eq}}} - \nu \left(\frac{T}{T_{eq}} \right)^{3/2} e^{-\frac{E_c - E_T}{k_B T}} \right]. \tag{3.131}$$

At $T = T_{eq}$ Eq. 3.131 reduces to

$$\frac{d\nu}{dt} = k_n^{eq} N_c^{eq} e^{-\frac{E_c - E_T}{k_B T}} \left[\frac{n_B}{n_B^{eq}} \left(\frac{1 - f_n^{eq}\nu}{1 - f_n^{eq}} \right) - \nu \right]. \tag{3.132}$$

Corrected rate equation

Eqs. 3.131 and 3.132 were derived from the rate equation of Eq. 3.107. Using the corrected rate equation of Eq. 3.119 instead yields

$$\frac{d\nu}{dt} = \frac{k_n^{eq} N_c^{eq} \sqrt{\frac{T}{T_{eq}}} \left[\frac{n_B}{n_B^{eq}} \left(\frac{1 - f_n^{eq}\nu}{1 - f_n^{eq}} \right) e^{-\frac{E_c - E_T}{k_B T_{eq}}} - \nu \left(\frac{T}{T_{eq}} \right)^{3/2} e^{-\frac{E_c - E_T}{k_B T}} \right]}{1 + \xi_{eq} \sqrt{\frac{T}{T_{eq}}} \left(\frac{1 - f_n^{eq}\nu}{f_n^{eq}\nu} \right)}, \tag{3.133}$$

where

$$\xi_{eq} = \frac{k_n^{eq} \varepsilon \eta}{q \mu}. \tag{3.134}$$

At $T = T_{eq}$ Eq. 3.133 reduces to

$$\frac{d\nu}{dt} = \frac{k_n^{eq} N_c^{eq} e^{-\frac{E_c - E_T}{k_B T}} \left[\frac{n_B}{n_B^{eq}} \left(\frac{1 - f_n^{eq}\nu}{1 - f_n^{eq}} \right) - \nu \right]}{1 + \xi_{eq} \left(\frac{1 - f_n^{eq}\nu}{f_n^{eq}\nu} \right)}. \tag{3.135}$$

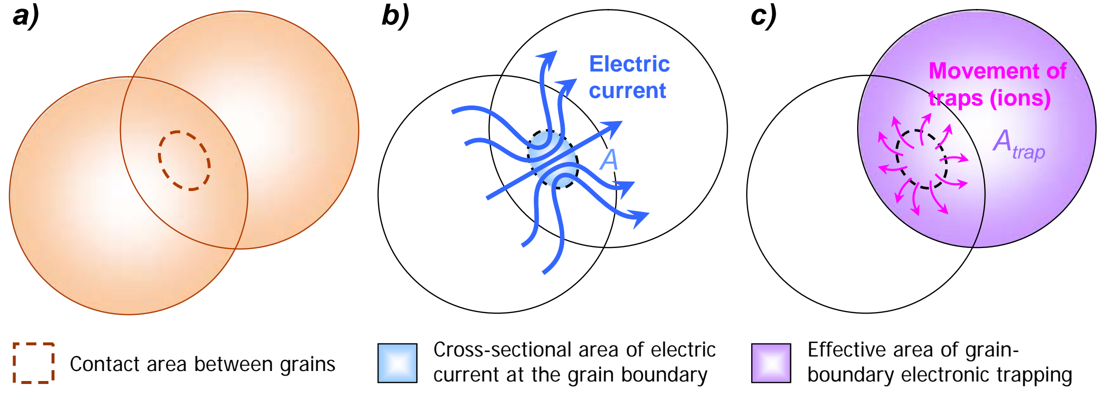

Figure 3.20: Schematic picture of *a)* two interconnected grains, *b)* flow of electric current through the grains, and *c)* movement of traps (i.e. in this case ions) across the surface of the whole grain. A is the cross-sectional area of the electric current flowing at the grain boundary and A_{trap} the effective area of trapping at the grain-boundary, respectively.

3.5 Dynamical electric model of grain boundary

In the dynamical (i.e. time-dependent) case the electric current flowing through the grain-boundary region is not constant due to the displacement current and the time-dependent grain-boundary charge N_B. Here it is assumed that no generation or recombination takes place in the depletion regions or in the bulk.

If the cross-sectional area of the path of current A is small compared to the dimensions of the grain boundary (i.e. the contact area between the grains) and the traps are mobile (i.e. mobile ions), trapping may take place in a larger area than A. This is phenomenon illustrated in Fig. 3.20. The mobile traps can easily exist in granular gas sensing materials, in which adsorbed atoms and molecules are mostly responsible for trapping (i.e. ionization) processes [5, 9]. This effect can be taken into account with a parameter

$$\eta = \frac{A_{trap}}{A}, \tag{3.136}$$

where A_{trap} is the cross-sectional area in which trapping can occur. Here all the equations are derived by using the parameter of Eq. 3.136. The parameter value of $\eta = 1$ corresponds to the usual case of immobile traps.

The density of current flowing in regions I and II (see Figs. 3.1 and 3.13) are denoted by J_I and J_{II}, respectively. At the grain boundary the continuity equation, $\vec{\nabla} \cdot \vec{J} =$

$-\frac{\partial \rho}{\partial t}$ [24], gives a relation between the current densities

$$J_{II} - J_I = q\eta \frac{dN_B}{dt}. \tag{3.137}$$

In steady state $J_I = J_{II}$ and the total current flowing through the barrier region is J_{GB}^{DC}. J_{GB}^{DC} is given by Eq. 3.56. J_I and J_{II} are related by Eq. 3.55. Substituting Eq. 3.56 in Eq. 3.55 gives

$$J_{GB}^{DC} = \frac{J_I \mathcal{I}_I + J_{II} \mathcal{I}_{II}}{\mathcal{I}_{tot}}, \tag{3.138}$$

where $\mathcal{I}_I$, $\mathcal{I}_{II}$, and $\mathcal{I}_{tot}$ are given by Eqs. 3.51, 3.54, and 3.57. Plugging Eq. 3.137 in Eq. 3.138 gives

$$J_I = J_{GB}^{DC} - \frac{\mathcal{I}_{II}}{\mathcal{I}_{tot}} q\eta \frac{dN_B}{dt}. \tag{3.139}$$

With the help of Eqs. 3.50 and 3.139 the density of electrons at the grain boundary in the dynamical case can be written as

$$n_B = e^{-\frac{qV_B}{k_B T}} \left[N_d + \frac{J_I \mathcal{I}_I}{qD} \right] = n_B^{DC} - \frac{\eta}{D} e^{-\frac{qV_B}{k_B T}} \cdot \frac{\mathcal{I}_I \mathcal{I}_{II}}{\mathcal{I}_{tot}} \cdot \frac{dN_B}{dt}, \tag{3.140}$$

where n_B^{DC} is the density of electrons at the grain boundary in steady state.

In the dynamical case the total current density is the sum of the free current density $\vec{J}$ and the displacement current:

$$\vec{J}_{tot} = \vec{J} + \vec{J}_D. \tag{3.141}$$

In a linear isotropic material the displacement current is given by

$$\vec{J}_D = \frac{\partial \vec{D}}{\partial t} = \varepsilon \frac{\partial \vec{E}}{\partial t}, \tag{3.142}$$

where $\vec{D}$ is the electric displacement field. In region I the total current density is given by

$$J_{GB}^{tot} = J_I + \varepsilon \frac{dE_I}{dt} = J_{GB}^{DC} - \frac{\mathcal{I}_{II}}{\mathcal{I}_{tot}} q\eta \frac{dN_B}{dt} + \varepsilon \frac{dE_I}{dt}, \tag{3.143}$$

where Eq. 3.139 was used.

3.5.1 Calculation using linear potential and approximations

When the linear potential profile is used, $E_I = E_I^{max}$ (Eq. 3.38) and the integrals $\mathcal{I}_I$ and $\mathcal{I}_{II}$ are given by Eqs. 3.58 and 3.59. These formulas and Eqs. 3.57 and 3.64 give

$$\frac{\mathcal{I}_{II}}{\mathcal{I}_{tot}} = \frac{\left(1+\frac{U_{GB}}{4V_{B_0}}\right)\left(1-e^{-\frac{qV_{B_0}}{k_BT}\left[1+\left(\frac{U_{GB}}{4V_{B_0}}\right)^2\right]+\frac{qU_{GB}}{2k_BT}}\right)}{2-2e^{-\frac{qV_{B_0}}{k_BT}\left[1+\left(\frac{U_{GB}}{4V_{B_0}}\right)^2\right]}\left(\cosh\frac{qU_{GB}}{2k_BT}+\frac{U_{GB}}{4V_{B_0}}\sinh\frac{qU_{GB}}{2k_BT}\right)} \approx \frac{1}{2}\left(1+\frac{U_{GB}}{4V_{B_0}}\right) \tag{3.144}$$

and

$$\begin{aligned}\frac{\mathcal{I}_I\mathcal{I}_{II}}{\mathcal{I}_{tot}} &= \frac{k_BT}{qE_0^{max}}e^{\frac{qV_B}{k_BT}}\cdot\frac{1+2e^{-\frac{qV_{B_0}}{k_BT}\left[1+\left(\frac{U_{GB}}{4V_{B_0}}\right)^2\right]}\cosh\frac{qU_{GB}}{2k_BT}+e^{-\frac{2qV_{B_0}}{k_BT}\left[1+\left(\frac{U_{GB}}{4V_{B_0}}\right)^2\right]}}{2-2e^{-\frac{qV_{B_0}}{k_BT}\left[1+\left(\frac{U_{GB}}{4V_{B_0}}\right)^2\right]}\left(\cosh\frac{qU_{GB}}{2k_BT}+\frac{U_{GB}}{4V_{B_0}}\sinh\frac{qU_{GB}}{2k_BT}\right)}\\ &\approx \frac{k_BT}{2qE_0^{max}}e^{\frac{qV_B}{k_BT}}.\end{aligned} \tag{3.145}$$

The time dependence of the electric field in the region I both with the linear and quadratic the potential profiles is given by

$$\frac{dE_I}{dt} = \frac{dE_I^{max}}{dt}, \tag{3.146}$$

where Eq. 3.39 and $\frac{dx_{d_1}}{dt} = \frac{x_{d_1}}{E_I^{max}-E_{bulk}}\left(\frac{dE_I^{max}}{dt}-\frac{dE_{bulk}}{dt}\right)$ (see Eqs. 3.31 and 3.39) were used. Plugging Eq. 3.38 in Eq. 3.146 gives

$$\begin{aligned}\frac{dE_I}{dt} &= \frac{dE_0^{max}}{dt}\left(1+\frac{U_{GB}}{4V_{B_0}}\right)+\frac{E_0^{max}}{4V_{B_0}}\frac{dU_{GB}}{dt}+\frac{E_0^{max}U_{GB}}{4}\underbrace{\frac{d}{dt}\left(\frac{1}{V_{B_0}}\right)}_{-\frac{2}{N_BV_{B_0}}\cdot\frac{dN_B}{dt}}\\ &= \frac{q}{2\varepsilon}\frac{dN_B}{dt}\left(1-\frac{U_{GB}}{4V_{B_0}}\right)+\frac{N_d}{N_B}\frac{dU_{GB}}{dt},\end{aligned} \tag{3.147}$$

where Eq. 3.17 was used. Substituting Eqs. 3.147 and 3.144 into Eq. 3.143 gives

$$J_{GB}^{tot} = J_{GB}^{DC}-\frac{1}{2}q\frac{dN_B}{dt}\left[\eta-1+\frac{U_{GB}}{4V_{B_0}}(\eta+1)\right]+\frac{\varepsilon}{L_d}\cdot\frac{dU_{GB}}{dt}, \tag{3.148}$$

where Eq. 3.23 was used. When $\eta = 1$ Eq. 3.148 reduces to [12]

$$J_{GB}^{tot} = J_{GB}^{DC} - \frac{U_{GB}}{4V_{B_0}} \cdot q\frac{dN_B}{dt} + \frac{\varepsilon}{L_d} \cdot \frac{dU_{GB}}{dt}. \tag{3.149}$$

In Eq. 3.149 it must be noted that L_d is dependent on N_B (see Eq. 3.11). The last term in Eqs. 3.148 and 3.149 corresponds to the characteristics of an ideal capacitor, $I = C\,\frac{dU}{dt}$ [52]. Thus the capacitance of the grain-boundary region is given by

$$C_{dep} = \varepsilon\,\frac{A}{L_d^{corr}}, \tag{3.150}$$

where L_d was replaced with L_d^{corr} (see Eq. 3.21) and A is the cross-sectional area of the grain-boundary region. Eq. 3.150 has exactly the same form as the formula of an ideal plate capacitor with the area A and the distance between the plates L_d^{corr}. If the grain-boundary charge does not change with time, Eq. 3.149 corresponds to a parallel RC circuit. A more detailed treatment of the first two terms in Eq. 3.149 requires the modelling of the dynamics of N_B.

Substitution of Eq. 3.145 in Eq. 3.140 gives

$$n_B = n_B^{DC} - \frac{\eta}{2\mu E_0^{max}} \cdot \frac{dN_B}{dt} = n_B^{DC} - \frac{\varepsilon\eta}{q\mu} \cdot \frac{1}{N_B} \cdot \frac{dN_B}{dt}, \tag{3.151}$$

where Einstein's relation (Eq. 2.10) was used. The term $2\mu E_0^{max}$ in the intermediate form of Eq. 3.151 is twice the drift velocity of electrons in the electric field with a magnitude of E_0^{max}. Hence, in the dynamical case the density of electrons at the grain boundary n_B is reduced or increased by the ratio of the rate of change of N_B and the drift velocity of electrons. In other words, the amount of trapped charge (determined by N_B) can only change through movement of electrons through the grain-boundary region. The speed of electrons is given by the drift velocity. The overall effect of this is finite speed is merely a delay effect when rapid changes in N_B take place: A rapid increase of N_B causes a brief reduction of the density of electrons n_B from its steady state value n_B^{DC}. In the opposite case, a rapid decrease of N_B causes a brief increase of n_B from its steady state value. Together with the electronic trapping rate equation Eq. 3.151 leads to the introduction of the delay coefficient ξ (see section 3.4.1).

3.5.2 Electrical equivalent circuit model

Here the electrical equivalent circuit (EEC) model for the grain boundary is obtained by linearizing the approximative formula of the density total current flowing through

the grain-boundary region (Eq. 3.148). The EEC model was originally briefly presented in Ref. [12]. In order to simplify the derivation the simplest formulas are used for the DC current flowing through the grain-boundary region (Eq. 3.71) and the electron density at the grain boundary (Eq. 3.72), which is with help of Eq. 3.117 written in the form

$$\frac{n_B}{n_B^{eq}} = \exp\left[-\left(\frac{qV_{B_0}^{eq}}{k_B T} - 1\right)\left(\nu^2 - 1\right)\right]\cosh\frac{qU_{GB}}{2k_B T}. \tag{3.152}$$

First, the rate equation describing the density of the occupied grain-boundary states is linearized. Here the normalized rate equation is used (see section 3.4.3). Using Eq. 3.152, Eq. 3.135 can be written as

$$\frac{d\nu}{dt} = \frac{k_{-i}^{eq}\left\{\exp\left[-\left(\frac{qV_{B_0}^{eq}}{k_B T} - 1\right)\left(\nu^2 - 1\right)\right]\cosh\frac{qU_{GB}}{2k_B T}\left(\frac{1-f_n^{eq}\nu}{1-f_n^{eq}}\right) - \nu\right\}}{1 + \xi_{eq}\left(\frac{1-f_n^{eq}\nu}{f_n^{eq}\nu}\right)}, \tag{3.153}$$

where ξ_{eq} is given by Eq. 3.134 and

$$k_{-i}^{eq} = k_n^{eq} N_c^{eq} e^{-\frac{E_c - E_T}{k_B T_{eq}}} \tag{3.154}$$

is the so-called reverse rate constant of ionization in the thermodynamical equilibrium (i.e. the prefactor of the normalized rate equation).

The linearization is performed by assuming that the voltage across the grain boundary U_{GB} and the normalized density of the occupied grain-boundary states ν can be written as the sum of DC (i.e. time-independent) and time-dependent components

$$U_{GB}(t) = U_{GB}^{DC} + \delta U_{GB}(t) \tag{3.155}$$

$$\nu(t) = \nu_{DC} + \delta\nu(t), \tag{3.156}$$

where the time-dependent components δU and $\delta\nu$ are assumed to be small. The linearized form of the normalized rate equation is given by

$$\frac{\delta\nu}{\delta t} = \frac{\partial}{\partial U}\left(\frac{d\nu}{dt}\right)\Bigg|_{\substack{\nu=\nu_{DC}\\ U_{GB}=U_{GB}^{DC}}} \delta U + \frac{\partial}{\partial \nu}\left(\frac{d\nu}{dt}\right)\Bigg|_{\substack{\nu=\nu_{DC}\\ U_{GB}=U_{GB}^{DC}}} \delta\nu. \tag{3.157}$$

The derivatives of Eq. 3.153 with respect to the voltage U_{GB} and ν are

$$\frac{\partial}{\partial U_{GB}}\left(\frac{d\nu}{dt}\right)\Bigg|_{\substack{\nu=\nu_{DC}\\ U_{GB}=U_{GB}^{DC}}} = \frac{k_{-i}^{eq} q\left(1 - f_n^{eq}\nu_{DC}\right)}{2k_B T} \cdot \frac{e^{-\left(\frac{qV_{B_0}^{eq}}{k_B T} - 1\right)\left(\nu_{DC}^2 - 1\right)}\sinh\left(\frac{qU_{GB}^{DC}}{2k_B T}\right)}{\left[1 + \xi_{eq}\left(\frac{1}{f_n^{eq}\nu_{DC}} - 1\right)\right]\left(1 - f_n^{eq}\right)} \tag{3.158}$$

and

$$\frac{\partial}{\partial \nu}\left(\frac{d\nu}{dt}\right)\Bigg|_{\substack{\nu=\nu_{DC}\\ U_{GB}=U_{GB}^{DC}}} = -\frac{k_{-i}^{eq}}{\left[1+\xi_{eq}\left(\frac{1}{f_n^{eq}\nu_{DC}}-1\right)\right]^2}\Bigg\{1+\xi_{eq}\left(\frac{2}{f_n^{eq}\nu_{DC}}-1\right)$$
$$+\frac{\exp\left[-\left(\frac{qV_{B_0}^{eq}}{k_BT}-1\right)\left(\nu_{DC}^2-1\right)\right]\cosh\left(\frac{qU_{GB}^{DC}}{2k_BT}\right)}{1-f_n^{eq}}\cdot\Bigg[\tag{3.159}$$
$$2\nu_{DC}\left(\frac{qV_{B_0}^{eq}}{k_BT}-1\right)\left(1-f_n^{eq}\nu_{DC}\right)\left(1+\xi_{eq}\left[\frac{1}{f_n^{eq}\nu_{DC}}-1\right]\right)+f_n^{eq}$$
$$-f_n^{eq}\xi_{eq}\left(\frac{1}{f_n^{eq}\nu_{DC}}-1\right)^2\Bigg]\Bigg\}.$$

When $\xi_{eq}=0$ Eqs. 3.158 and 3.159 reduce to

$$\frac{\partial}{\partial U_{GB}}\left(\frac{d\nu}{dt}\right)\Bigg|_{\substack{\nu=\nu_{DC}\\ U_{GB}=U_{GB}^{DC}}} = \frac{k_{-i}^{eq}q\left(1-f_n^{eq}\nu_{DC}\right)}{2k_BT}\cdot\frac{e^{-\left(\frac{qV_{B_0}^{eq}}{k_BT}-1\right)\left(\nu_{DC}^2-1\right)}\sinh\left(\frac{qU_{GB}^{DC}}{2k_BT}\right)}{1-f_n^{eq}} \tag{3.160}$$

and

$$\frac{\partial}{\partial \nu}\left(\frac{d\nu}{dt}\right)\Bigg|_{\substack{\nu=\nu_{DC}\\ U_{GB}=U_{GB}^{DC}}} = -k_{-i}^{eq}\Bigg\{\frac{\exp\left[-\left(\frac{qV_{B_0}^{eq}}{k_BT}-1\right)\left(\nu_{DC}^2-1\right)\right]\cosh\left(\frac{qU_{GB}^{DC}}{2k_BT}\right)}{1-f_n^{eq}}$$
$$\cdot\left[2\nu_{DC}\left(\frac{qV_{B_0}^{eq}}{k_BT}-1\right)\left(1-f_n^{eq}\nu_{DC}\right)+f_n^{eq}\right]+1\Bigg\}. \tag{3.161}$$

Writing Eq. 3.157 in Fourier space and solving $\delta\nu$ gives

$$\frac{\delta\nu}{\delta t}=i\omega\delta\nu=\frac{\partial}{\partial U_{GB}}\left(\frac{d\nu}{dt}\right)\Bigg|_{\substack{\nu=\nu_{DC}\\ U_{GB}=U_{GB}^{DC}}}\delta U_{GB}+\frac{\partial}{\partial \nu}\left(\frac{d\nu}{dt}\right)\Bigg|_{\substack{\nu=\nu_{DC}\\ U_{GB}=U_{GB}^{DC}}}\delta\nu$$
$$\Rightarrow \delta\nu=\frac{\frac{\partial}{\partial U_{GB}}\left(\frac{d\nu}{dt}\right)\Big|_{\substack{\nu=\nu_{DC}\\ U_{GB}=U_{GB}^{DC}}}}{-\frac{\partial}{\partial \nu}\left(\frac{d\nu}{dt}\right)\Big|_{\substack{\nu=\nu_{DC}\\ U_{GB}=U_{GB}^{DC}}}+i\omega}\delta U_{GB}. \tag{3.162}$$

The density of the total current flowing through the grain-boundary region is given by Eq. 3.148. However, because of the electronic trapping the normalized density

of occupied states is time-dependent (cf. Eq. 3.156), the term J_{GB}^{DC} consists of two components: the normal grain-boundary barrier limited current and a term which is caused by the modulation of the grain-boundary barrier. Using the simplest formula for J_{GB}^{DC} (Eq. 3.71) and Eq. 3.117 the DC electric current can be written as

$$I_{GB}^{DC} = I_0 \nu \sqrt{2} \sqrt{V_{B_0}^{eq} - \frac{k_B T}{q}} \exp\left[-\nu^2 \left(\frac{qV_{B_0}^{eq}}{k_B T} - 1\right) - 1\right] \sinh \frac{qU_{GB}}{2k_B T}, \tag{3.163}$$

where $I_0 = AJ_0$ (see Eq. 3.66). The linearized I_{GB}^{DC} is given by

$$\delta I_{GB}^{DC} = \overbrace{\left.\frac{\partial I_{GB}^{DC}}{\partial U_{GB}}\right|_{\substack{\nu=\nu_{DC} \\ U_{GB}=U_{GB}^{DC}}} \delta U_{GB}}^{I_{diff}} + \overbrace{\left.\frac{\partial I_{GB}^{DC}}{\partial \nu}\right|_{\substack{\nu=\nu_{DC} \\ U_{GB}=U_{GB}^{DC}}} \delta \nu}^{I_{mod}}, \tag{3.164}$$

where I_{diff} and I_{mod} are the currents corresponding to the differential (i.e. AC) barrier-limited conductance and the modulation of the grain-boundary potential barrier, respectively. The derivatives of Eq. 3.163 are

$$\left.\frac{\partial I_{GB}^{DC}}{\partial U_{GB}}\right|_{\substack{\nu=\nu_{DC} \\ U_{GB}=U_{GB}^{DC}}} = \frac{qI_0 \nu_{DC}}{\sqrt{2}\, k_B T} \sqrt{V_{B_0}^{eq} - \frac{k_B T}{q}} e^{-\nu_{DC}^2 \left(\frac{qV_{B_0}^{eq}}{k_B T} - 1\right) - 1} \cosh \frac{qU_{GB}^{DC}}{2k_B T}. \tag{3.165}$$

and

$$\left.\frac{\partial I_{GB}^{DC}}{\partial \nu}\right|_{\substack{\nu=\nu_{DC} \\ U_{GB}=U_{GB}^{DC}}} =$$
$$- I_0 \sqrt{2} \sqrt{V_{B_0}^{eq} - \frac{k_B T}{q}} e^{-\nu_{DC}^2 \left(\frac{qV_{B_0}^{eq}}{k_B T} - 1\right) - 1} \sinh \frac{qU_{GB}^{DC}}{2k_B T} \left[2\nu_{DC}^2 \left(\frac{qV_{B_0}^{eq}}{k_B T} - 1\right) - 1\right]. \tag{3.166}$$

Finally, the total current flowing through the grain-boundary region can be written as

$$I_{GB}^{tot} = \overbrace{I_{diff} + I_{mod}}^{I_{GB}^{DC}} \overbrace{- \frac{1}{2} qA \frac{dN_B}{dt} \left[\eta - 1 + \frac{U_{GB}^{DC}}{4V_{B_0}} (\eta + 1)\right]}^{I_{char}} + \overbrace{A \frac{\varepsilon}{L_d} \cdot \frac{dU_{GB}}{dt}}^{I_{cap}}, \tag{3.167}$$

where I_{char} is the current corresponding to charging and discharging (i.e. trapping and releasing) of the grain boundary electronic states and I_{cap} the capacitive current, respectively.

The differential conductance is given by

$$\delta G = I_{diff}/\delta U_{GB} = \frac{qI_0\nu_{DC}}{\sqrt{2}\,k_BT}\sqrt{V_{B_0}^{eq} - \frac{k_BT}{q}}e^{-\nu_{DC}^2\left(\frac{qV_{B_0}^{eq}}{k_BT}-1\right)-1}\cosh\frac{qU_{GB}^{DC}}{2k_BT}, \tag{3.168}$$

where Eqs. 3.164 and 3.165 were used.

The modulating current is given by Eqs. 3.162 and 3.166:

$$I_{mod} = \left.\frac{\partial I_{GB}^{DC}}{\partial \nu}\right|_{\substack{\nu=\nu_{DC}\\ U_{GB}=U_{GB}^{DC}}}\delta\nu = \frac{\left.\frac{\partial I_{GB}^{DC}}{\partial \nu}\right|_{\substack{\nu=\nu_{DC}\\ U_{GB}=U_{GB}^{DC}}} \left.\frac{\partial}{\partial U_{GB}}\left(\frac{d\nu}{dt}\right)\right|_{\substack{\nu=\nu_{DC}\\ U_{GB}=U_{GB}^{DC}}}}{-\left.\frac{\partial}{\partial \nu}\left(\frac{d\nu}{dt}\right)\right|_{\substack{\nu=\nu_{DC}\\ U_{GB}=U_{GB}^{DC}}} + i\omega}\delta U_{GB}. \tag{3.169}$$

The response function of Eq. 3.169 can be represented by a series RL circuit. The admittance Y of an ideal series RL circuit is given by

$$Y = \frac{1}{R+i\omega L} = \frac{\frac{1}{L}}{\frac{1}{\tau}+i\omega} = \frac{1}{R}\cdot\frac{1-i\omega\tau}{\tau^2\omega^2+1}, \tag{3.170}$$

where $\tau = L/R$ is the time constant of the circuit. Comparison of Eqs. 3.169 and 3.170 gives

$$L_{mod} = \left[\left.\frac{\partial I_{GB}^{DC}}{\partial \nu}\right|_{\substack{\nu=\nu_{DC}\\ U_{GB}=U_{GB}^{DC}}} \left.\frac{\partial}{\partial U_{GB}}\left(\frac{d\nu}{dt}\right)\right|_{\substack{\nu=\nu_{DC}\\ U_{GB}=U_{GB}^{DC}}}\right]^{-1} \tag{3.171}$$

$$\tau_{mod} = -\left[\left.\frac{\partial}{\partial \nu}\left(\frac{d\nu}{dt}\right)\right|_{\substack{\nu=\nu_{DC}\\ U_{GB}=U_{GB}^{DC}}}\right]^{-1} \tag{3.172}$$

$$R_{mod} = L_{mod}/\tau_{mod}. \tag{3.173}$$

With the help of Eqs. 3.115 and 3.117 the formula of the charging current can be written as

$$I_{char} = -\frac{1}{2}qA\frac{dN_B}{dt}\left[\eta - 1 + \frac{U_{GB}}{4V_{B_0}}(\eta+1)\right] = -I_{char}^0\frac{d\nu}{dt}, \tag{3.174}$$

where the prefactor is defined by

$$I_{char}^0 = \frac{1}{2}qAN_B^{eq}\left[\eta - 1 + \frac{U_{GB}(\eta+1)}{4\left[\nu^2\left(V_{B_0}^{eq}-\frac{k_BT}{q}\right)+\frac{k_BT}{q}\right]}\right]. \tag{3.175}$$

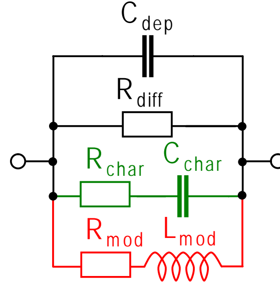

Figure 3.21: Electrical equivalent circuit (EEC) of the grain-boundary region [12]. C_{dep} is the depletion region capacitance and R_{diff} the resistor corresponding to the differential conductance. The circuit branch R_{char}–C_{char} (*green*) corresponds to the charging and discharging current and the circuit branch R_{mod}–L_{mod} (*red*) to the modulation of the grain-boundary potential barrier. The values of the circuit elements in the circuit branches R_{char}–C_{char} and R_{mod}–L_{mod} are negative.

Writing linearized Eq. 3.174 in Fourier space and plugging in Eq. 3.162 gives

$$\delta I_{char} = -I^0_{char} \cdot \frac{\partial}{\partial U_{GB}} \left(\frac{d\nu}{dt} \right) \Bigg|_{\substack{\nu=\nu_{DC} \\ U_{GB}=U_{GB}^{DC}}} \cdot \frac{i\omega}{-\frac{\partial}{\partial \nu}\left(\frac{d\nu}{dt}\right)\Big|_{\substack{\nu=\nu_{DC} \\ U_{GB}=U_{GB}^{DC}}} + i\omega} \delta U_{GB}. \quad (3.176)$$

Eq. 3.176 represents a series RC circuit. The admittance Y of an ideal series RC circuit is given by

$$Y = \frac{1}{R + \frac{1}{i\omega C}} = \frac{i\omega C}{i\tau\omega + 1} = \frac{i\omega \cdot \frac{1}{R}}{\frac{1}{\tau} + i\omega} = \frac{\frac{1}{R} \cdot \tau^2\omega^2 + i\omega C}{\tau^2\omega^2 + 1}, \quad (3.177)$$

where $\tau = RC$ is the time constant of the circuit. Comparison of Eqs. 3.176 and 3.177 yields

$$R_{char} = -\frac{1}{I^0_{char}} \cdot \left[\frac{\partial}{\partial U_{GB}} \left(\frac{d\nu}{dt} \right) \Bigg|_{\substack{\nu=\nu_{DC} \\ U_{GB}=U_{GB}^{DC}}} \right]^{-1} \quad (3.178)$$

$$\tau_{char} = -\left[\frac{\partial}{\partial \nu} \left(\frac{d\nu}{dt} \right) \Bigg|_{\substack{\nu=\nu_{DC} \\ U_{GB}=U_{GB}^{DC}}} \right]^{-1} = \tau_{mod} \quad (3.179)$$

$$C_{char} = \tau_{char}/R_{char}. \quad (3.180)$$

The electrical equivalent circuit (EEC) model of the grain-boundary region derived here is shown in Fig. 3.21. In Fig. 3.21 C_{dep} is the capacitance originating from the depletion region (Eq. 3.150) and R_{diff} the resistor corresponding to the differential

conductance (Eq. 3.168) which represents the ordinary AC current passing through the grain-boundary region, respectively. The circuit branch R_{char}–C_{char} shown in green in Fig. 3.21 corresponds to the charging and discharging current (see Eqs. 3.167 and 3.174), which is caused by any change in the density of the grain-boundary charge N_B. The last circuit branch shown in red in Fig. 3.21 is the circuit branch R_{mod}–L_{mod}, which corresponds to the modulation of the grain-boundary potential barrier. Usually the circuit branch R_{char}–C_{char} can be neglected (see below). This is due to the fact that often the current corresponding to the change in the grain-boundary charge is very small compared to the currents in the other circuit branches.

The values of the circuit elements in the circuit branches R_{char}–C_{char} and R_{mod}–L_{mod} are negative, i.e. they both have negative admittances [12]. However, since this kind of behaviour is not physically possible without input of additional energy, these branches disappear at zero DC bias voltage (see below). Different circuit elements in Fig. 3.21 contribute to different parts of the admittance or impedance spectrum of the EEC: At very low frequencies AC current cannot pass through the capacitors C_{dep} and C_{char} and the inductor L_{mod} can be neglected, thus the resistors R_{diff} and R_{mod} define the total admittance of the EEC. At low frequencies the branches R_{char}–C_{char} and R_{mod}–L_{mod} and the resistor R_{diff} define the total admittance of the EEC. At higher frequencies the inductor L_{mod} blocks the flow of AC current in the branch R_{mod}–L_{mod} and the capacitor C_{char} can be neglected due to the short circuit effect. In addition, some AC current begins to pass though the capacitor C_{dep}. At high frequencies the total admittance of the EEC is determined by the resistors R_{diff} and R_{char} and the capacitor C_{dep}.

The normalized density of the occupied grain-boundary states ν_{DC} and the values of the circuit elements R_{diff} and C_{dep} are plotted as a function of the DC voltage U_{GB}^{DC} across the grain boundary in Fig. 3.22. In Fig. 3.22 ν_{DC} increases with U_{GB}^{DC} due to electronic trapping. The decrease of C_{dep} with U_{GB}^{DC} in Fig. 3.22 is caused by increase of the total width of the depletion region L_d^{corr} due to increase of ν_{DC}. The exponential dependence of R_{diff} on U_{GB}^{DC} in Fig. 3.22 is mostly due to the cosh-term in Eq. 3.168.

The effect of the parameter η (see Eq. 3.136) to the values and the admittance spectrum of the grain boundary is shown in Figs. 3.23 and 3.24, respectively. Fig. 3.23 shows that the values of the resistors R_{mod} and R_{char} approach $-\infty$ at the zero DC bias voltage U_{GB}^{DC}, i.e. the current through the R_{char}–C_{char} and R_{mod}–L_{mod} branches disappears at $U_{GB}^{DC} = 0$. In Fig. 3.24 the admittance is represented by the effec-

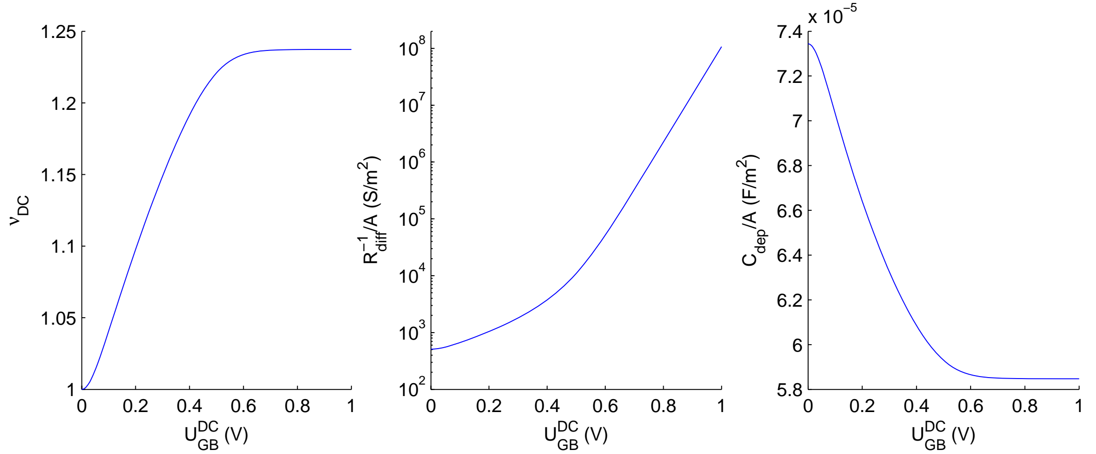

Figure 3.22: Normalized density of the occupied grain-boundary states ν_{DC} and the values of the circuit elements R_{diff} and C_{dep} plotted as a function of the DC voltage U_{GB}^{DC} across the grain boundary. Calculated using Eqs. 3.126, 3.150, 3.152, and 3.168. The parameter values are $\mu = 1000\ \mathrm{cm}^2/(\mathrm{Vs})$, $N_d = 10^{21}\ \mathrm{m}^{-3}$ ($E_c - E_F = 0.22$ eV), $N_B^{tot} = 1.4 \cdot 10^{15}\ \mathrm{m}^{-2}$, $E_c - E_T = 0.60$ eV ($f_n^{eq} = 0.81$), $V_{B_0}^{eq} = 0.348$ V, and $T = 300$ K.

tive parallel conductance (i.e. the real part of admittance $\Re\{Y\}$) and the effective parallel capacitance (i.e. the imaginary part of admittance $\Im\{Y\}$ normalized by angular frequency ω). The low frequency value of the effective parallel conductance in Fig. 3.24 is given by the resistors R_{diff} and R_{mod}. The high frequency value of the effective parallel capacitance in Fig. 3.24 is given by the capacitor C_{dep}.

The parameter η affects only the time constant of the circuit branches $\tau = \tau_{mod} = \tau_{char}$ (see Eqs. 3.134, 3.159, 3.172, and 3.179 and Fig. 3.23) and the values of the circuit elements of the charging and discharging branch R_{char} and C_{char} (see Eqs. 3.134, 3.159, 3.175, 3.178, and 3.180 and Fig. 3.23). The essential effect of the parameter η is the determination of the magnitude of the charging and discharging current I_{char} (see Eqs. 3.167 and 3.174). When the value of η is high enough ($\eta > 100$ in Fig. 3.24), I_{char} (i.e. the admittance of the branch R_{char}–C_{char}) begins to affect the admittance spectrum of the grain-boundary region (see Fig. 3.24). With even higher values of η ($\eta > 5000$ in Fig. 3.24) the contribution of I_{char} is such a high that the shape of the admittance spectrum changes (see Fig. 3.24).

The effect of the delay coefficient ξ (see Eqs. 3.120 and 3.134) to the values and the admittance spectrum of the grain boundary is shown in Figs. 3.25 and 3.26, respectively. The delay coefficient ξ affects only the time constant of the circuit branches $\tau = \tau_{mod} = \tau_{char}$ (see Eqs. 3.134, 3.159, 3.172, and 3.179 and Fig. 3.25)

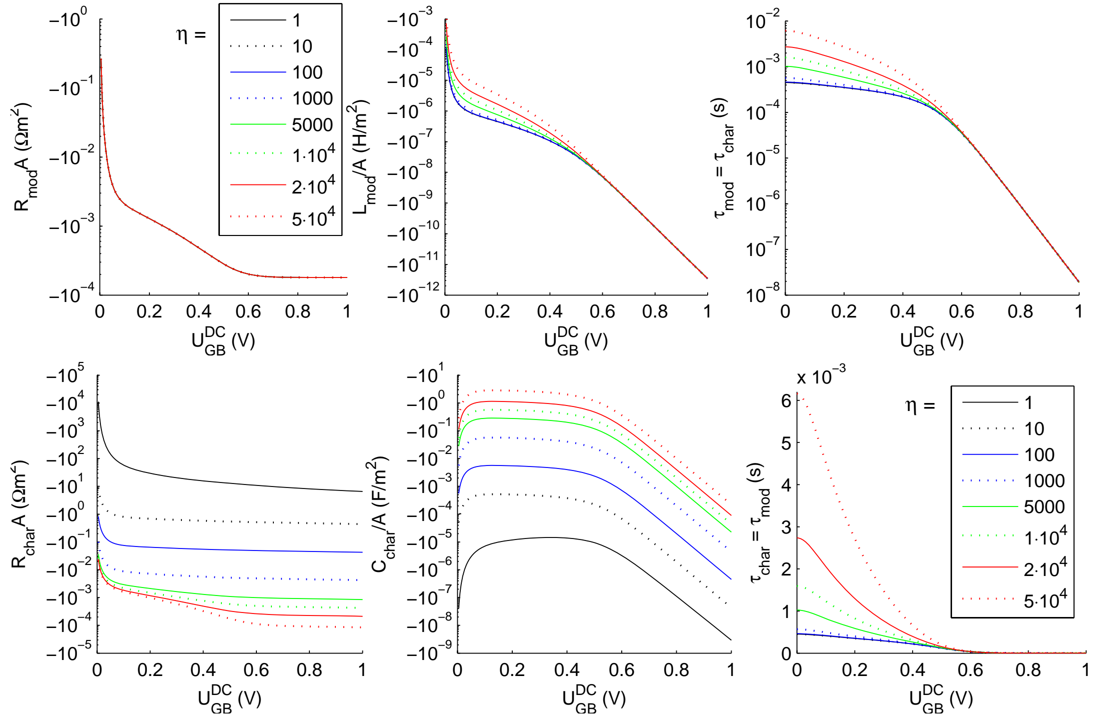

Figure 3.23: Values of the circuit elements of the modulation (*top*) and charging (*bottom*) branches as a function of the DC voltage U_{GB}^{DC} across the grain boundary with various values of the parameter η. Calculated using Eqs. 3.171, 3.173, 3.178, 3.179, and 3.180. The values of ν_{DC} are from Fig. 3.22. The parameter values are $\mu = 1000$ cm^2/(Vs), $N_d = 10^{21}$ m^{-3} ($E_c - E_F = 0.22$ eV), $N_B^{tot} = 1.4 \cdot 10^{15}$ m^{-2}, $E_c - E_T = 0.60$ eV ($f_n^{eq} = 0.81$), $V_{B_0}^{eq} = 0.348$ V, $k_{-i}^{eq} = 73.2$ s^{-1} ($\sigma_n = 10^{-14}$ cm^2), $\xi_{eq}(\eta = 1) = 1.06 \cdot 10^{-3}$, and $T = 300$ K.

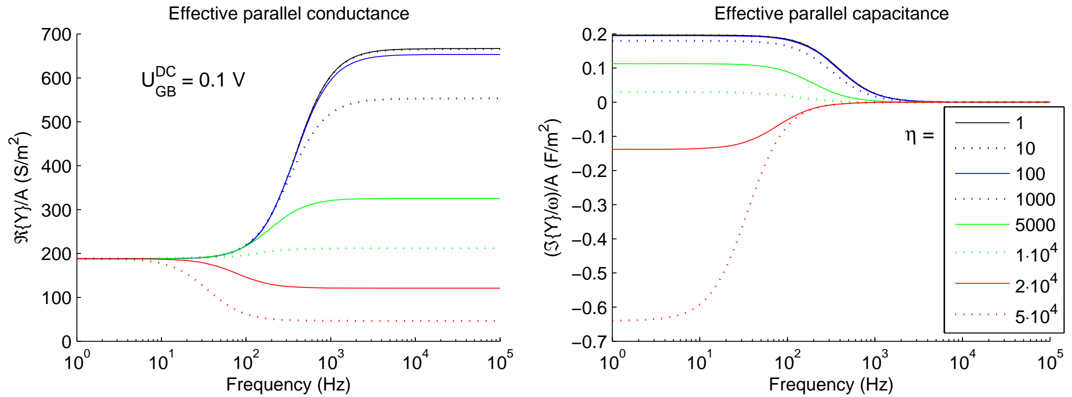

Figure 3.24: Effective parallel conductance and capacitance of the EEC shown in Fig. 3.21 plotted as a function of frequency with various values of η. The values of the circuit elements and parameters are from Figs. 3.22 and 3.23.

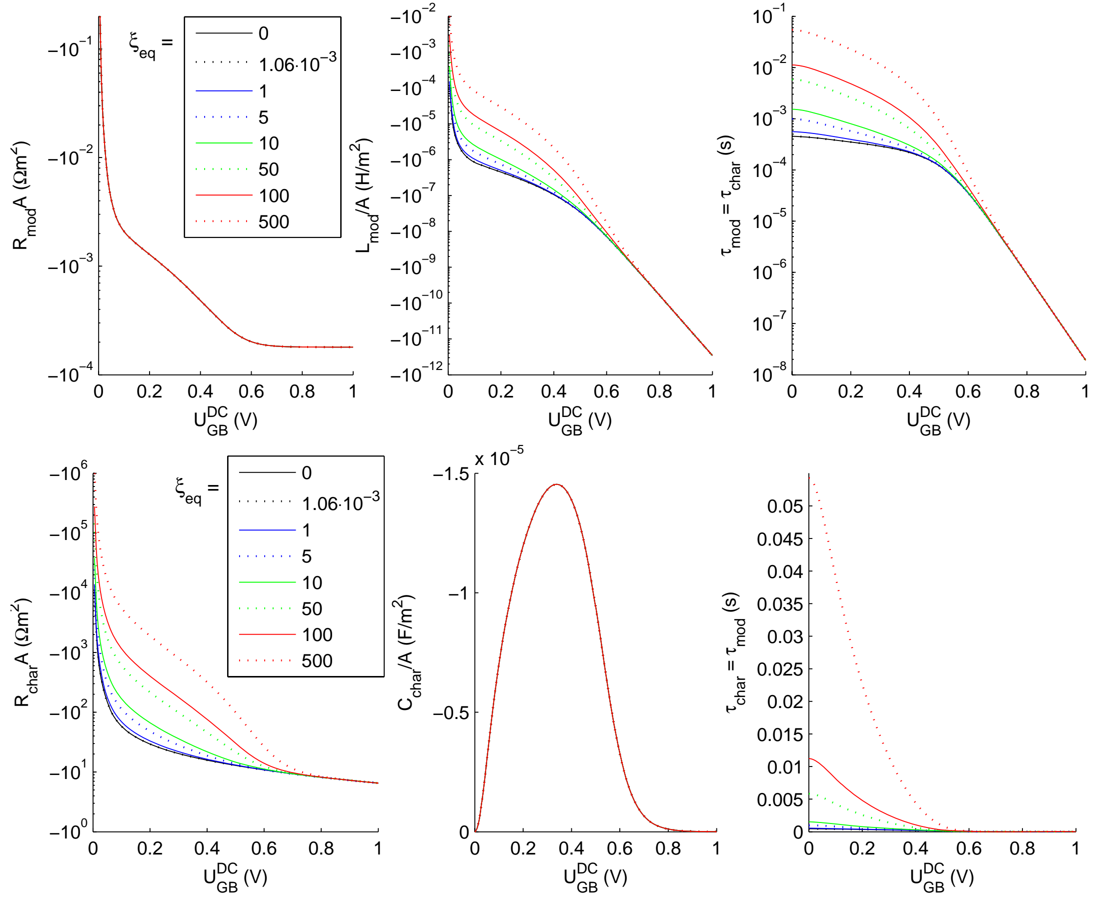

Figure 3.25: Values of the circuit elements of the modulation (*top*) and charging (*bottom*) branches as a function of the DC voltage U_{GB}^{DC} across the grain boundary with various values of the delay coefficient ξ_{eq}. Calculated using Eqs. 3.171, 3.173, 3.178, 3.179, and 3.180. The values of ν_{DC} are from Fig. 3.22. The parameter values are $\mu = 1000$ cm^2/(Vs), $N_d = 10^{21}$ m^{-3} ($E_c - E_F =$ 0.22 eV), $N_B^{tot} = 1.4 \cdot 10^{15}$ m^{-2}, $E_c - E_T = 0.60$ eV ($f_n^{eq} = 0.81$), $V_{B0}^{eq} = 0.348$ V, $k_{-i}^{eq} = 73.2$ s^{-1} ($\sigma_n = 10^{-14}$ cm^2), $\eta = 1$, and $T = 300$ K. The value $\xi_{eq} = 1.06 \cdot 10^{-3}$ is given by Eq. 3.134.

and the values of the circuit elements L_{mod} and R_{char} (see Eqs. 3.134, 3.158, 3.171, and 3.178 and Fig. 3.25). As the name indicates the essential effect of the delay coefficient ξ is addition of delay to those parts of the EEC which describe the electronic trapping process. This shown in Fig. 3.26 where the step in the admittance spectrum of the EEC moves to lower frequencies when ξ_{eq} is increased. In addition to the frequency shift the magnitude of the effective parallel capacitance increases at the low frequencies with increasing values of ξ_{eq}.

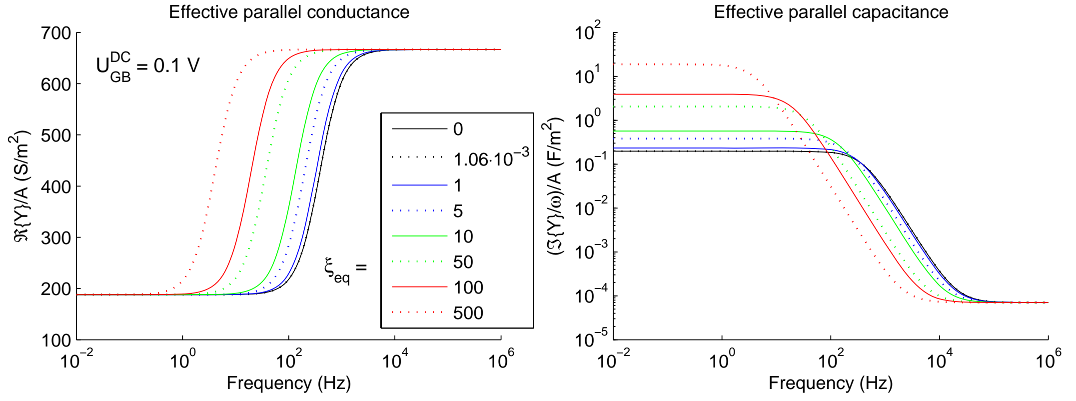

Figure 3.26: Effective parallel conductance and capacitance of the EEC shown in Fig. 3.21 plotted as a function of frequency with various values of ξ. The values of the circuit elements and parameters are from Figs. 3.22 and 3.23.

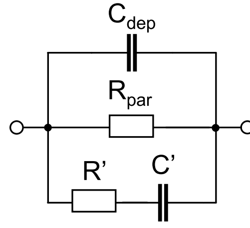

Figure 3.27: Converted circuit.

3.5.3 Electrical equivalent circuit conversion

As Eqs. 3.179 and 3.172 show, the time constants τ_{char} and τ_{mod} of the series RC and RL circuits are equal. This allows the circuit consisting of the branches $R_{char}C_{char}$ and $R_{mod}L_{mod}$ in parallel (see Fig. 3.21) to be converted into a circuit with a resistor R_{mod} and a series RC branch in parallel. The converted EEC of the grain boundary is shown in Fig. 3.27.

The values of the circuit elements are given by [12]

$$\begin{aligned} R_{par} &= \frac{R_{diff}R_{mod}}{R_{diff}+R_{mod}} \\ R' &= \frac{R_{mod}R_{char}}{R_{mod}-R_{char}} \\ C' &= C_{char}\left(1-\frac{R_{char}}{R_{mod}}\right). \end{aligned} \tag{3.181}$$

The time constant of the $R'C'$ branch is the same as in the modulation and charging branches: $\tau = R'C' = \tau_{char} = \tau_{mod}$.

3.6 Additional modelling considerations

In addition to the effects listed in section 2.3.2 the other effects which were not considered in the models presented in this chapter are listed. Some assumptions which were made during the derivation of the models are also discussed.

- Possible temperature dependencies, which were not considered: dielectric constant, Fermi levels in bulk (ionization of dopants) and interface [1], energy levels of bulk and interface traps [1], band gap narrowing [18], mobility [18], and capture cross-sections of electrons and holes.
- Failure of the depletion region approximation at low grain-boundary potential barrier heights and high applied voltages.
- Detailed modelling of mobility.
  - Temperature and field dependence (i.e. velocity of charge carriers).
  - Velocity of charge carriers. In general, the density of electric current can be written as $J = qnv$, where v is the velocity of electrons. In the DC case J is constant, therefore at the grain boundary v must be high because n is low. This could lead to saturation of v.
  - Surface scattering [16, 17], when the bulk mean free path is comparable with the film thickness [2].
  - Grain-boundary scattering [2, 25].
- Properties of the grain-boundary interface.
  - Bias voltage dependence of the quasi Fermi level at the grain boundary (a small correction) [1, 53].
  - Shape of density of interface states as a function of energy [1]. Localised vs. extended states [1].
  - Existence of additional different types of trap states (for example donor-type interface states and chemically induced states [5]) in the interface.

  - Spatial statistical fluctuations of the potential barrier [1].
  - Shape and dimension of the interface [1]. Non-symmetrical grain boundaries due to electrical degradation and growth and processing [1].

- Effect of contacts (electrodes): the metal-semiconductor junction.
- Electronic bulk trap states.
  - Gives additional dynamic features in the bulk regions.
  - Changes the bulk electron density.
  - Trapping in bulk states in the depletion region [1, 4, 16] (changes the solution of Poisson's equation performed in section 3.2).

Chapter 4

I–V characteristics of granular semiconductor

In this chapter the analytical DC model of a grain boundaries in n-type semiconductor (see section 3.3) is applied to the calculation of I–V characteristics of granular n-type semiconductor. In addition, the analytical results are compared with results obtained from the numerical simulations with Silvaco ATLAS.

4.1 DC model of granular semiconductor

The one-dimensional geometrical model of a granular n-type semiconductor employed in this work is illustrated in Fig. 4.1. In the model the granular film has N_{GB} identical grain boundaries. The voltage across a single barrier is U_{GB}, and the voltage across the whole sample is U. In Fig. 4.1a l is the length of the sample or distance between the electrodes and L_d^{corr} the total length of the depletion regions of a single grain boundary (see Eq. 3.21), respectively.

The electric current flowing through the grain-boundary regions can be calculated with the formulas given in the previous chapter. Although the equations for the current are nonlinear, the resistance of a single barrier can be defined as

$$R_{GB} = \frac{U_{GB}}{I} = \frac{U_{GB}}{AJ}, \tag{4.1}$$

where I is the electric current and A the cross-sectional area of the sample, respec-

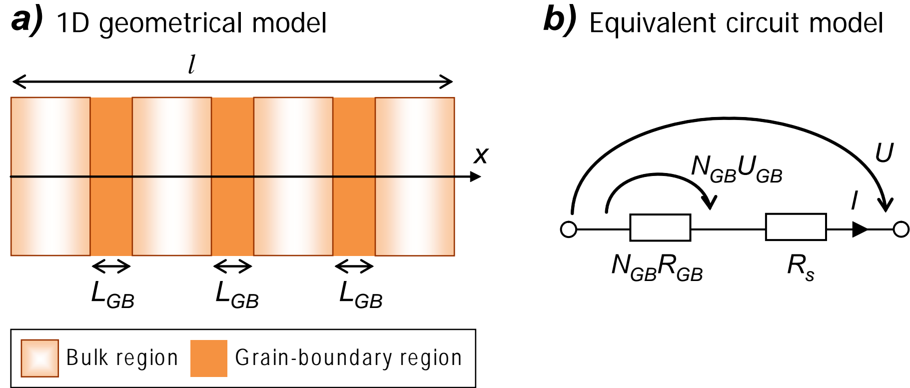

Figure 4.1: *a)* One-dimensional geometrical model of a granular semiconductor. l is the length of the sample and $L_{GB} = L_d^{corr}$ the total length of the depletion regions in the grain-boundary region, respectively. *b)* A corresponding equivalent circuit of the 1D geometrical model of a granular semiconductor. U is the voltage across the sample, U_{GB} the voltage across a single grain boundary region, I the electric current flowing through the sample, R_{GB} the resistance of a single grain boundary region, R_s the series resistance consisting of the resistance of the bulk part of the sample, and N_{GB} the number of grain boundaries, respectively.

tively. An equivalent-circuit representation of the 1D geometrical model is shown in Fig. 4.1b. The series resistance is given by

$$R_s = \frac{l - L_d^{corr} N_{GB}}{\sigma_{bulk} A} = \left(1 - N_{GB} \frac{L_d^{corr}}{l}\right) R_{bulk}, \tag{4.2}$$

where R_{bulk} is the bulk resistance

$$R_{bulk} = \frac{l}{\sigma_{bulk} A}, \tag{4.3}$$

which is the resistance of a sample without any grain boundaries (i.e. a sample consisting of bulk only). Kirchhoff's and Ohm's laws and Eq. 4.2 give for the total current flowing through the material

$$I = \frac{U}{N_{GB} R_{GB} + R_s} \tag{4.4}$$

and for the single grain boundary voltage

$$U_{GB} = \frac{U - R_s I}{N_{GB}} = \frac{U - \left(1 - N_{GB} \frac{L_d^{corr}}{l}\right) R_{bulk} I}{N_{GB}}. \tag{4.5}$$

The electric field in the bulk part of the material is given by

$$E_{bulk} = \frac{J}{\sigma_{bulk}} = \frac{I}{\sigma_{bulk} A} = \frac{R_s I}{l - N_{GB} L_d^{corr}}, \tag{4.6}$$

where Eqs. 4.2 and 4.3 were used.

4.2 Comparison of modelling results

In this section I–V characteristics of n-type granular semiconductor calculated with various analytical formulas and numerical simulation are compared. In addition, the effect of trapping on the I–V characteristics are discussed.

First, the case without the electronic trapping at the grain boundary (i.e. the case where the grain-boundary traps are filled) is considered. The current density J, the normalized electron density n_B/N_d, and the voltage across the grain-boundary U_{GB} calculated with Silvaco ATLAS and various analytical formulas as a function of voltage U applied across the sample of granular n-type semiconductor are plotted in Fig. 4.2. The different analytical formulas describing the current density J_{GB}^{DC} through the grain-boundary region and the density of electrons at the grain boundary n_B are formulas of the quadratic potential profile with E_{bulk} (Eqs. 3.105 and 3.106), the quadratic potential profile without the bulk electric field (Eqs. 3.90 and 3.91), the linear potential profile (Eqs. 3.65 and 3.68), the 1$^{\text{st}}$ approximation of linear potential profile (Eqs. 3.69 and 3.70), and the 2$^{\text{nd}}$ approximation of linear potential profile (Eqs. 3.71 and 3.72), respectively. In addition, Eqs. 3.17 and 3.21 and the formulas for the derived in this chapter in section 4.1 (Eqs. 4.4, 4.5, and 4.6) were used. These analytical formulas were numerically solved by using the MATLAB function `fsolve`. The erfi function in Eqs. 3.90, 3.91, 3.105, and 3.106 was calculated with the complex function error function implemented in MATLAB [49]. In addition to the parameter values listed in Fig. 4.2 the parameter values listed in Table 3.1 were used.

In the case where all the grain-boundary traps are filled the I–V curve of the granular semiconductor shown in Fig. 4.2 has three characteristic regions: Linear, super-linear (nonlinear), and series resistance limited (linear). At low voltages the I–V curve is linear. The electrical conduction limited by the potential barrier V_B at the grain boundary. At higher voltages the super-linear (nonlinear) region appears. In the super-linear region the effective potential barrier decreases with increasing voltage and the current increases exponentially (see sections 3.2.5 and 3.3). At high voltages the resistance of the bulk regions of the granular semiconductor begins to limit the nonlinear increase of current. In this the series resistance limited region the I–V

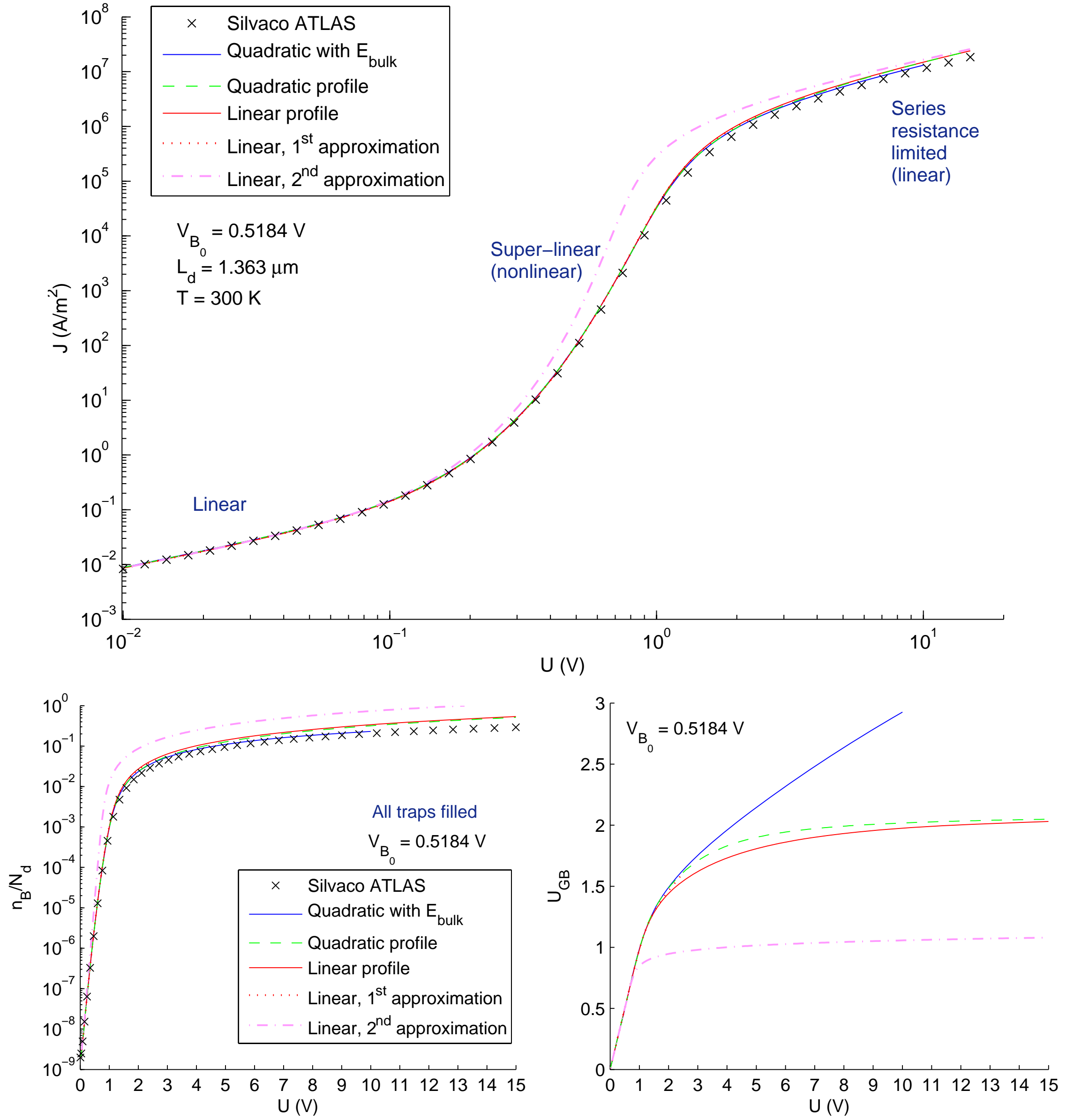

Figure 4.2: Current density J, normalized electron density n_B/N_d, and voltage across the grain-boundary U_{GB} plotted as a function of voltage U applied across the sample. Calculated using Silvaco ATLAS and various formulas: Quadratic potential profile with E_{bulk} (Eqs. 3.105 and 3.106), quadratic profile (Eqs. 3.90 and 3.91), linear profile (Eqs. 3.65 and 3.68), 1$^{\text{st}}$ approximation of linear profile (Eqs. 3.69 and 3.70), and 2$^{\text{nd}}$ approximation of linear profile (Eqs. 3.71 and 3.72). In addition, Eqs. 3.17, 3.21, 4.4, 4.5, and 4.6 were used. The parameter values are $l = 10$ μm, $N_d = 10^{21}$ m^{-3} ($E_c - E_F = 0.22$ eV), $\mu = 1000$ cm^2/(Vs), $N_{GB} = 1$, $N_B^{tot} = 1.4 \cdot 10^{15}$ m^{-2}, $E_c - E_T = 2$ eV (all traps filled), and $T = 300$ K. The parameters are the same as in Figs. 3.10, 3.11, and 3.12.

characteristics return back to linear.

In the linear region ($U \lesssim 0.1$ V in Fig. 4.2) all the analytical formulas are in excellent agreement with the numerical simulation results. In the super-linear regime (0.1 V$\lesssim U \lesssim 1$ V in Fig. 4.2) only the 2nd approximation formulas of the linear potential profile (Eqs. 3.71 and 3.72) are not in agreement with the numerical simulation results due to overestimation of current density and grain-boundary electron density. However, due to the bulk resistance the overestimation is not as poor as in the case of the grain boundary alone (see section 3.3.5).

In the series resistance limited region (at $U \approx 2.5$ V in Fig. 4.2) the 1st approximation formulas of the linear profile (Eqs. 3.69 and 3.70) fail due to the numerical convergence problems (see discussion in section 3.3.5). In the series resistance limited region ($U \gtrsim 2$ V in Fig. 4.2) all the analytical formulas overestimate the current density and grain-boundary electron density. The smallest difference between the numerical simulation results and the formulas of the quadratic potential profile with E_{bulk} (Eqs. 3.105 and 3.106). The reason for this is that with E_{bulk} taken into account the voltage across the grain-boundary region U_{GB} (see Fig. 4.2) increases with the applied voltage U, thus increasing the voltage across the bulk regions (see Fig. 4.1) and thereby limiting the increase of current due to the series-resistance effect. However, some overestimation of current still exist due to the faulty form of Eq. 3.105. These overestimation problems are generally caused by the fact that depletion region approximation fails at high voltages (see discussion in section 3.2.6).

In the case with electronic trapping at the grain boundary the current density J, the normalized electron density n_B/N_d, and the voltage across the grain-boundary U_{GB} calculated with Silvaco ATLAS and various analytical formulas as a function of voltage U applied across the sample of granular n-type semiconductor are plotted in Fig. 4.3. The trapping effect was calculated with Eqs. 3.114, 3.116, 3.117, 3.118, and 3.126. In Fig. 4.3 calculations were not performed with the formulas of quadratic potential profile with E_{bulk} (Eqs. 3.105 and 3.106) and the 1st approximation of the linear profile (Eqs. 3.69 and 3.70) because of the numerical convergence problems (see discussion in section 3.3.5). All the other analytical formulas performed as well as in the previous case of filled traps.

In addition to the three regions observed in the I–V curve of the case with all traps filled a fourth region appears (see Fig. 4.3): At low voltages after the linear region there is a sub-linear region where the increase of current with voltage is less than

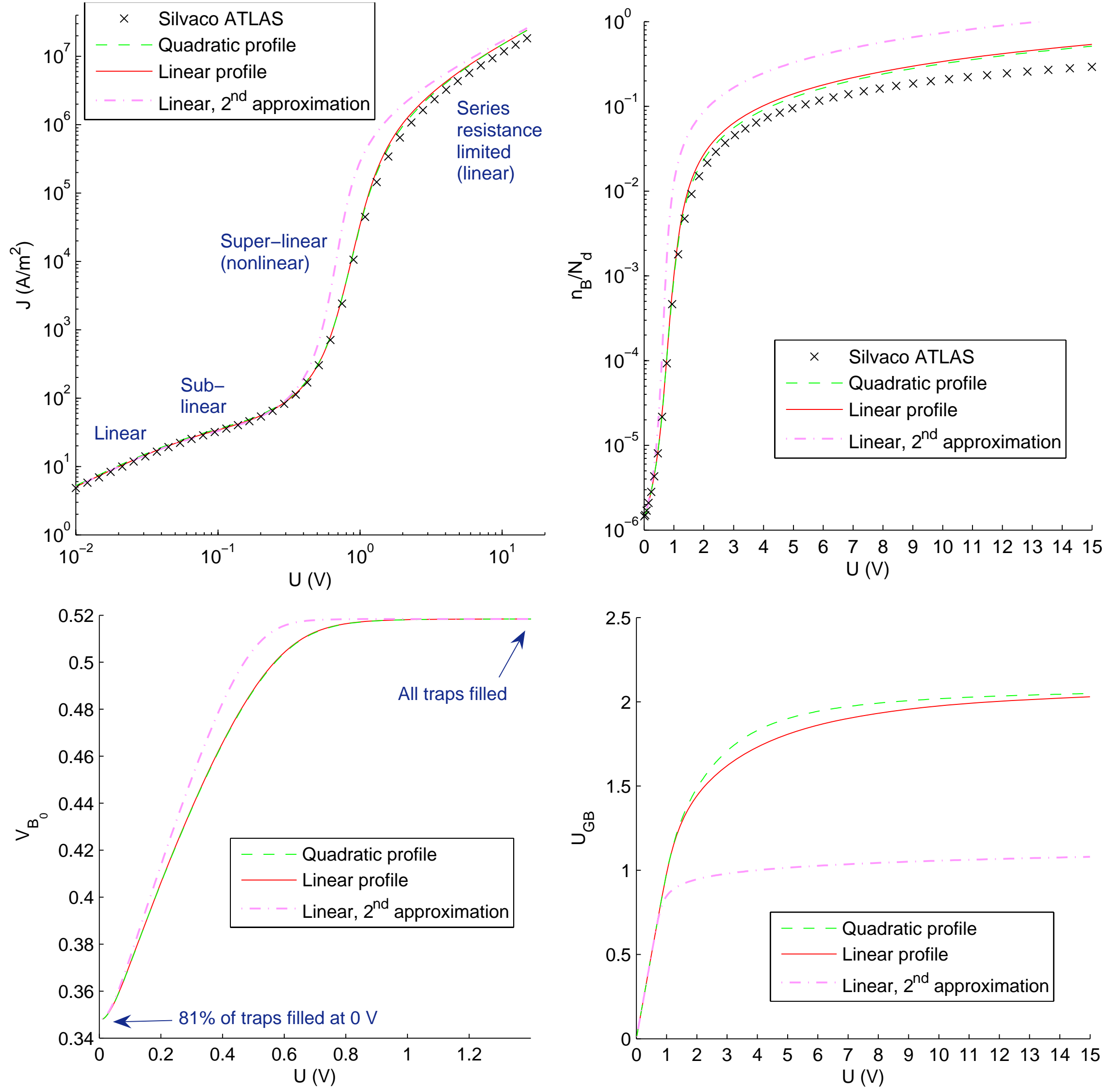

Figure 4.3: Current density J, normalized electron density n_B/N_d, the zero-voltage potential at the grain boundary V_{B_0}, and voltage across the grain-boundary U_{GB} plotted as a function of voltage U applied across the sample. Calculated using Silvaco ATLAS and various formulas: Quadratic potential profile (Eqs. 3.90 and 3.91), linear profile (Eqs. 3.65 and 3.68), and 2$^{\text{nd}}$ approximation of linear profile (Eqs. 3.71 and 3.72). In addition, Eqs. 3.17, 3.21, 3.114, 3.116, 3.117, 3.118, 3.126, 4.4, and 4.5 were used. The parameter values are $l = 10$ μm, $N_d = 10^{21}$ m^{-3} ($E_c - E_F = 0.22$ eV), $\mu = 1000$ cm^2/(Vs), $N_{GB} = 1$, $N_B^{tot} = 1.4 \cdot 10^{15}$ m^{-2}, $E_c - E_T = 0.6$ eV, and $T = 300$ K. The same case but without trapping is shown in Fig. 4.2.

in the linear region. This is caused by filling of the grain-boundary traps, what in turn increases the zero-voltage grain-boundary potential V_{B_0} (see Fig. 4.3 and Eq. 3.17) thereby limiting the flow of current. In spite of the filling of the traps the sub-linear region changes into the super-linear or nonlinear region at higher voltages (at $U \approx 0.15$ V in Fig. 4.3).

4.3 Effect of parameters

In this section the effect of the most important parameters of the model on I–V characteristics of n-type granular semiconductor are discussed.

The I–V characteristics are calculated with the numerical simulation software Silvaco ATLAS and the analytical formulas of the quadratic potential profile without the bulk electric field (Eqs. 3.90 and 3.91) and the linear potential profile (Eqs. 3.65 and 3.68), respectively. In addition, Eqs. 3.17, 3.21, 3.114, 3.116, 3.117, 3.118, 3.126, 4.4, and 4.5 were used. These analytical formulas were numerically solved by using the MATLAB function `fsolve`. The erfi function in Eqs. 3.90, 3.91, 3.105, and 3.106 was calculated with the complex function error function implemented in MATLAB [49]. In addition to the parameter values listed in Fig. 4.2 the parameter values listed in Table 3.1 were used. The current density J, the normalized electron density n_B/N_d, and the voltage across the grain-boundary U_{GB} calculated with Silvaco ATLAS and the analytical formulas and with various values of the parameters as a function of voltage U applied across the sample of granular n-type semiconductor are plotted in Figs. 4.4, 4.5, 4.6, 4.7, 4.8, 4.9, and 4.10. In all figures the analytical formulas and the numerical results are in excellent agreement in all of the regions of the I–V curves (see section 4.2), except in the series resistance limited region (at high voltages). In addition, the quadratic and linear potential profile formulas give very similar results.

In Fig. 4.4 the energy level of the grain-boundary state $E_c - E_T$ is varied. $E_c - E_T$ has a huge effect on the I–V characteristic because it defines the magnitude of the trapping process and the occupancy of the grain-boundary states in the thermodynamical equilibrium f_n^{eq} (i.e. the occupancy at zero voltage). Fig. 4.4 shows that f_n^{eq} increases with $E_c - E_T$. When $f_n^{eq} = 1$ (i.e. all traps filled at 0 V), the sub-linear regime disappears in the I–V curve (see Fig. 4.4 and discussion in section 4.2).

The total density of grain-boundary states N_B^{tot} is varied in Fig. 4.5. N_B^{tot} determines

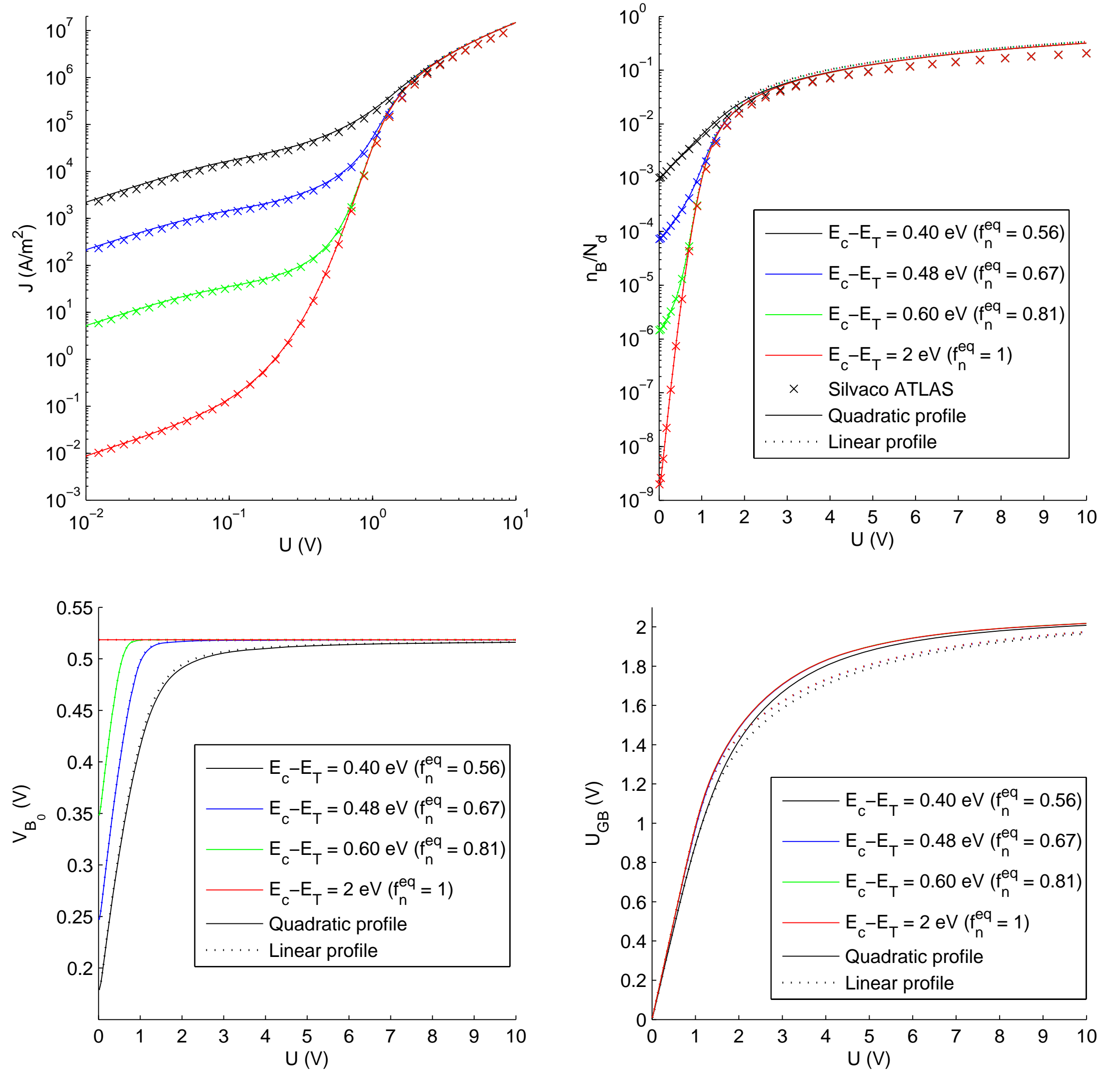

Figure 4.4: Current density J, normalized electron density n_B/N_d, the zero-voltage potential at the grain boundary V_{B_0}, and voltage across the grain-boundary U_{GB} plotted as a function of voltage U applied across the sample with various values of the energy level of the grain-boundary state $E_c - E_T$. Calculated using Silvaco ATLAS, and quadratic (Eqs. 3.90 and 3.91) and linear potential profile formulas (Eqs. 3.65 and 3.68), respectively. In addition, Eqs. 3.17, 3.21, 3.114, 3.116, 3.117, 3.118, 3.126, 4.4, and 4.5 were used. The parameter values are $l = 10$ μm, $\mu = 1000$ cm^2/(Vs), $N_d = 10^{21}$ m^{-3} ($E_c - E_F = 0.22$ eV), $N_{GB} = 1$, $N_B^{tot} = 1.4 \cdot 10^{15}$ m^{-2}, and $T = 300$ K.

mostly the maximum of the zero-voltage grain-boundary potential, which is given by V_B^{tot} (see Eq. 3.114), and the occupancy of the grain-boundary states in the thermodynamical equilibrium f_n^{eq}. Higher values of N_B^{tot} result in lower values for current and grain-boundary electron density (especially in the linear regime at low voltages), and larger sub-linear region (see Fig. 4.5). However, the effect is reduced considerably in the series resistance limited region at high voltages (see Fig. 4.5) due to the bulk resistance.

In Fig. 4.6 the length of the sample, l, is varied. l affects only the series resistance limited region of the I–V curve at high voltages (see Fig. 4.6). The donor density N_d is varied in Fig. 4.7. In addition to the bulk regions and the series resistance limited region N_d has also an effect on the zero-voltage grain-boundary potential V_{B_0} (see Eq. 3.17). The final bulk-related effect is the mobility μ, which is varied in Fig. 4.8. μ affects only the flow of current in the bulk and the grain-boundary regions (see section 3.3 and Eqs. 3.90 and 3.65).

The final parameter under consideration is the absolute temperature T. The effect of the temperature in two different cases with the energy level of the grain-boundary state $E_c - E_T$ of 0.60 eV and 1.00 eV is shown in Figs. 4.9 and 4.10, respectively. In the model the electronic trapping and most of the formulas describing the grain boundary region are highly dependent on temperature. Hence, the I–V characteristics change considerably when temperature is changed. The major effects of a temperature increase are increased current and grain-boundary electron density (see Figs. 4.9 and 4.10).

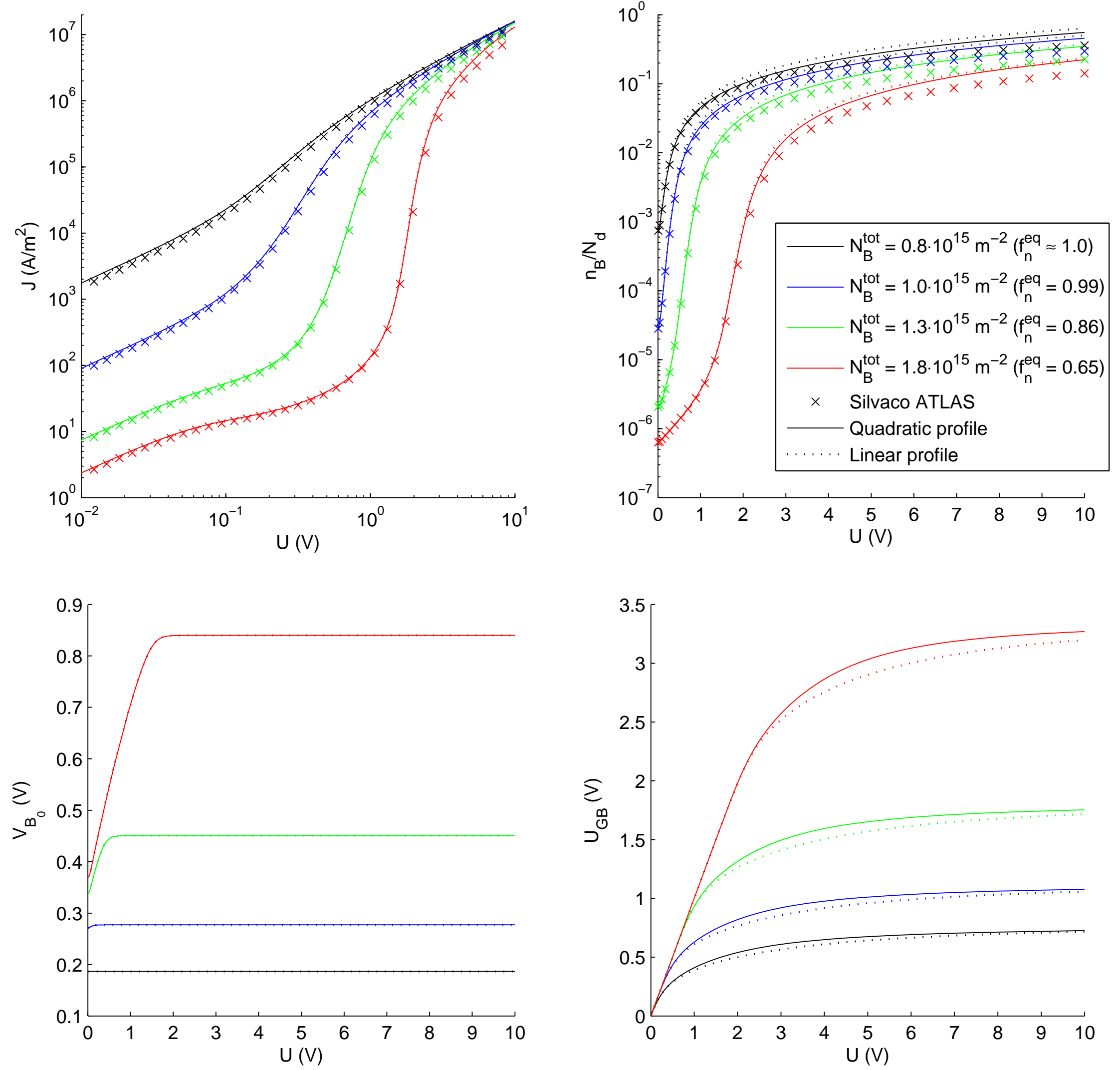

Figure 4.5: Current density J, normalized electron density n_B/N_d, the zero-voltage potential at the grain boundary V_{B_0}, and voltage across the grain-boundary U_{GB} plotted as a function of voltage U applied across the sample with various values of the total density of grain-boundary states N_B^{tot}. Calculated using Silvaco ATLAS, and quadratic (Eqs. 3.90 and 3.91) and linear potential profile formulas (Eqs. 3.65 and 3.68), respectively. In addition, Eqs. 3.17, 3.21, 3.114, 3.116, 3.117, 3.118, 3.126, 4.4, and 4.5 were used. The parameter values are $l = 10\ \mu$m, $\mu = 1000\ \text{cm}^2/(\text{Vs})$, $N_d = 10^{21}\ \text{m}^{-3}$ ($E_c - E_F = 0.22$ eV), $N_{GB} = 1$, $E_c - E_T = 0.60$ eV, and $T = 300$ K.

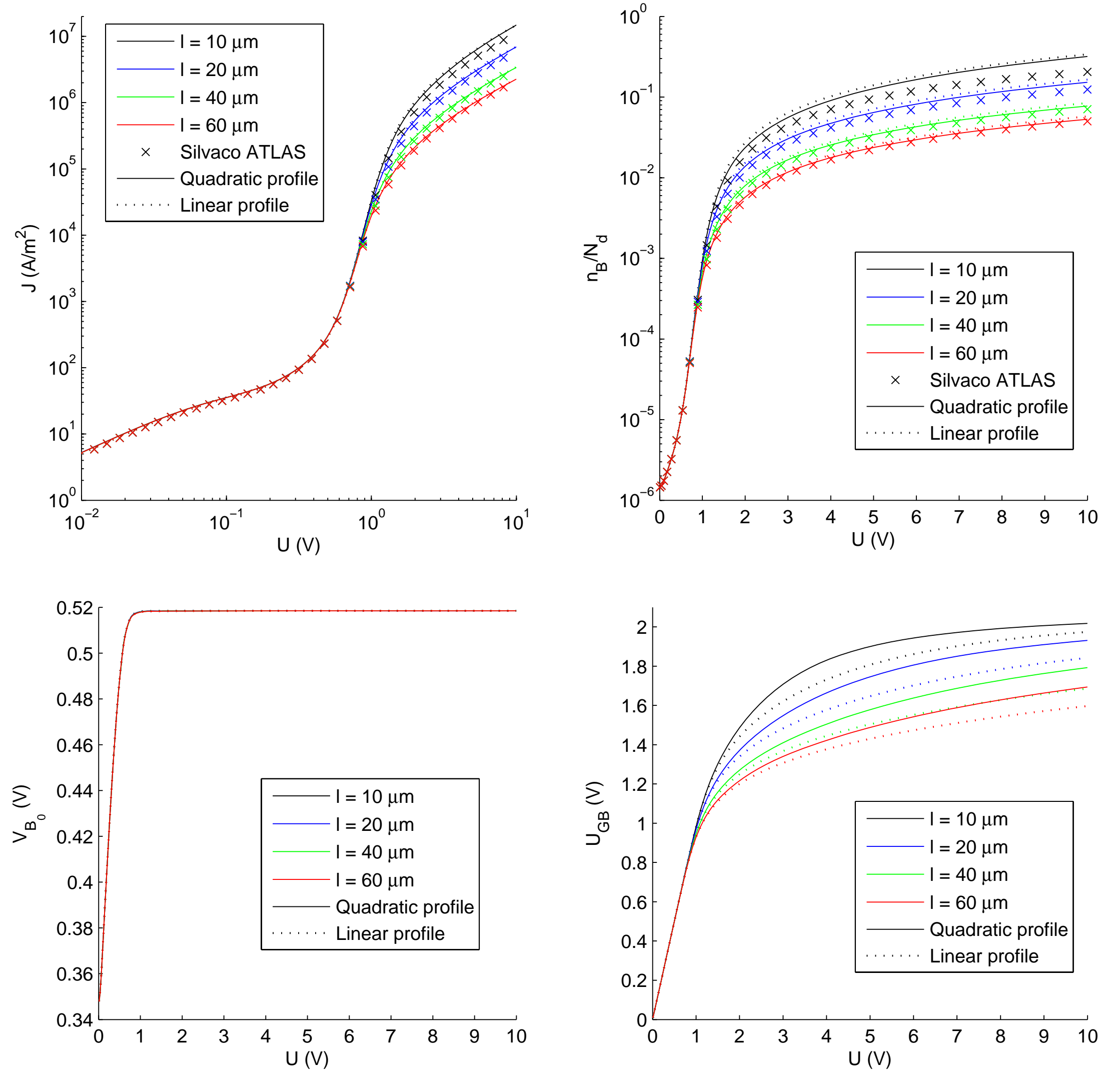

Figure 4.6: Current density J, normalized electron density n_B/N_d, the zero-voltage potential at the grain boundary V_{B_0}, and voltage across the grain-boundary U_{GB} plotted as a function of voltage U applied across the sample with various values of the sample length l. Calculated using Silvaco ATLAS, and quadratic (Eqs. 3.90 and 3.91) and linear potential profile formulas (Eqs. 3.65 and 3.68), respectively. In addition, Eqs. 3.17, 3.21, 3.114, 3.116, 3.117, 3.118, 3.126, 4.4, and 4.5 were used. The parameter values are $\mu = 1000$ cm^2/(Vs), $N_d = 10^{21}$ m^{-3} ($E_c - E_F = 0.22$ eV), $N_{GB} = 1$, $N_B^{tot} = 1.4 \cdot 10^{15}$ m^{-2}, $E_c - E_T = 0.60$ eV ($f_n^{eq} = 0.81$), and $T = 300$ K.

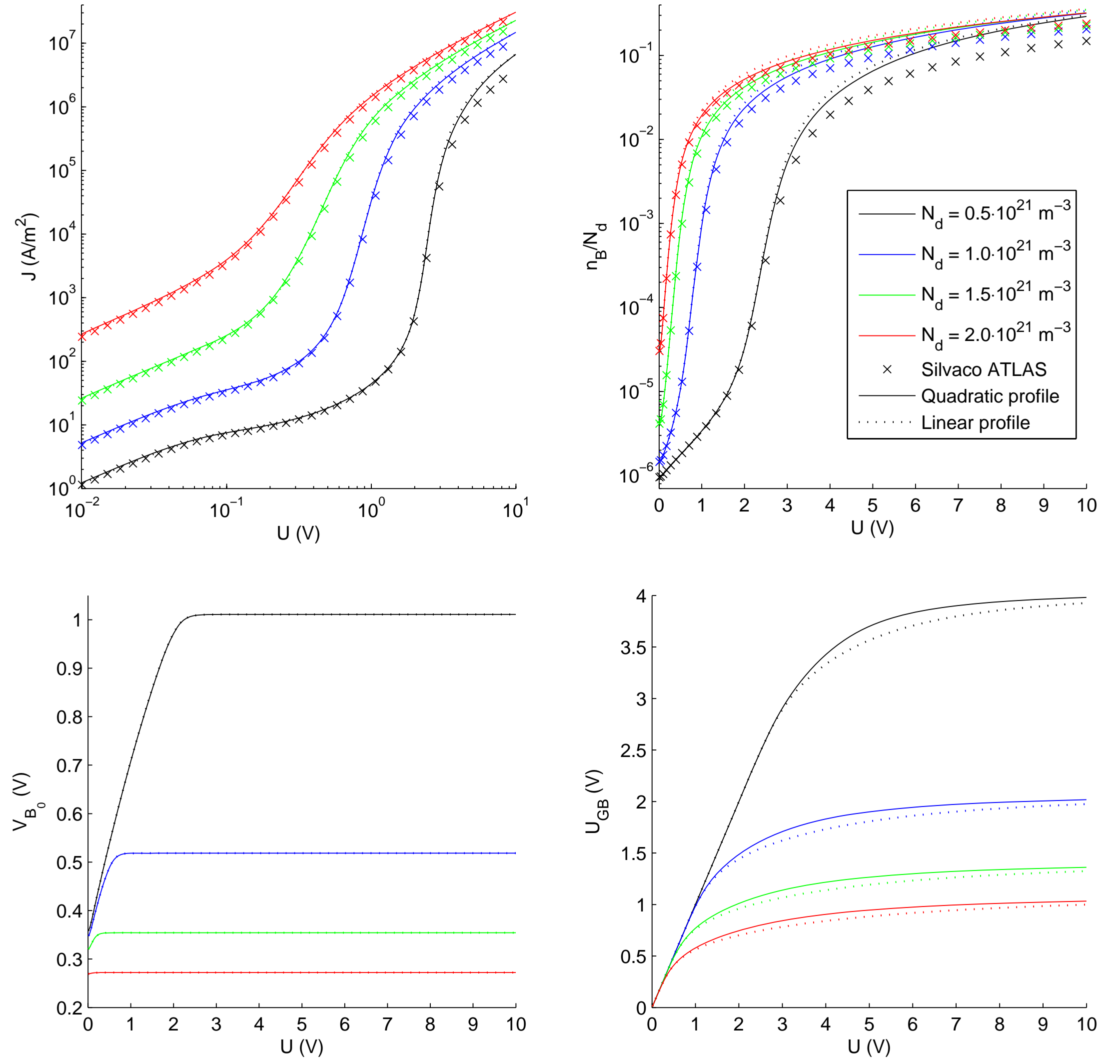

Figure 4.7: Current density J, normalized electron density n_B/N_d, the zero-voltage potential at the grain boundary V_{B_0}, and voltage across the grain-boundary U_{GB} plotted as a function of voltage U applied across the sample with various values of the donor density N_d. Calculated using Silvaco ATLAS, and quadratic (Eqs. 3.90 and 3.91) and linear potential profile formulas (Eqs. 3.65 and 3.68), respectively. In addition, Eqs. 3.17, 3.21, 3.114, 3.116, 3.117, 3.118, 3.126, 4.4, and 4.5 were used. The parameter values are $l = 10\ \mu\text{m}$, $\mu = 1000\ \text{cm}^2/(\text{Vs})$, $N_{GB} = 1$, $N_B^{tot} = 1.4 \cdot 10^{15}\ \text{m}^{-2}$, $E_c - E_T = 0.60$ eV, and $T = 300$ K.

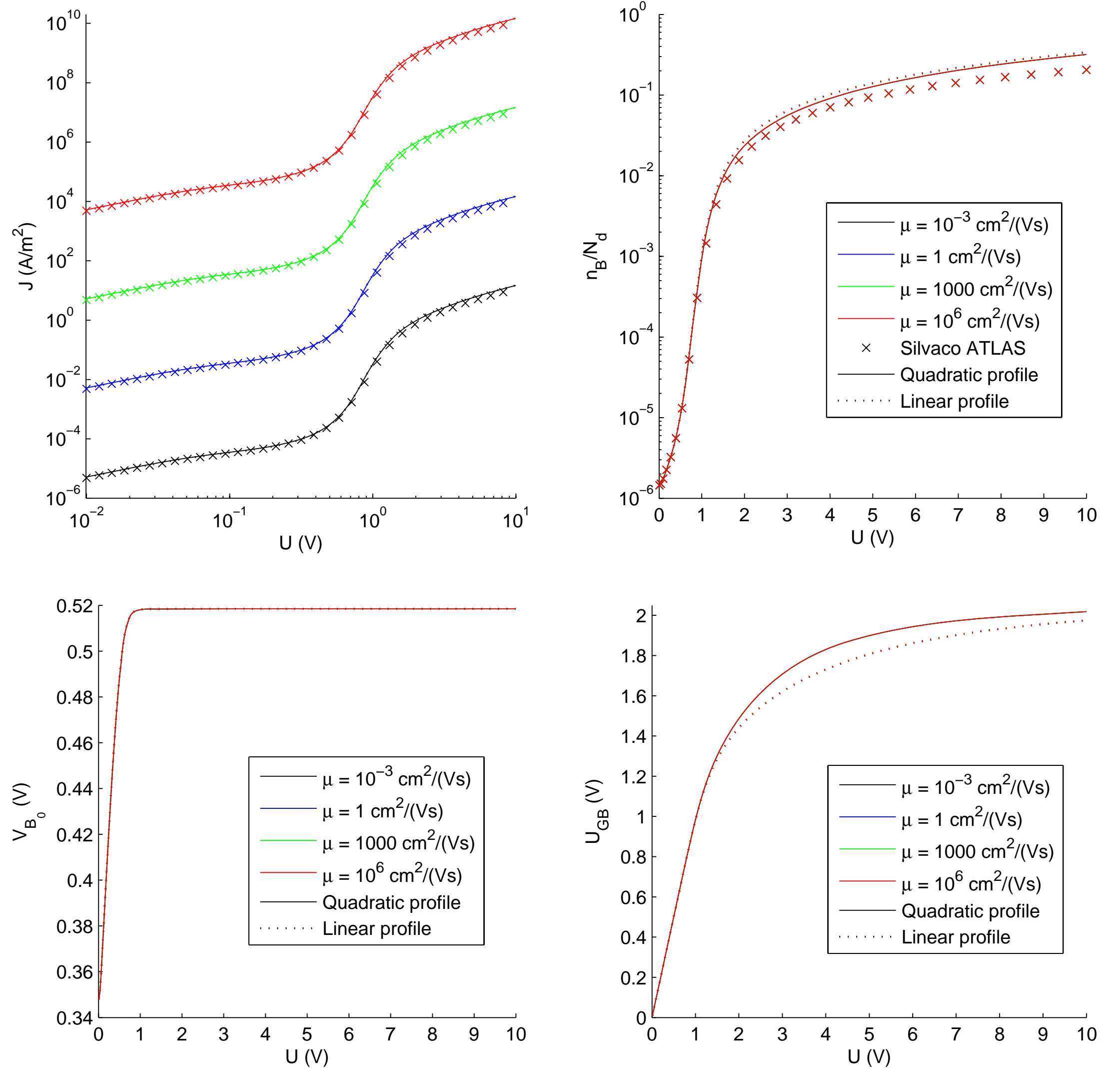

Figure 4.8: Current density J, normalized electron density n_B/N_d, the zero-voltage potential at the grain boundary V_{B_0}, and voltage across the grain-boundary U_{GB} plotted as a function of voltage U applied across the sample with various values of the mobility μ. Calculated using Silvaco ATLAS, and quadratic (Eqs. 3.90 and 3.91) and linear potential profile formulas (Eqs. 3.65 and 3.68), respectively. In addition, Eqs. 3.17, 3.21, 3.114, 3.116, 3.117, 3.118, 3.126, 4.4, and 4.5 were used. The parameter values are $l = 10$ μm, $N_d = 10^{21}$ m^{-3} ($E_c - E_F = 0.22$ eV), $N_{GB} = 1$, $N_B^{tot} = 1.4 \cdot 10^{15}$ m^{-2}, $E_c - E_T = 0.60$ eV ($f_n^{eq} = 0.81$), and $T = 300$ K.

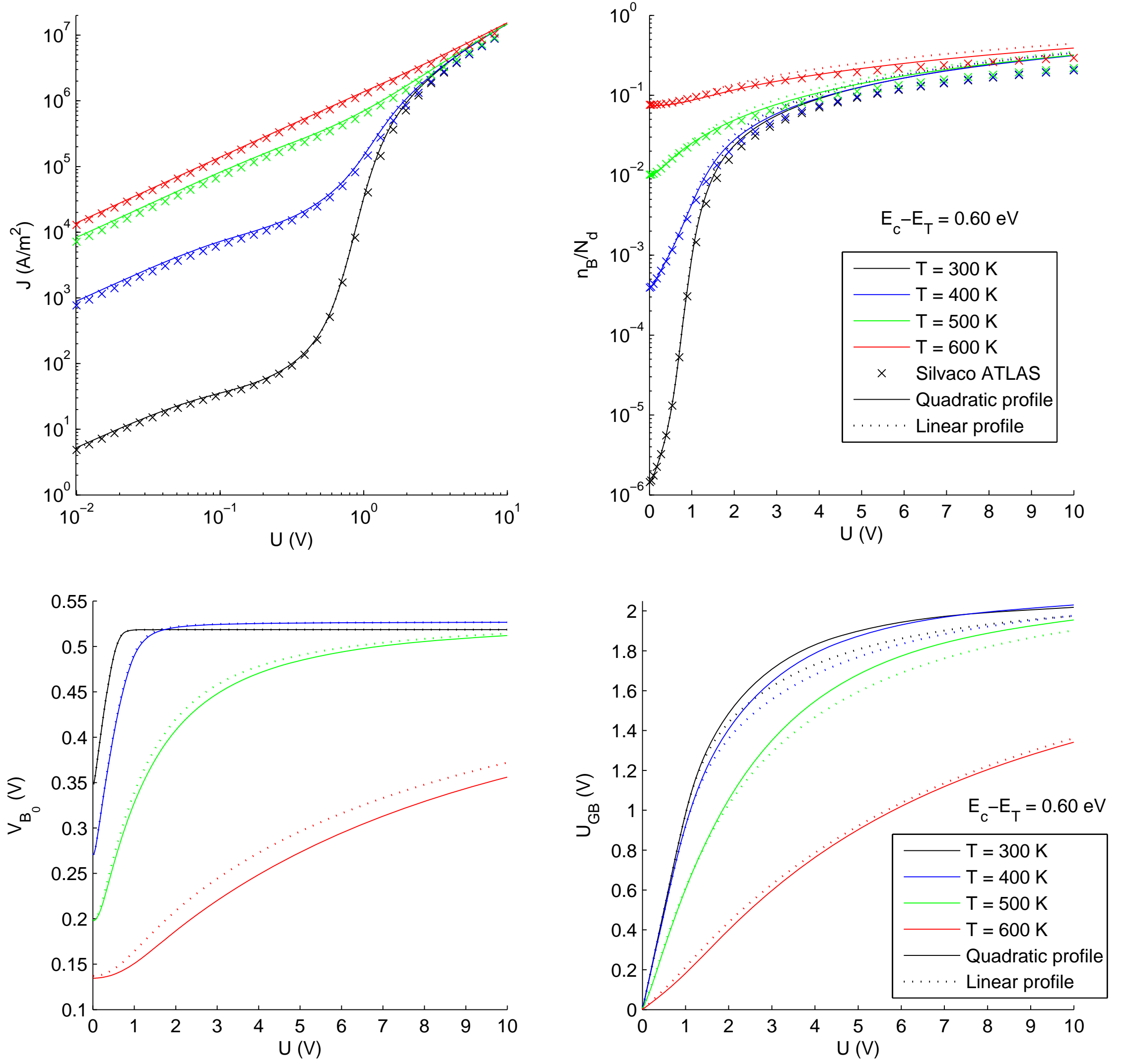

Figure 4.9: Current density J, normalized electron density n_B/N_d, the zero-voltage potential at the grain boundary V_{B_0}, and voltage across the grain-boundary U_{GB} plotted as a function of voltage U applied across the sample with various values the absolute temperature T. Calculated using Silvaco ATLAS, and quadratic (Eqs. 3.90 and 3.91) and linear potential profile formulas (Eqs. 3.65 and 3.68), respectively. In addition, Eqs. 3.17, 3.21, 3.114, 3.116, 3.117, 3.118, 3.125, 4.4, and 4.5 were used. The parameter values are $l = 10$ μm, $\mu = 1000$ cm^2/(Vs), $N_d = 10^{21}$ m^{-3} ($E_c - E_F = 0.22$ eV), $N_{GB} = 1$, $N_B^{tot} = 1.4 \cdot 10^{15}$ m^{-2}, $E_c - E_T = 0.60$ eV ($f_n^{eq}(T_{eq}) = 0.81$), and $T_{eq} = 300$ K.

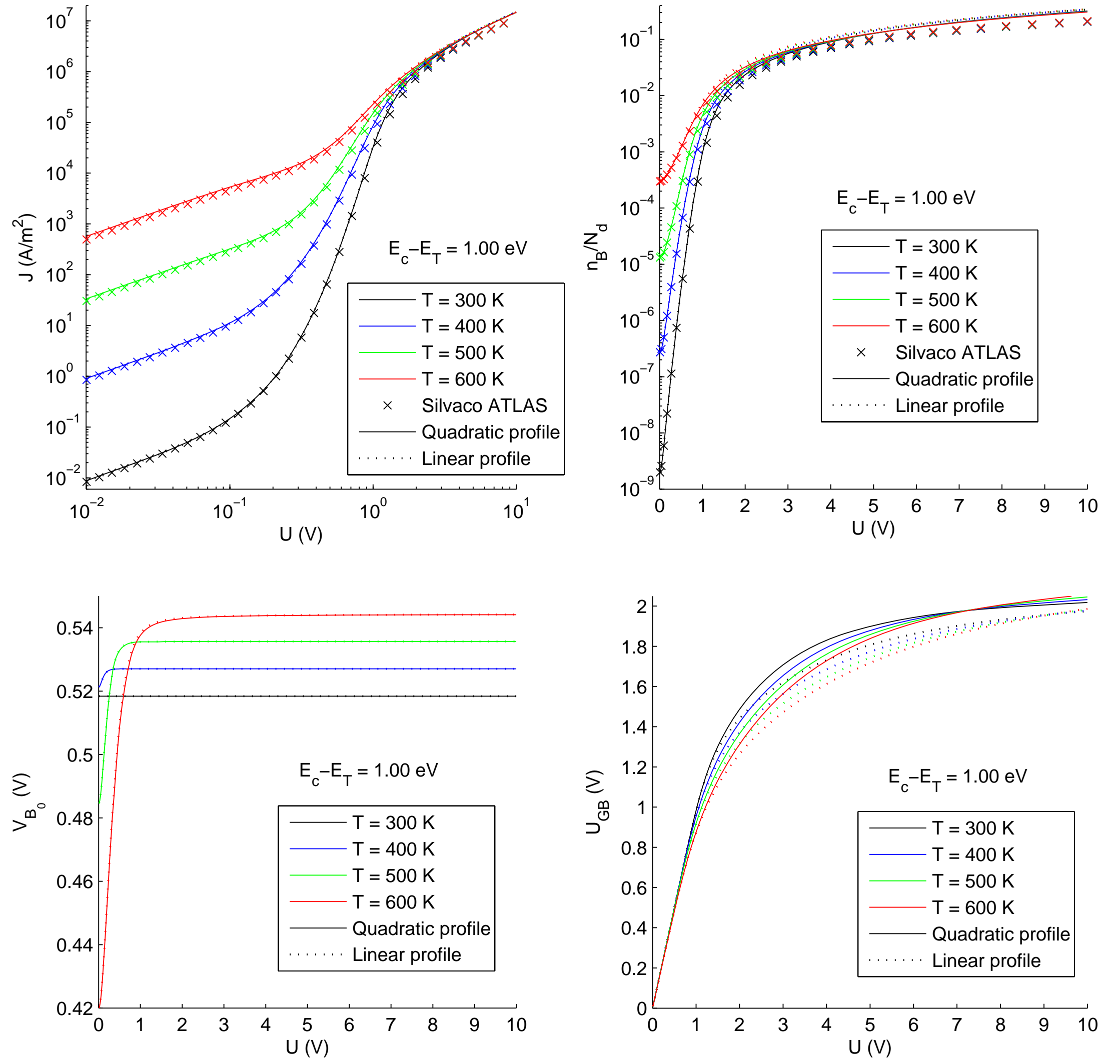

Figure 4.10: Current density J, normalized electron density n_B/N_d, the zero-voltage potential at the grain boundary V_{B_0}, and voltage across the grain-boundary U_{GB} plotted as a function of voltage U applied across the sample with various values the absolute temperature T. Calculated using Silvaco ATLAS, and quadratic (Eqs. 3.90 and 3.91) and linear potential profile formulas (Eqs. 3.65 and 3.68), respectively. In addition, Eqs. 3.17, 3.21, 3.114, 3.116, 3.117, 3.118, 3.125, 4.4, and 4.5 were used. The parameter values are $l = 10$ μm, $\mu = 1000$ cm^2/(Vs), $N_d = 10^{21}$ m^{-3} ($E_c - E_F = 0.22$ eV), $N_{GB} = 1$, $N_B^{tot} = 1.4 \cdot 10^{15}$ m^{-2}, $E_c - E_T = 1.00$ eV ($f_n^{eq}(T_{eq}) \approx 1.0$), and $T_{eq} = 300$ K.

Chapter 5

Small signal analysis of granular semiconductor

In this chapter the AC model of a grain boundaries in n-type semiconductor (see section 3.5) is applied to the small signal analysis of granular n-type semiconductor. In addition, the analytical results are compared with results obtained from the numerical simulations with Silvaco ATLAS.

5.1 Electrical equivalent circuit model

The EEC model for granular semiconductor is shown in Fig. 5.1. Although the model in Fig. 5.1 applies to a semiconductor with a single grain boundary, the model can be easily extended to the case of multiple grain boundaries by connecting additional grain-boundary and bulk regions in series.

The impedance of the granular semiconductor consisting of N_{GB} identical grain boundaries (see Fig. 4.1a) and represented by the EEC shown in Fig. 5.1b is given by

$$Z = \frac{1}{\frac{1}{R_s} + i\omega C_s} + \frac{N_{GB}}{\frac{1}{R_{diff}} + i\omega C_{dep} + \left(R_{char} + \frac{1}{i\omega C_{char}}\right)^{-1} + \left(R_{mod} + i\omega L_{mod}\right)^{-1}}, \tag{5.1}$$

where the series resistance of the bulk region R_s is given by Eq. 4.2 and the series

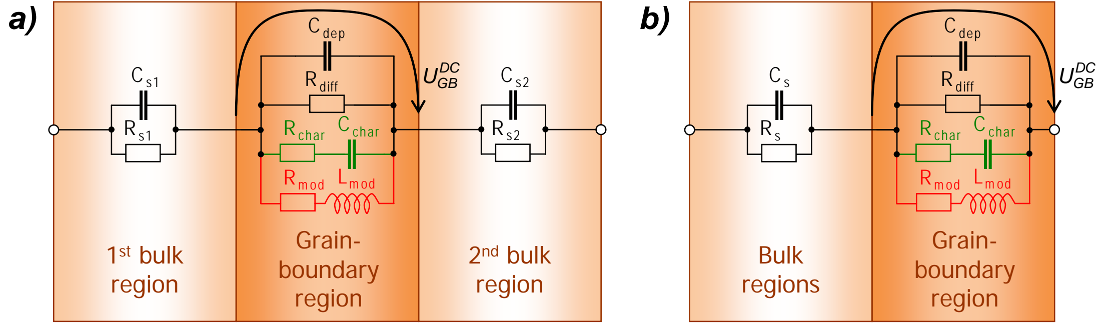

Figure 5.1: Electrical equivalent circuit (EEC) model of granular semiconductor with a single grain boundary. Either the EEC representation (a) or (b) can be employed. U_{GB}^{DC} is the DC bias voltage across the grain boundary.

capacitance caused by the bulk region by

$$C_s = \frac{\varepsilon A}{l - N_{GB} L_d^{corr}}. \tag{5.2}$$

The formulas for the values of the other circuit elements in Fig. 5.1 are given in section 3.5.2.

In order to calculate the values of all the circuit elements in Fig. 5.1 the values of the DC bias voltage across a single grain-boundary region U_{GB}^{DC} and the normalized density of the occupied grain-boundary states in steady state ν_{DC} must be known (see section 3.5.2). For this the DC solution (see section 4.1) must be calculated first. Here the formulas of the 2$^{\text{nd}}$ approximation of linear profile (Eqs. 3.71 and 3.72), and Eqs. 3.17, 3.21, 3.114, 3.116, 3.117, 3.118, 3.126, 4.4, and 4.5 are used in the calculation of U_{GB}^{DC} and ν_{DC}.

The admittance spectra of a granular n-type semiconductor as a function of frequency with various values of the DC bias voltage U_{DC} across the sample are plotted in Fig. 5.2. The admittance spectra are represented by the effective parallel conductance (i.e. the real part of admittance, $\Re\{Y\}$) and the effective parallel capacitance (i.e. the imaginary part of admittance normalized by angular frequency, $\Im\{Y\}/\omega$) in Fig. 5.2. The data in Fig. 5.2 was calculated using Silvaco ATLAS and the analytical model presented in this section (Eq. 5.1).

The various phenomena in the granular semiconductor indicated in Fig. 5.2 occur in different frequency ranges: At very high frequencies ($> 10^{11}$ Hz in Fig. 5.2) only the conductance and capacitance of the bulk regions of the material (i.e. R_s and C_s in Fig. 5.1b) are visible. At intermediate frequencies (around 10^4–10^8 Hz in Fig. 5.2)

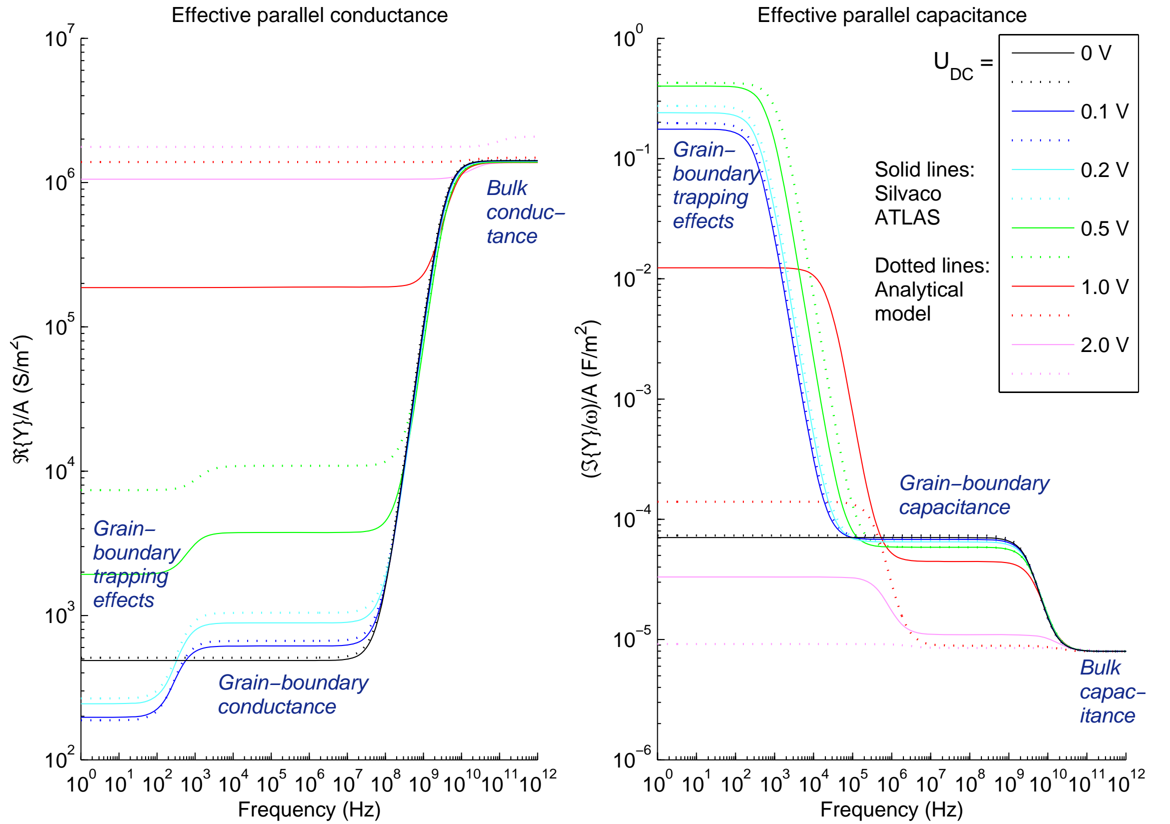

Figure 5.2: Effective parallel conductance and capacitance plotted as a function of frequency with various values of the DC bias voltage U_{DC} across the sample. The regions of spectra corresponding to the various phenomena are indicated. The grain-boundary conductance and capacitance correspond to R_{diff} and C_{dep}, respectively. Calculated using Silvaco ATLAS and the analytical model presented in this section (Eq. 5.1). The parameter values are $l = 10$ μm, $\mu = 1000$ cm^2/(Vs), $N_d = 10^{21}$ m^{-3} ($E_c - E_F = 0.22$ eV), $N_{GB} = 1$, $\eta = 1$, $N_B^{tot} = 1.4 \cdot 10^{15}$ m^{-2}, $E_c - E_T = 0.60$ eV ($f_n^{eq} = 0.81$), $\sigma_n = 10^{-14}$ cm^2, and $T = 300$ K.

the ordinary grain-boundary AC conductance and capacitance (i.e. R_{diff} and C_{dep} in Fig. 5.1) define the AC response of the material. At very low frequencies ($< 10^2$ Hz in Fig. 5.2) the electronic trapping effects at the grain boundaries (i.e. the circuit branches R_{char}–C_{char} and R_{mod}–L_{mod} in Fig. 5.1) dominate the admittance spectrum. Fig. 5.2 shows that the grain-boundary trapping effects in the admittance spectrum disappear at zero DC bias voltage as it was discussed earlier (see section 3.5.2).

Fig. 5.2 shows that the agreement between the analytical model and the numerical simulation results is very good in the whole frequency range at low DC bias voltages

($U_{DC} \lesssim 0.2$ V). At higher voltages the analytical model overestimates the grain-boundary conductance and underestimates the grain-boundary capacitance and the effective capacitance of the grain-boundary trapping effects (see Fig. 5.2). In fact the discrepancy between the models at higher voltages is such a large that the analytical model should not be used at high voltages ($U_{DC} \gtrsim 0.5$ V in the case of Fig. 5.2). The poor performance of the analytical model is mostly caused by the simplest approximative formulas (Eqs. 3.71 and 3.72) used in the derivation of the model (see sections 3.5.1 and 3.5.2).

5.2 Effect of parameters

In this section the effect of the most important parameters of the model on the admittance spectrum of n-type granular semiconductor are discussed.

Here the admittance spectra are represented by the effective parallel conductance and capacitance. They were calculated at three different DC bias voltages (0 V, 0.1 V, and 1.0 V) using Silvaco ATLAS and the analytical model presented in section (Eq. 5.1). The effective parallel conductance and capacitance as a function of frequency with various values of the parameters of the model are plotted in Figs. 5.3, 5.4, 5.5, 5.6, 5.7, 5.8, 5.9, and 5.10. In all of the figures at 0 V and 0.1 V DC bias voltages the analytical model and the numerical results are in a very good agreement in the whole frequency range. At the high DC bias voltage of 1.0 V the performance of the analytical model is poor, as it was discussed in section 5.1.

In Fig. 5.3 the value of the electron capture cross-section σ_n is varied. σ_n determines the rate of the electronic trapping process, hence it only affects the grain-boundary trapping section of the admittance spectrum of the material. When σ_n is increased the characteristic step in the admittance step shifts roughly by the same amount to higher frequencies (see the $U_{DC} = 0.1$ V plot in Fig. 5.3). In addition, the magnitude of the effective capacitance of the trapping effect changes.

The energy level of the grain-boundary state $E_c - E_T$ is varied in Fig. 5.4. In addition to the trapping process $E_c - E_T$ determines the zero-voltage grain-boundary potential V_{B_0}. This is the reason why also the grain-boundary conductance and capacitance change with $E_c - E_T$ in Fig. 5.4. Similar effect is also shown in Fig. 5.5 in which the total density of grain-boundary states N_B^{tot} is varied. However, because N_B^{tot}

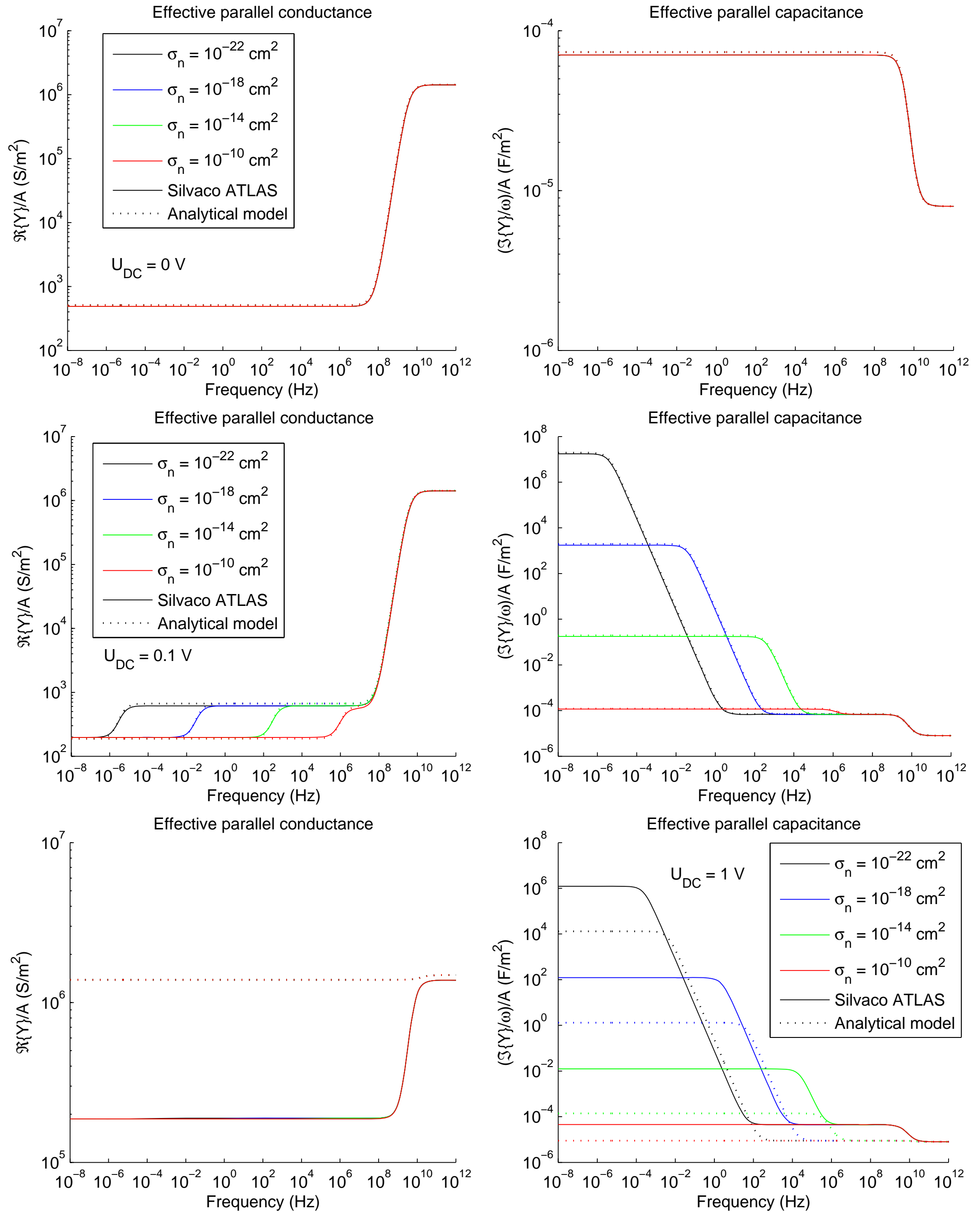

Figure 5.3: Effective parallel conductance and capacitance plotted as a function of frequency with various values of the electron capture cross-section σ_n and the DC bias voltage U_{DC} across the sample. Calculated using Silvaco ATLAS and the analytical model presented in section 5.1 (Eq. 5.1). The parameter values are $l = 10$ μm, $\mu = 1000$ cm^2/(Vs), $N_d = 10^{21}$ m^{-3} ($E_c - E_F = 0.22$ eV), $N_{GB} = 1$, $\eta = 1$, $N_B^{tot} = 1.4 \cdot 10^{15}$ m^{-2}, $E_c - E_T = 0.60$ eV ($f_n^{eq} = 0.81$), and $T = 300$ K.

does not directly determine the rate of the trapping, the effect of N_B^{tot} on the low frequency part of the admittance spectrum is weaker than with $E_c - E_T$.

The effect of the length of the sample l on the admittance spectrum is shown in Fig. 5.6. Mostly the high-frequency part of the spectrum, where the bulk effect exist, changes with l. However, slight changes occur also in the whole spectrum due to the decrease of the DC bias voltage across the grain boundary U_{GB}^{DC} with l.

In Fig. 5.7 the donor density N_d is varied. N_d affects the bulk conductance regions and the zero-voltage grain-boundary potential V_{B_0} (see Eq. 3.17). Therefore only the bulk capacitance region (at high frequencies) does not change in the admittance spectrum when N_d is changed.

The mobility μ is varied in Fig. 5.8. μ determines both the grain-boundary and bulk conductances. μ has also an effect on the grain-boundary trapping process via the delay coefficient ξ (see Eq. 3.120). This effect is shown at $U_{DC} = 0.1$ V in Fig. 5.8: When $\mu = 10^{-3}$ cm$^2/(Vs)$ the step corresponding to the grain-boundary step in the effective parallel conductance spectrum is at much lower frequencies (at around 1 Hz) than with higher values of μ (at around 10^3 Hz). In addition the magnitude of the effective parallel capacitance at low frequencies changes with μ due to L_{mod} (see section 3.5.2).

Finally, the effect of the absolute temperature T is shown in Figs. 5.9 and 5.10, in which two different values for the energy levels of the grain-boundary state $E_c - E_T$, 0.60 eV and 1.00 eV, are used. Due to the various temperature dependencies the trapping process and grain-boundary conductance is highly dependent on temperature. Only the bulk region of the admittance spectrum does not change with temperature.

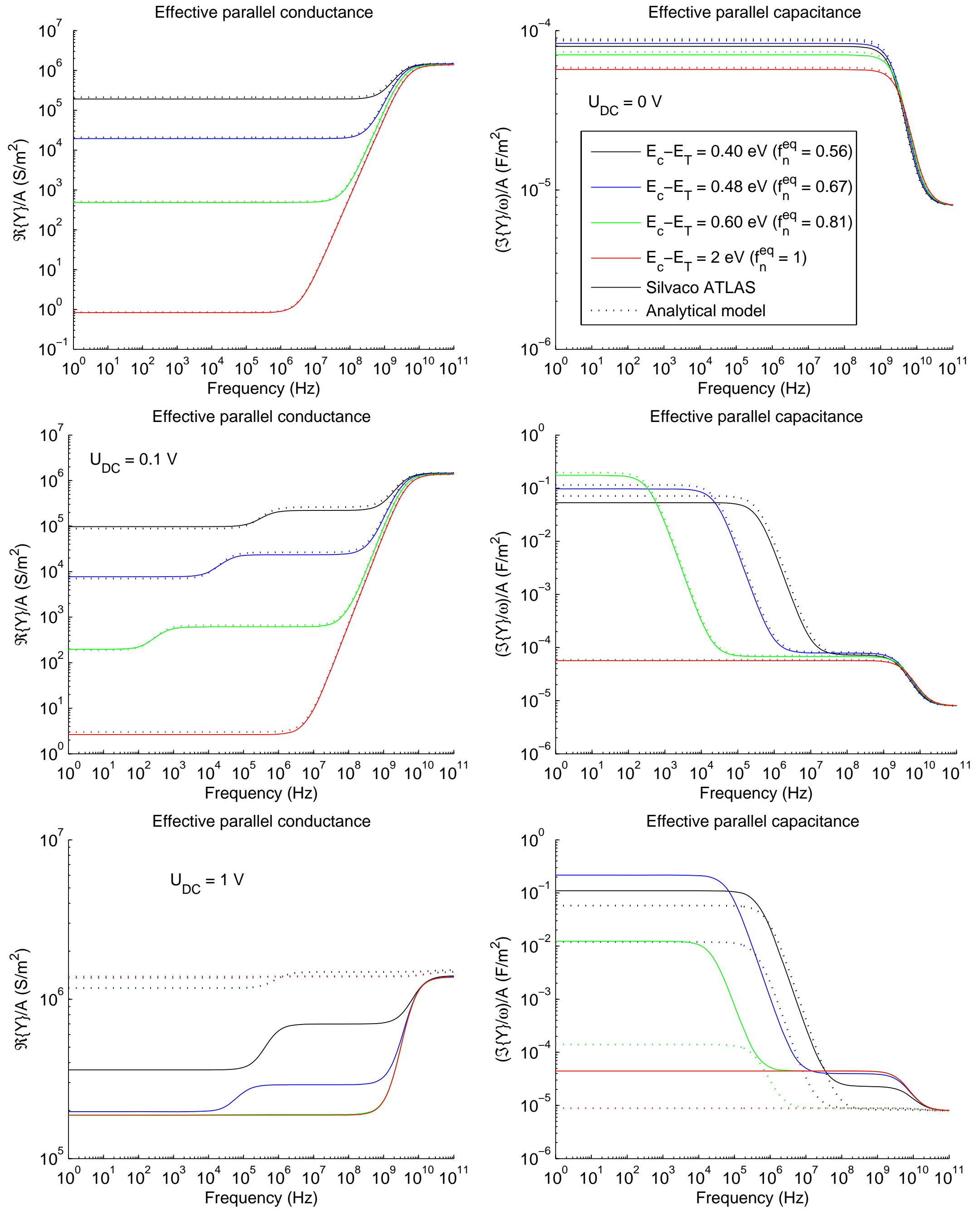

Figure 5.4: Effective parallel conductance and capacitance plotted as a function of frequency with various values of the energy level of the grain-boundary state $E_c - E_T$ and the DC bias voltage U_{DC} across the sample. Calculated using Silvaco ATLAS and the analytical model presented in section 5.1 (Eq. 5.1). The parameter values are $l = 10$ μm, $\mu = 1000$ cm^2/(Vs), $N_d = 10^{21}$ m^{-3} ($E_c - E_F = 0.22$ eV), $N_{GB} = 1$, $\eta = 1$, $N_B^{tot} = 1.4 \cdot 10^{15}$ m^{-2}, $\sigma_n = 10^{-14}$ cm^2, and $T = 300$ K.

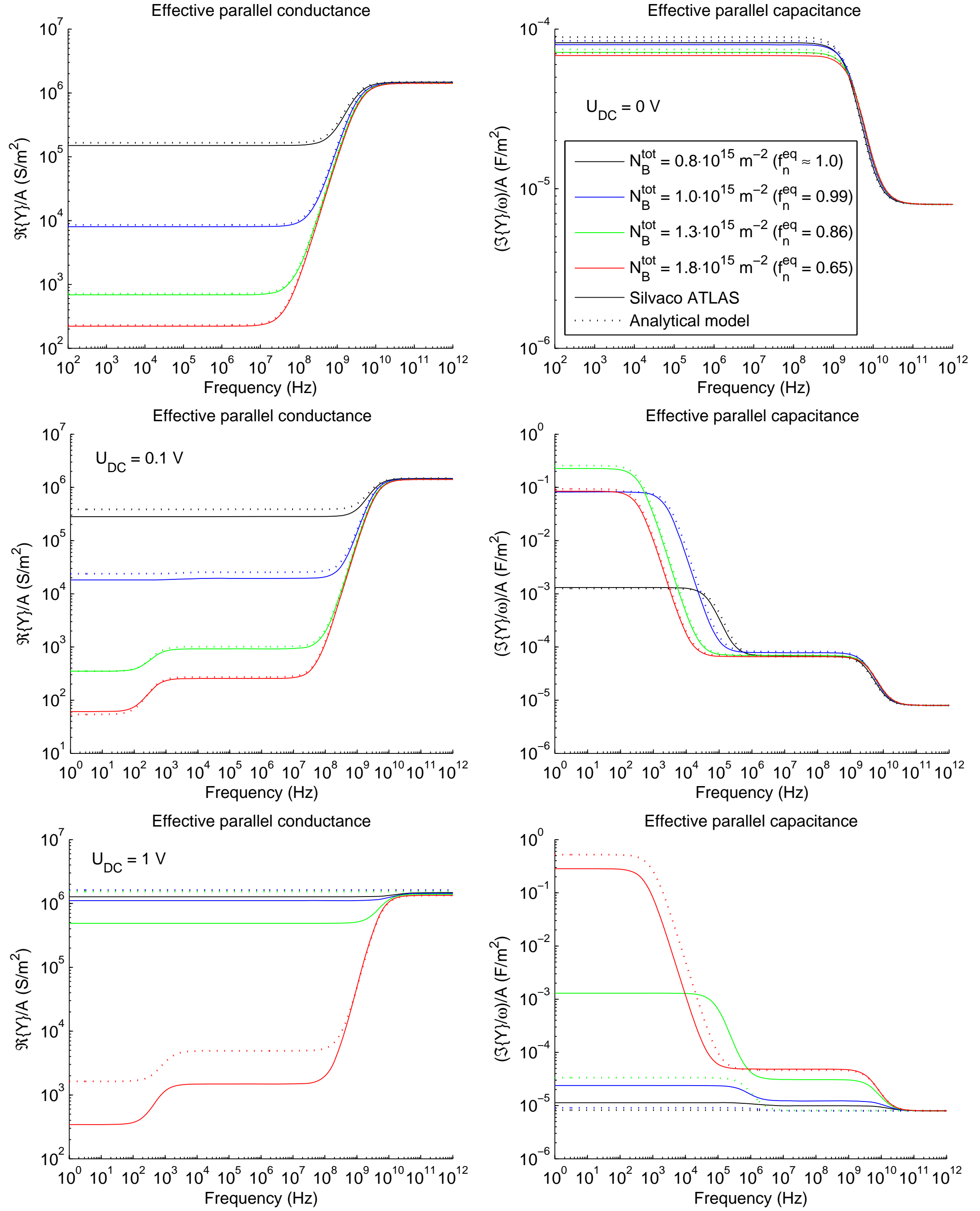

Figure 5.5: Effective parallel conductance and capacitance plotted as a function of frequency with various values of the total density of grain-boundary states N_B^{tot} and the DC bias voltage U_{DC} across the sample. Calculated using Silvaco ATLAS and the analytical model presented in section 5.1 (Eq. 5.1). The parameter values are $l = 10$ μm, $\mu = 1000$ cm^2/(Vs), $N_d = 10^{21}$ m^{-3} ($E_c - E_F = 0.22$ eV), $N_{GB} = 1$, $\eta = 1$, $E_c - E_T = 0.60$ eV, $\sigma_n = 10^{-14}$ cm^2, and $T = 300$ K.

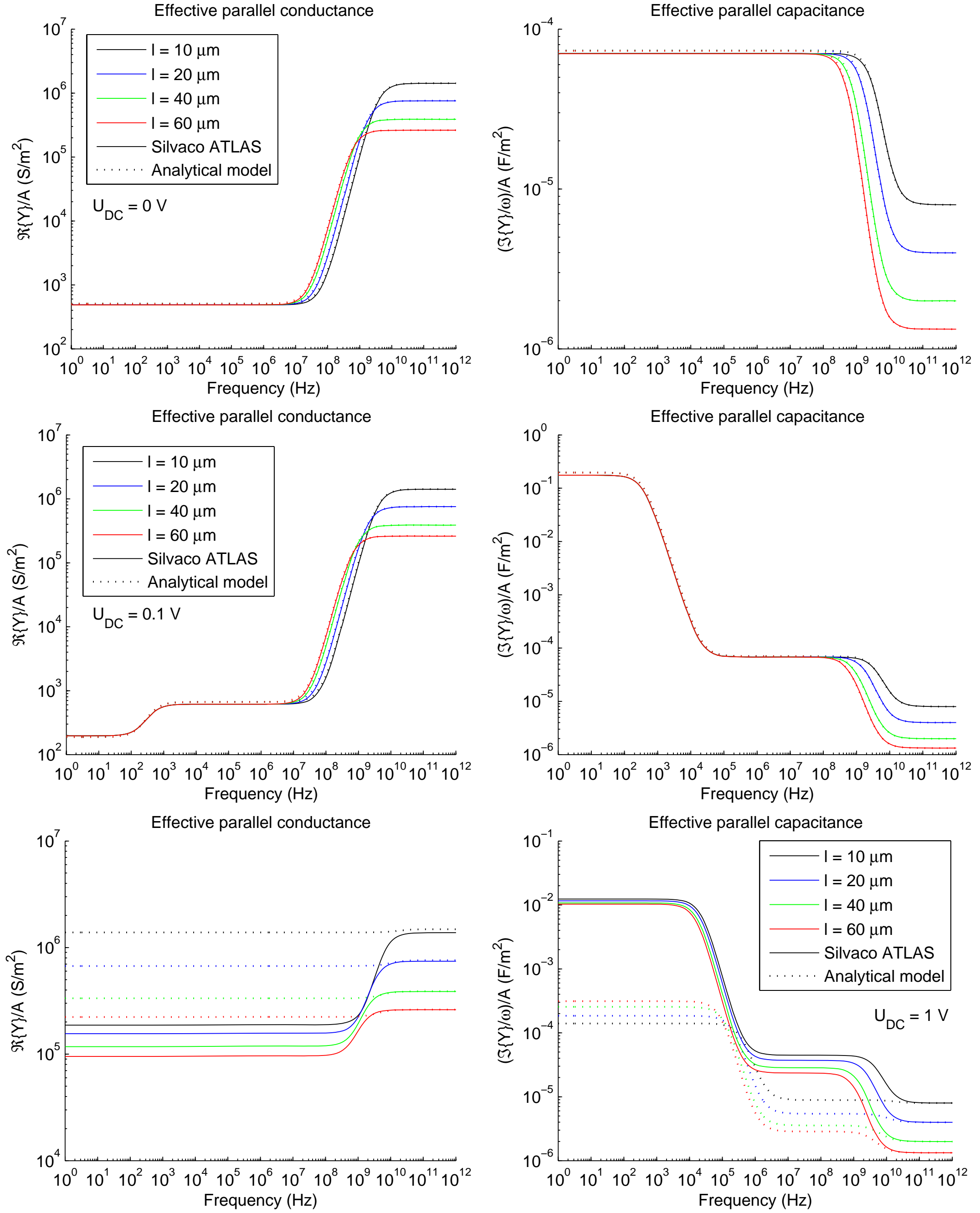

Figure 5.6: Effective parallel conductance and capacitance plotted as a function of frequency with various values of the sample length l and the DC bias voltage U_{DC} across the sample. Calculated using Silvaco ATLAS and the analytical model presented in section 5.1 (Eq. 5.1). The parameter values are $\mu = 1000$ cm^2/(Vs), $N_d = 10^{21}$ m^{-3} ($E_c - E_F = 0.22$ eV), $N_{GB} = 1$, $\eta = 1$, $N_B^{tot} = 1.4 \cdot 10^{15}$ m^{-2}, $E_c - E_T = 0.60$ eV ($f_n^{eq} = 0.81$), $\sigma_n = 10^{-14}$ cm^2, and $T = 300$ K.

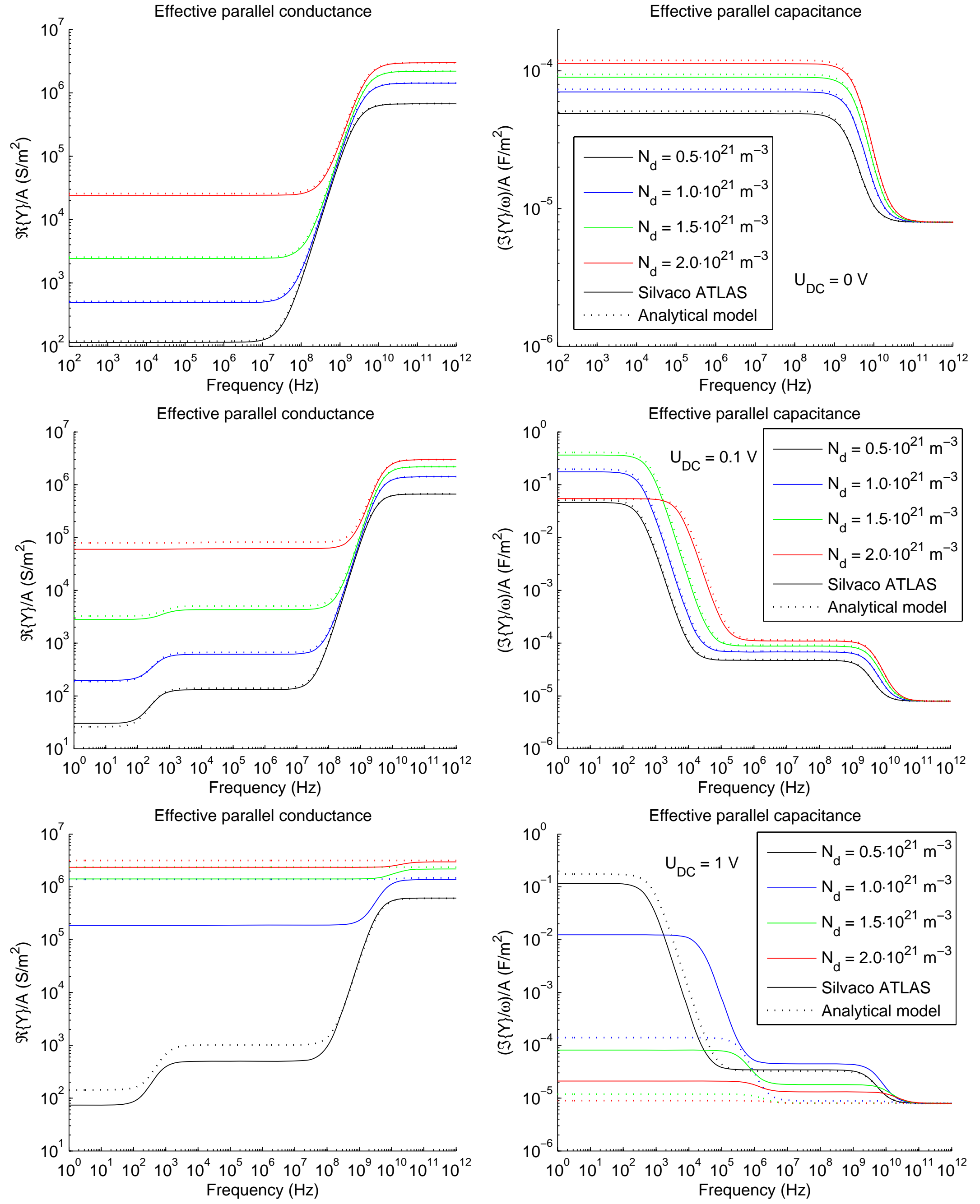

Figure 5.7: Effective parallel conductance and capacitance plotted as a function of frequency with various values of the donor density N_d and the DC bias voltage U_{DC} across the sample. Calculated using Silvaco ATLAS and the analytical model presented in section 5.1 (Eq. 5.1). The parameter values are $l = 10\ \mu\text{m}$, $\mu = 1000\ \text{cm}^2/(\text{Vs})$, $N_{GB} = 1$, $\eta = 1$, $N_B^{tot} = 1.4 \cdot 10^{15}\ \text{m}^{-2}$, $E_c - E_T = 0.60$ eV, $\sigma_n = 10^{-14}\ \text{cm}^2$, and $T = 300$ K.

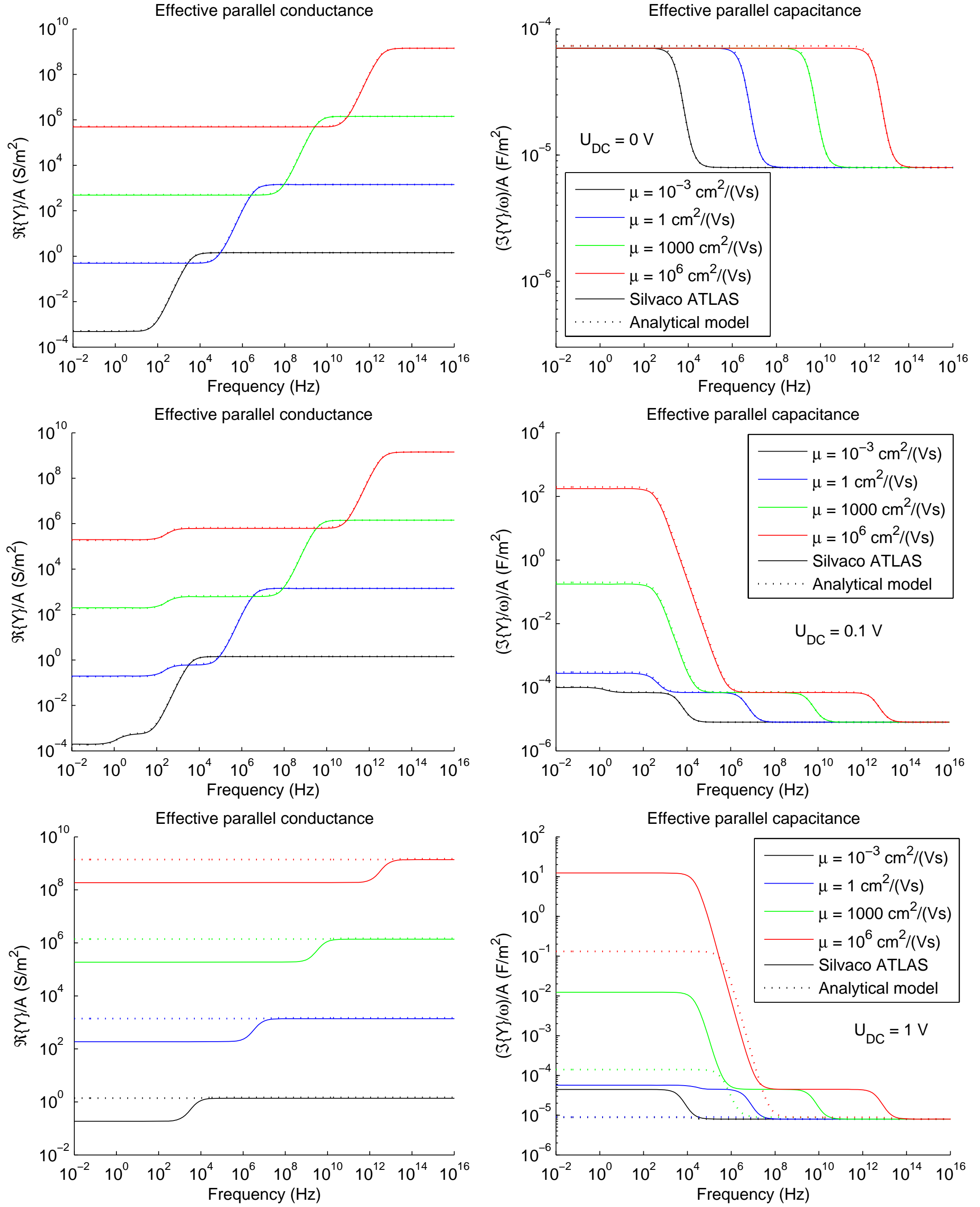

Figure 5.8: Effective parallel conductance and capacitance plotted as a function of frequency with various values of the mobility μ and the DC bias voltage U_{DC} across the sample. Calculated using Silvaco ATLAS and the analytical model presented in section 5.1 (Eq. 5.1). The parameter values are $l = 10\ \mu$m, $N_d = 10^{21}$ m^{-3} ($E_c - E_F = 0.22$ eV), $N_{GB} = 1$, $\eta = 1$, $N_B^{tot} = 1.4 \cdot 10^{15}$ m^{-2}, $E_c - E_T = 0.60$ eV ($f_n^{eq} = 0.81$), $\sigma_n = 10^{-14}$ cm^2, and $T = 300$ K.

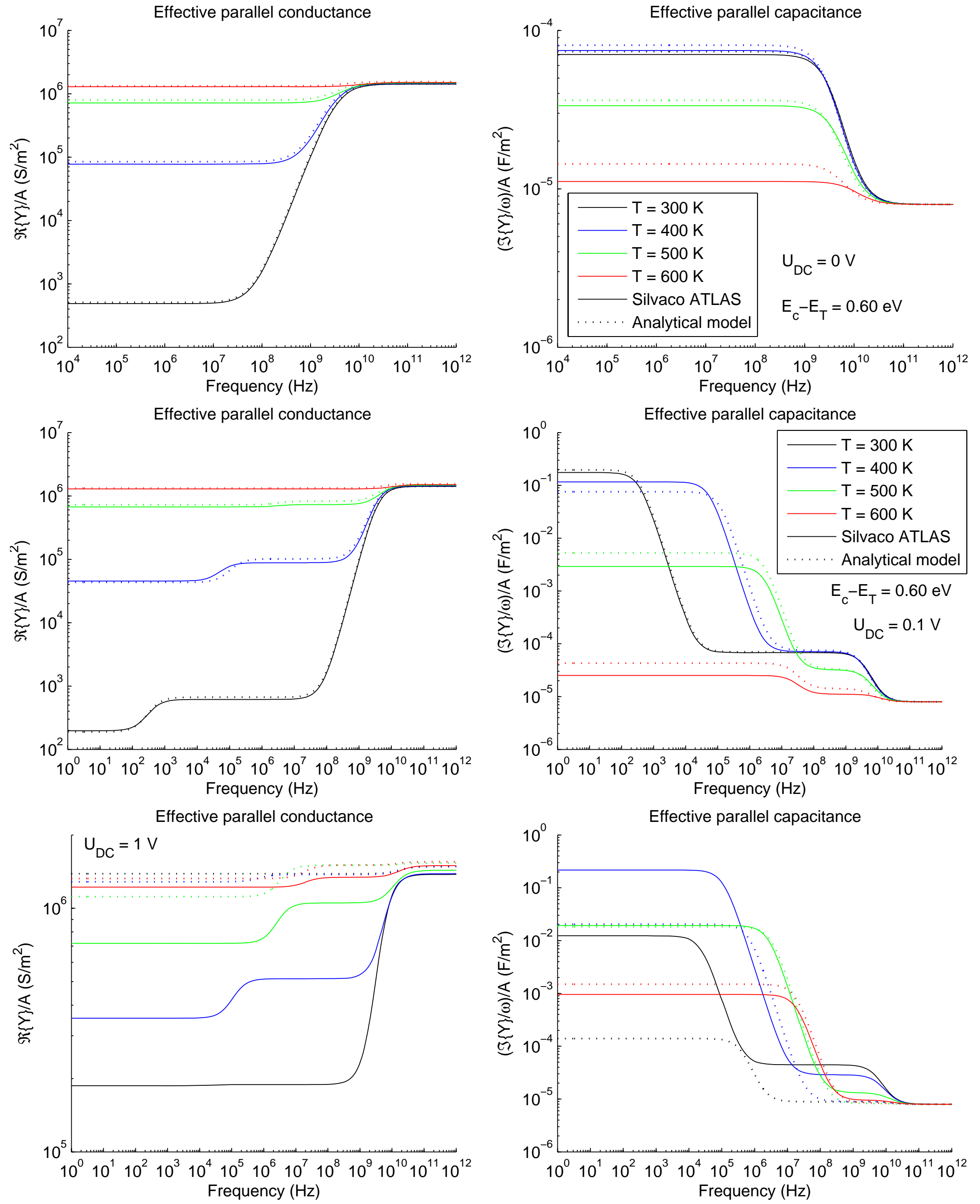

Figure 5.9: Effective parallel conductance and capacitance plotted as a function of frequency with various values of the absolute temperature T and the DC bias voltage U_{DC} across the sample. Calculated using Silvaco ATLAS and the analytical model presented in section 5.1 (Eq. 5.1). The parameter values are $l = 10\ \mu$m, $\mu = 1000$ cm^2/(Vs), $N_d = 10^{21}$ m^{-3} ($E_c - E_F = 0.22$ eV), $N_{GB} = 1$, $\eta = 1$, $N_B^{tot} = 1.4 \cdot 10^{15}$ m^{-2}, $E_c - E_T = 0.60$ eV ($f_n^{eq}(300\text{ K}) = 0.81$), and $\sigma_n = 10^{-14}$ cm^2.

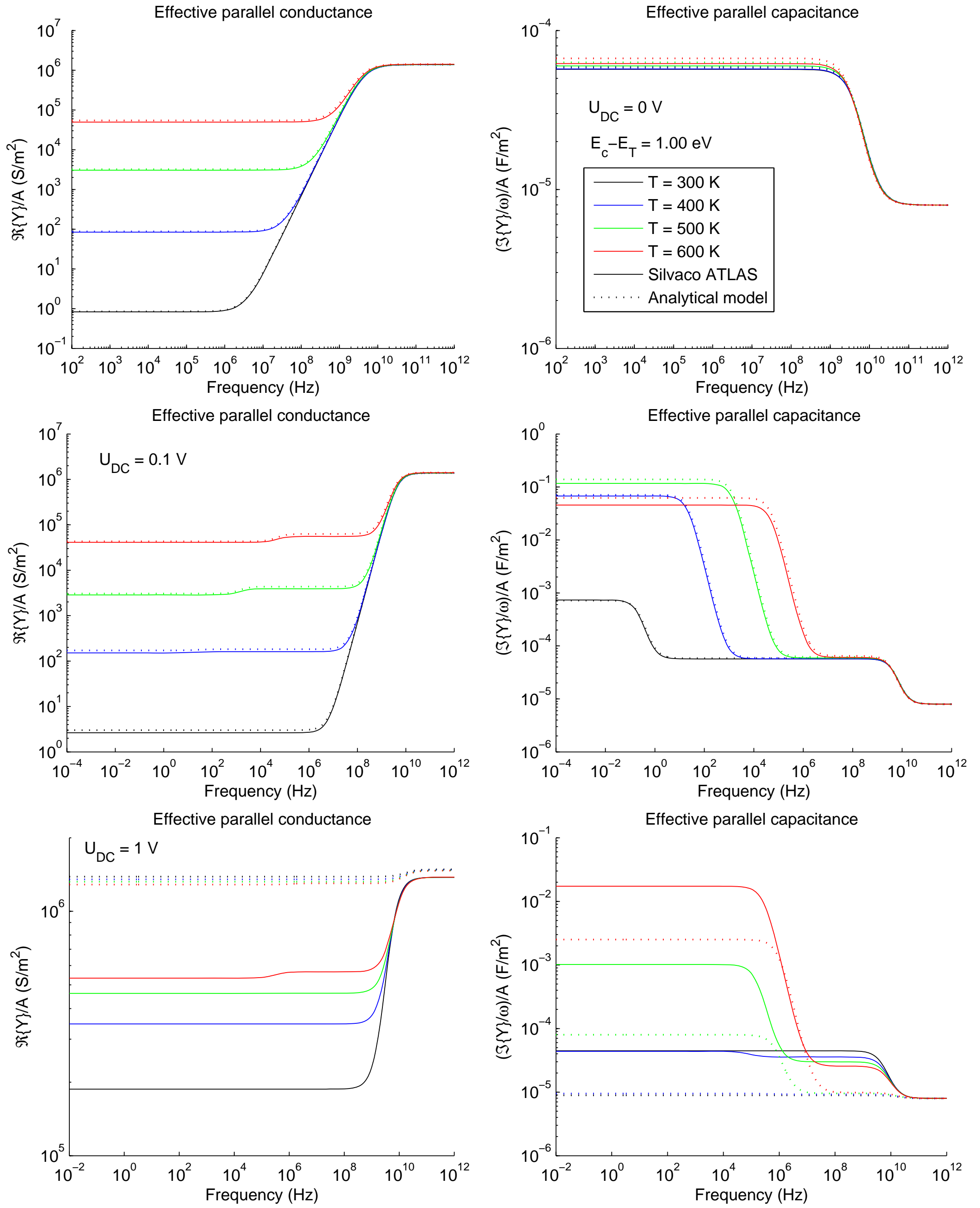

Figure 5.10: Effective parallel conductance and capacitance plotted as a function of frequency with various values of the absolute temperature T and the DC bias voltage U_{DC} across the sample. Calculated using Silvaco ATLAS and the analytical model presented in section 5.1 (Eq. 5.1). The parameter values are $l = 10$ μm, $\mu = 1000$ cm^2/(Vs), $N_d = 10^{21}$ m^{-3} ($E_c - E_F = 0.22$ eV), $N_{GB} = 1$, $\eta = 1$, $N_B^{tot} = 1.4{\cdot}10^{15}$ m^{-2}, $E_c - E_T = 1.00$ eV ($f_n^{eq}(300\text{ K}) \approx 1.0$), and $\sigma_n = 10^{-14}$ cm^2.

Chapter 6

Conclusions

In this work the electrical properties of granular large band-gap n-type semiconductor were modelled using analytical and numerical simulation methods. The effect of holes in the material was neglected. However, with very small changes, the results presented in this work can also be applied to a p-type semiconductor. The analytical model was compared with the results from the SILVACO ATLAS device simulation software.

In this work the analytical DC and AC models of the granular n-type semiconductor were presented. The grain boundaries were modelled with infinitely thin interfaces that have acceptor-type electronic interface states with a single discrete energy level. The whole granular material was modelled with a number of identical grain boundaries separated by bulk regions.

The potential in the grain-boundary region was modelled with three different profiles: the quadratic potential profile with the bulk electric field taken into account, the quadratic potential profile without the bulk electric field, and the linear potential profile. The comparison of the DC current density and the electron density at the grain boundary calculated with different potential profiles showed that all potential profiles gave very similar results. In other words, it seems that when the electric properties are calculated only the region near the top of the grain-boundary potential barrier needs to be considered.

Using the models the I–V characteristics of the granular semiconductor was calculated in the case with and without electronic trapping at the grain boundaries. The

results showed that I–V curves had four characteristic regions: linear, sub-linear, super-linear (nonlinear), and series resistance limited (linear). In the linear regime at low voltages the electrical conduction is limited by the grain-boundary potential barrier. The sub-linear region is caused by the electronic trapping at grain boundaries. In the super-linear region at higher voltages the effective potential barrier decreases with increasing voltage and the current increases exponentially. In the series resistance limited region at high voltages the resistance of the bulk parts of the granular material the I–V curves return back to linear. The agreement between the analytical and numerical results was excellent in a large voltage range. The poorer performance at high voltages was explained by the failure of the depletion region approximation, which was also seen in the potential profile calculations.

In the small-signal AC analysis of the granular semiconductor the electrical equivalent circuit (EEC) model of the granular semiconductor material was presented. The model shows that a granular semiconductor material exhibits negative admittance and capacitance, when the electronic trapping at grain boundaries is present and a DC bias voltage is applied across the material. The analytical and numerical results were in a very good agreement in the whole frequency range. However, at high DC bias voltages the analytical model fails due to the simple approximative formulas used in the derivation of the analytical model.

Bibliography

[1] F. Greuter and G. Blatter. Electrical properties of grain boundaries in polycrystalline compound semiconductors. *Semicond. Sci. Technol.*, 5:111–137, 1990.

[2] J. W. Orton and M. J. Powell. The Hall effect in polycrystalline and powdered semiconductors. *Reports on Progress in Physics*, 43:1263–1307, 1980.

[3] Aapo Varpula. AFM and XPS characterization of the iron oxide thin film growth process. Special Assignment, Helsinki University of Technology, 2004.

[4] Paolo R. Bueno, José A. Varela, and Elson Longo. SnO_2, ZnO and related polycrystalline compound semiconductors: An overview and review on the voltage-dependent resistance (non-ohmic) feature. *Journal of the European Ceramic Society*, 28:505–529, 2008.

[5] C. O. Park and S. A. Akbar. Ceramics for chemical sensing. *Journal of Materials Science*, 38:4611–4637, 2003.

[6] G. Eranna, B.C. Joshi, D.P. Runthala, and R.P. Gupta. Oxide materials for development of integrated gas sensors - a comprehensive review. *Critical Reviews in Solid State and Materials Sciences*, 29:111–188, 2004.

[7] Dieter Kohl. Function and applications of gas sensors. *Journal of Physics D: Applied Physics*, 34:R125–R149, 2001.

[8] Isolde Simon, Nicolae Bârsan, Michael Bauer, and Udo Weimar. Micromachined metal oxide gas sensors: opportunities to improve sensor performance. *Sensors and Actuators B, Chemical*, 73:1–26, 2001.

[9] Nicolae Barsan and Udo Weimar. Conduction model of metal oxide gas sensors. *Journal of Electroceramics*, 7:143–167, 2001.

[10] Silvaco Data Systems Inc. *ATLAS User's Manual*, June 2008.

[11] A. Varpula, S. Novikov, J. Sinkkonen, and M. Utriainen. Bias dependent sensitivity in metal-oxide gas sensors. *Sensors and Actuators B, Chemical*, 131:134–142, 2008.

[12] Aapo Varpula, Sergey Novikov, Juha Sinkkonen, and Mikko Utriainen. Negative admittance in resistive metal oxide gas sensors. *Journal of Physics: Conference Series*, 100:082036, 2008.

[13] Juha Sinkkonen. *Puolijohdeteknologian perusteet*. Helsinki University of Technology, Espoo, Finland, 1996.

[14] Stephen Elliot. *The Physics and Chemistry of Solids*. John Wiley & Sons, West Sussex, England, 2nd edition, 2000.

[15] Hans Lüth. *Solid surfaces, interfaces and thin films*. Springer, Berlin, Germany, 4th edition, 2001.

[16] A. Many, Y. Goldstein, and N. B. Grover. *Semiconductor Surfaces*. North-Holland Publishing Company, Amsterdam, The Netherlands, 1965.

[17] Dieter K. Schroder. *Semiconductor material and device characterization*. Wiley-Interscience, Hoboken, the United States of America, 3rd edition, 2006.

[18] S. M. Sze. *Physics of Semiconductor Devices*. Wiley-Interscience, New York, the United States of America, 2nd edition, 1981.

[19] T. Wolkenstein. *Electronic Processes on Semiconductor Surfaces during Chemisorption*. Plenum Publishing Corporation, New York, the United States of America, 1991.

[20] Junhua Ding, Thomas J. McAvoy, Richard E. Cavicchi, and Steve Semancik. Surface state trapping models for SnO_2-based microhotplate sensors. *Sensors and Actuators B, Chemical*, 77:597–613, 2001.

[21] F.F. Vol'kenshtein. *The Electronic Theory of Catalysis on Semiconductors*. Pergamon Press Ltd., New York, U.S.A., 1963.

[22] C. R. M. Grovenor. Grain boundaries in semiconductors. *Journal of Physics C: Solid State Physics*, 18:4079–4119, 1985.

[23] Avner Rothschild and Yigal Komem. On the relationship between the grain size and gas-sensitivity of chemo-resistive metal-oxide gas sensors with nanosized grains. *Journal of Electroceramics*, 13:697–701, 2004.

[24] Jack Vanderlinde. *Classical Electromagnetic Theory*. Kluwer, 2nd edition, 2004.

[25] A. Oprea, E. Moretton, N. Bârsan, W. J. Becker, J. Wöllenstein, and U. Weimar. Conduction model of SnO_2 thin films based on conductance and Hall effect measurements. *Journal of Applied Physics*, 100(033716), 2006.

[26] V.K. Sikka and C.J. Rosa. The oxidation kinetics of tungsten and the determination of oxygen diffusion coefficient in tungsten trioxide. *Corrosion Science*, 20:1201–1219, 1980.

[27] B. Kamp, R. Merkle, R. Lauck, and J. Maier. Chemical diffusion of oxygen in tin dioxide: Effects of dopants and oxygen partial pressure. *Journal of Solid State Chemistry*, 178:3027–3039, 2005.

[28] J. W. Essam. Percolation theory. *Reports on Progress in Physics*, 43:833–912, 1980.

[29] Scott Kirkpatrick. Percolation and conduction. *Reviews of Modern Physics*, 45:574–588, 1973.

[30] Muhammad Sahimi. *Applications of Percolation Theory*. Taylor & Francis, 1994.

[31] J. P. Clerc, G. Giraud, J. M. Laugier, and J. M. Luck. The electrical conductivity of binary disordered systems, percolation clusters, fractals and related models. *Advances is Physics*, 39(3):191–309, 1990.

[32] Rolf Landauer. The electrical resistance of binary metallic mixtures. *Journal of Applied Physics*, 23:779–784, 1952.

[33] W. R. Tinga, W. A. G. Voss, and D. F. Blossey. Generalized approach to multiphase dielectric mixture theory. *Journal of Applied Physics*, 44(9):3897–3902, 1973.

[34] Johan Helsing and Andreas Helte. Effective conductivity of aggregates of anisotropic grains. *Journal of Applied Physics*, 69(6):3583–3588, 1991.

[35] G. Dezanneau, A. Morata, A. Tarancón, M. Salleras, F. Peiró, and J. R. Morante. Grain-boundary resistivity versus grain size distribution in three-dimensional polycrystals. *Applied Physics Letters*, 88:141920, 2006.

[36] J. Fleig and J. Maier. A finite element study on the grain boundary impedance of different microstructures. *Journal of The Electrochemical Society*, 145:2081–2089, 1998.

[37] J. Sinkkonen. DC conductivity of a random barrier network. *Physica Status Solidi (b)*, 102:621–627, 1980.

[38] Leora Sali and David J. Bergman. Effective medium approximation for strongly nonlinear media. *Journal of Statistical Physics*, 86:455–479, 1997.

[39] K. W. Yu and G. Q. Gu. Effective conductivity of nonlinear composites. II. Effective-medium approximation. *Physical Review B*, 47(12):7568–7571, 1993.

[40] Wei En-bo, Song Jin-bao, and Gu Guo-qing. Effective response of a non-linear composite in external AC electric field. *Physica B*, 324:322–328, 2002.

[41] Matthias Batzill and Ulrike Diebold. The surface and materials science of tin oxide. *Progress in Surface Science*, 79:47–154, 2005.

[42] K. Ellmer. Resistivity of polycrystalline zinc oxide films: current status and physical limit. *Journal of Physics D: Applied Physics*, 34:3097–3108, 2001.

[43] Karl W. Böer. *Survey of Semiconductor Physics, Volume II*. Van Nostrand Reinhold, New York, the United States of America, 1992.

[44] Ulrike Diebold. The surface science of titanium dioxide. *Surface Science Reports*, 48:53–229, 2003.

[45] G. Blatter and F. Greuter. Carrier transport through grain boundaries in semiconductors. *Physical Review B*, 33(6):3952–3966, 1986.

[46] Lennart Råde and Bertil Westergren. *Mathematics Handbook for Science and Engineering*. Studentlitteratur, Lund, Sweden, 4th edition, 1998. On page 196.

[47] Wolfram Research Inc. Wolfram Mathematica Online Integrator. `http://integrals.wolfram.com/`, 2009.

[48] Eric W. Weisstein. Erfi, 2004. From MathWorld `http://mathworld.wolfram.com/Erfi.html`.

[49] Paul Godfrey and Peter J. Acklam. erfz, error function for complex inputs implemented in MATLAB. Available at MATLAB Central, `http://www.mathworks.com/matlabcentral/fileexchange/3574`, 2001.

[50] Juha Sinkkonen, Sergey Novikov, Aapo Varpula, and J. Haapamaa. Characterization of epiready n^+-GaAs (100) surfaces by SPV-transient. *Proceedings of SPIE*, 6800:68001D, 2008.

[51] Avner Rothschild and Yigal Komem. Numerical computation of chemisorption isotherms for device modeling of semiconductor gas sensors. *Sensors and Actuators B, Chemical*, 93:362–369, 2003.

[52] Kimmo Silvonen. *Sähkötekniikka ja elektroniikka*. Otatieto, Helsinki, Finland, 2nd edition, 2003.

[53] G. E. Pike. Diffusion-limited quasi Fermi level near a semiconductor grain boundary. *Physical Review B*, 30(6):3274–3276, 1984.